

DOE/ET-53088-386

IFSR #386

**A Study of Runaway Electron Confinement
and Theory of Neoclassical MHD Turbulence**

O. J. Kwon

Institute for Fusion Studies
The University of Texas at Austin
Austin, Texas 78712

July 1989

A STUDY OF RUNAWAY ELECTRON TRANSPORT
AND THEORY OF NEOCLASSICAL
MHD TURBULENCE

Publication No. _____

Oh Jin Kwon, Ph.D.

The University of Texas at Austin, 1989

Supervising Professor: Herbert L. Berk

Due to their high sensitivity to magnetic fluctuations, runaway electrons can be used to probe the structure of electromagnetic turbulence that causes anomalous electron heat transport in the L-mode confinement regime. The results of runaway confinement experiments from ASDEX are analyzed and the radial scale length of the magnetic turbulence is determined to be about 1 mm. Using this value and that of experimentally deduced electron thermal diffusivity, we determine the radial magnetic fluctuation level at the plasma edge in the L-mode to be about 2×10^{-4} . From a comparison of these results with the predictions of various theoretical models, it is concluded that resistive-ballooning modes offer the best possibility for a consistent interpretation of the data.

Neoclassical MHD equations, which are valid in the experimentally relevant, low-collisionality regimes, support instabilities which might be responsible

for anomalous heat transport and high turbulence level of the tokamak edge. From the nonlinear study of neoclassical pressure-gradient-driven turbulence (NPGDT), the turbulent pressure diffusivity is obtained as an eigenvalue of the renormalized equations. The levels and radial scales of turbulence are also determined, and are shown to exceed mixing length estimates by powers of a nonlinear enhancement factor. The reconsideration of the radial structure of magnetic flutter driven by NPGDT leads to estimates of the electron heat transport and magnetic fluctuation levels which differ substantially from previous calculations. Neoclassical rippling modes can tap the density gradient expansion free energy source through the density dependence of the neoclassical resistivity. The turbulent radial diffusivities of the temperature and the density are obtained as eigenvalues of the renormalized eigenmode equations at steady state. The density gradient acts to enhance the level of turbulence, compared to that driven by the temperature gradient alone. The saturated turbulent state is characterized by: current decoupling, the breakdown of Boltzmann relation, a radial mode scale of density fluctuations exceeding that of temperature fluctuations.

A STUDY OF RUNAWAY ELECTRON CONFINEMENT
AND THEORY OF NEOCLASSICAL
MHD TURBULENCE

APPROVED BY
SUPERVISORY COMMITTEE:

Robert L. Berk

Marshall N. Rosenbluth

Peter H. Rost

F. W. Dulla

D. E. Baker

Edward J. Powers

To
my mom, Jin Sook,
and Jong Wan

A STUDY OF RUNAWAY ELECTRON CONFINEMENT
AND THEORY OF NEOCLASSICAL
MHD TURBULENCE

by

OH JIN KWON, M.A.

DISSERTATION

Presented to the Faculty of the Graduate School of
The University of Texas at Austin
in Partial Fulfillment
of the Requirements
for the Degree of
DOCTOR OF PHILOSOPHY

THE UNIVERSITY OF TEXAS AT AUSTIN

May, 1989

ACKNOWLEDGEMENTS

It has been a great privilege to learn from and to work with Prof. P. H. Diamond. His ingenuity as a physicist and his decisiveness as a guide in the maze of turbulence theory have been stimulating through the years. Without his help, this thesis would not have been possible.

I am grateful to Prof. M. N. Rosenbluth for his creative lectures upon which I founded my knowledge about plasma physics.

I would like to thank Prof. H. Berk for serving as the official supervising professor since Prof. M. Rosenbluth and Prof. P. Diamond left the University of Texas. I would also like to thank Prof. D. Baldwin, Dr. A. Wootton, and Prof. E. Powers for serving in my committee.

I am greatly indebted to Dr. F. Wagner and the ASDEX group for providing me with many valuable data about runaway electrons and for sharing their physical insights with me.

I learned a lot from lectures by Prof. W. Horton, Prof. H. Berk, and Dr. J. Van Dam.

I would like to acknowledge my gratitude to Prof. J. Callen and Dr. B. Carreras for stimulating discussions and helpful suggestions.

I express my gratitude to many people in IFS for supporting me before and after I moved to San Diego to finish my doctorate.

Discussions with Dr. P. Terry, Dr. T. S. Hahm, Dr. G. S. Lee, Dr. H. Biglari, and Dr. Y. B. Kim have been fruitful. I especially thank Dr. G. S. Lee who made it easier for me to adapt to a new culture when I first came to the States, and who introduced me to Prof. P. Diamond.

Associations with my fellow students have been extremely rewarding.

Among those are: H. T. Kook and Y. J. Kim, both of whom took care of administrative nuisances for me while I was away, N. Mattor who patiently and carefully read the manuscript, B. G. Hong, J. H. Han, G. Craddock, X. Q. Xu, F. Y. Gang, F. L. Waelbroeck, C. Y. Chen, and Q. Chen in Austin, and B. W. Lee, Y. D. Jung, and W. P. Hong in San Diego.

Due to my short memory, I must have left out many people who deserve a lot of credit.

Finally, I would like to express my special thanks to my mom, parents-in-law, my brother and sister, my wife Jin Sook, and my son Jong Wan who have stayed behind me all through those years. With those special people, my life has never been boring.

TABLE OF CONTENTS

I.	INTRODUCTION	1
II.	A STUDY OF RUNAWAY ELECTRON CONFINEMENT	14
	2.1 Introduction	14
	2.2 Experimental Results	20
	2.3 General Theory of Electron Thermal Diffusivity	36
	A. Electron Thermal Diffusivity	36
	B. Magnetic Fluctuation Spectrum	38
	C. Basic Scales and Regimes	40
	D. Comparison of χ_e for Thermal Runaway Electrons	41
	2.4 Analysis of Data	44
	2.5 Conclusions	53
III.	THEORY OF NEOCLASSICAL PRESSURE-GRADIENT-DRIVEN TURBULENCE	55
	3.1 Introduction	55
	3.2 Basic Equations	60
	3.3 Linear Theory	65
	A. Resistive Interchange Modes	69
	B. Energetic Trapped-Particle-Induced Resistive Interchange Modes	70
	C. Neoclassical Pressure-Gradient-Driven Modes	71
	D. Complete Description	72
	3.4 Nonlinear Theory	75

3.5	Electron Heat Transport	85
3.6	Summary	91
IV.	THEORY OF NEOCLASSICAL RESISTIVITY-GRADIENT-DRIVEN TURBULENCE	94
4.1	Introduction	94
4.2	Neoclassical Resistivity-Gradient-Driven Turbulence Model	99
4.3	Linear Theory	106
4.4	Nonlinear Theory	113
4.5	Summary and Conclusions	125
V.	CONCLUSIONS.....	129
	APPENDICES.....	134
	REFERENCES	140

CHAPTER I

INTRODUCTION

This thesis consists of two major studies: a study of runaway electron confinement (Chap. II) and a theory of neoclassical MHD turbulence (Chap. III and IV). The aim of the former is to study the structure of internal magnetic turbulence in tokamaks, which is thought by many to be responsible the heat transport. The aim of latter is to extend existing theories of MHD turbulence in tokamaks into experimentally relevant low-collisionality regimes. This section contains a theory of neoclassical pressure-gradient-driven turbulence (Chap. III) and a theory of neoclassical resistivity-gradient-driven turbulence (Chap. IV).

One of the primary goals of magnetic fusion research is to sustain a high-density and high-temperature plasma for a period of time, sufficient to generate fusion power greater than input power. To this end, the tokamak appears to be the most efficient device. Hence lots of experimental and theoretical efforts has been focused on understanding the behavior of the tokamak plasma. However, it is well known¹ that the energy confinement time (τ_E) of the tokamak plasma is much shorter than what is predicted by the classical Coulomb-collision-induced transport theory for tokamak magnetic geometry² (neoclassical transport). This excessive loss of the plasma heat is dubbed *anomalous* transport. Furthermore,

it seems inevitable that auxiliary heating such as neutral beam injection (NBI) will be necessary to heat plasmas to thermonuclear temperatures. With the onset of auxiliary heating, the decrease of τ_E by a factor of 2 to 4 from the value with only Ohmic heating (OH-mode) has been observed³ universally. This deterioration of τ_E , referred to as the low-energy-confinement mode (L-mode), becomes more severe³ with increased auxiliary heating power.

Magnetic fluctuations are often suggested⁴ as the cause of the anomalous transport (especially in the L-mode) since even very small levels of magnetic flutter⁵ can destroy magnetic flux surfaces, thus leading to enhanced transport. When two adjacent magnetic islands overlap, magnetic field lines wander stochastically, and particles can transport energy along perturbed field lines due to random-walk processes. Since electrons are more mobile than ions, they are more effective heat carriers. It is important to note that electron dissipation is essential for generating perpendicular magnetic fluctuations, since it relaxes the ideal frozen-in constraint.⁶ Thus, it induces parallel current fluctuations which, in turn, induce magnetic fluctuations through Ampere's law. With the level and structure of magnetic fluctuations specified, the electron heat transport coefficient (χ_e) has been calculated by many authors.^{7,8} However, these models are not self-consistent in that electron motions are not allowed to affect magnetic

fluctuations. Also, the actual source and the structure of magnetic fluctuations are not well understood yet.

Runaway electrons (REs) can serve as test particles to elucidate the nature of magnetic turbulence, since they are collisionless and sensitive to magnetic fluctuations due to their large parallel velocity. Most runaways are produced during the initial discharge phase, when the electric field inside the plasma exceeds the Dreicer electric field.⁹ Later, they are accelerated and in the current plateau phase, they are lost, due to magnetic turbulent transport. One unexpected aspect of the behavior of REs is that the RE confinement time (τ_R) is found to exceed τ_E , in the contrary to intuition and earlier theoretical prediction.⁷ It was shown^{10,11} that this discrepancy can be remedied when RE drift effects across magnetic field lines were considered. Therefore, REs can be used to determine the radial scale length of the magnetic turbulence.

The motivation behind Chap. II is the fact that τ_R and τ_E are well correlated in the L-mode and that they track the OH \rightarrow L transition. The experiments were performed on ASDEX. We develop a simple, generalized theory of electron heat transport, applicable to REs as well, to estimate W from the experimentally determined ratio of τ_E/τ_R . This, in turn, is used to estimate the level of magnetic turbulence by equating the measured electron heat diffusivity to the

theoretical electron heat transport coefficient due to stochastic magnetic fields. The parameter dependences of W and the level of turbulence are determined from parameter scan experiments. These results are compared to theoretical predictions in order to determine consistencies of existing theoretical models.

As resistive modes¹² seem to offer the most consistent interpretation, we further investigate the turbulence evolving from these instabilities. Also, the turbulence in tokamaks evolves from instabilities due to relaxation of the infinite conductivity constraint,⁶ since tokamaks are designed to be stable in ideal MHD. The peculiar feature of resistive instabilities is that magnetic reconnection between separate magnetic flux surfaces can occur, leading to deterioration of heat confinement. The important parameter, here, is the magnetic Reynolds number, $S_M = \tau_\eta / \tau_A$, where τ_η is the resistive timescale, associated with the magnetic reconnection, and τ_A is the poloidal Alfvén transit timescale, associated with magnetic free energy. The value of S_M for present-day tokamak parameters reaches 10^9 , and is expected to reach 10^{10} for future devices. The growth rate (γ) of resistive instabilities is slower than that of ideal MHD modes and it scales as $\gamma \sim S_M^s \tau_A^{-1}$, where s is a fraction between 0 and 1.

Three basic resistive modes were first identified by Furth, Killeen, and Rosenbluth,¹² and extensive investigations followed. These still remain topics of

current research. The three modes are: (i) the tearing mode, due to the relaxation of magnetic free energy associated with the gradient in the current profile (expressed by Δ'), with $s = 3/5$, (ii) the resistive- g mode (resistive interchange mode), due to the interaction of the pressure gradient with unfavorable curvature (curvature was effectively replaced by gravity in Ref. 12), with $s = 1/3$, (iii) the rippling mode, due to the resistivity gradient, with $s = 3/5$. Although resistive interchange modes are unstable, thus possibly accounting for anomalous transport, in stellarators¹³ and reversed-field pinches,¹⁴ the average favorable curvature¹⁵ (minimum- B configuration) in tokamaks can stabilize these modes. In addition, it may act to suppress^{12,16} the growth of the unstable tearing and rippling modes. Therefore, attention has shifted to resistive ballooning modes,¹⁷ where the pressure gradient in the localized outer region of unfavorable curvature forces modes to *balloon* outwards.

The resistive instabilities have been successful¹⁸ in identifying many characteristics, universally observed in tokamaks. The Mirnov oscillations,¹⁹ salient in the current ramp-up phases, are associated with $m \geq 2$ (m is the poloidal mode number) tearing modes.²⁰ The sawtooth oscillations²¹ may possibly be explained by $m = 1$ tearing modes.²² When a magnetic island from the $m = 2$ tearing modes grow, nonlinearly in the Rutherford regime,²³ and contacts with

islands of different helicity (usually $m = 3/n = 2$ and $m = 5/n = 3$, where n is the toroidal mode number), it may lead²⁴ to major disruptions.²⁵ The resistive ballooning modes have been well correlated with anomalous transport in the auxilarily heated ISX-B tokmak.²⁵ The energy confinement scaling is best described²⁷ in terms of dimensionless parameters, derived from resistive MHD equations. The rippling modes²⁸⁻³⁴ may be responsible for the highly turbulent characteristics of the tokamak plasma edge³⁵: a broadband spectrum of frequencies, high levels of density fluctuations ($\tilde{n}/n_0 = 10 \sim 100\%$, where n_0 is the density) increasing radially, high level of electrostatic fluctuations, large diffusivities which are possibly correlated with fluctuation levels, and the violation of Boltzmann relation ($\tilde{n}/n_0 \neq e\tilde{\phi}/T_e$, where $\tilde{\phi}$ is the electrostatic potential fluctuation, T_e is the electron temperature).

The resistive MHD model, however, is based on a short mean-free-path description³⁶ of the plasma, valid only in the Pfirsch-Schlüter regime,³⁷ where $\nu_{*e} \gg 1$ ($\nu_{*e} = \nu_e/\epsilon^{3/2}\omega_{be}$, ϵ is the inverse aspect ratio, ν_e is the electron collision rate, and ω_{be} is the electron bounce frequency). This renders the application of these models to present-day tokamak operational regimes rather dubious, since the temperature is so high that even the edge plasma falls into the low-collisionality, banana-plateau regimes. Recently, the reduced equations³⁸ of

resistive MHD have been extended³⁹ into the experimentally relevant banana-plateau regimes by incorporating the parallel viscous stress effects. The resultant neoclassical MHD equations include a bootstrap current,^{2,40} an enhancement of the inertia⁴¹ (an enhancement of the perpendicular dielectric constant by a factor of B^2/B_θ^2), trapped particle effects² in the resistivity, and the neoclassical damping of the vorticity, as well as other properties.

The neoclassical MHD equations support a pressure-gradient-driven instability,^{39,42,43} analogous to the resistive ballooning instabilities,^{17,25,44} in that the growth rate scales as $\gamma \sim \beta^{2/3} S_M^{-1/3} \tau_A^{-1}$ (β is the ratio of the kinetic pressure to the magnetic pressure) and that the structure is quite similar. However, the neoclassical pressure-gradient-driven instabilities are more virulent in that they are unstable for arbitrary β , S_M , etc., and that the neoclassical drive dominates over the magnetic field line curvature in providing access to the expansion free energy. The turbulence evolving from the neoclassical pressure-gradient-driven turbulence is the subject of Chap. III.

The rippling modes^{12,28-34} can couple to the density gradient through the neoclassical correction to the resistivity, since the effective neoclassical resistivity is a function of the density as well as the temperature while, the classical Spitzer resistivity³⁶ depends on the temperature only. This coupling is signif-

icant when $\nu_{*e} \sim 1$, where most tokamaks operate. The density fluctuation dynamics change the evolution of the rippling mode. In Chap. IV, we investigate the neoclassical modification of rippling modes and the characteristics of the turbulence evolving from the linearly unstable *neoclassical rippling* modes. The modification of the tearing modes will be discussed in the Appendix.

Since the thesis contains three relatively independent works (Chapters III, IV, and V), the discussion of each of them is self-contained. Note that the similar notation might have different meaning in different chapters, so that some notation may have been redefined. A substantial amount of introduction is required to each chapter. It will be given at the beginning of each work, and will not be repeated here. In the remainder of this chapter, we will give a brief summary of the individual works.

In Chap. II, we investigate the nature of magnetic turbulence. Section 2.1 contains the introduction to this work and in Sec. 2.2, we summarize experimental results, related to this work. In Sec. 2.3, we derive the electron heat diffusivity (χ_e) due to electron motion along perturbed magnetic field lines, starting from the electron drift kinetic equation.⁴⁵ Magnetic flutter nonlinearity is retained. It is shown that the calculated χ_e reduces to that of Ref. 7 in the quasilinear approximation. For REs, the Doppler shift due to radial excursions

across the mode rational surface reduces the effect of magnetic fluctuations on RE transport. Therefore, the ratio of τ_E/τ_R can be expressed as:

$$\frac{\tau_E}{\tau_R} = \frac{V_{\parallel,R}}{V_{\parallel,th}} S \left(\frac{V_{D,R} L_s}{V_{\parallel,R} W} \right).$$

Here, V_{\parallel} is the parallel velocity, V_D is the drift velocity, L_s is the shear length, and S is the radial structure function of magnetic fluctuations. Also, the subscripts, 'R' and 'th' denote REs and thermal electrons, respectively. When $S(V_{D,R}L_s/V_{\parallel,R}W) < V_{\parallel,th}/V_{\parallel,R}$, one finds $\tau_E/\tau_R < 1$, consistent with experimental results.¹⁰ In Sec. 2.4, we analyze experimental data from ASDEX to obtain values and scalings of W and magnetic fluctuation levels (\tilde{B}_r/B_0). We test the consistency of existing theories by comparing our results to theoretical predictions. If S function is determined from the experimental runaway energy spectrum, it can be inverted to find W . We use a Gaussian S function for simplicity in this investigation to find $W \sim 0.1cm$ from τ_E/τ_R . We can also determine \tilde{B}_r/B_0 if W is known. It is higher in the L-mode than in the OH-mode, and is higher at the edge than interior to account for experimentally measured,⁴⁶ radially increasing $\chi_e(r)$. The magnitude of \tilde{B}_r/B_0 at the plasma edge in the L-mode is determined to be about 2×10^{-4} , consistent with the theoretical prediction of resistive ballooning modes.¹⁷ The scalings of W and \tilde{B}_r/B_0 are also determined from parameter-scan experiments. As well as the

three resistive instabilities identified in Ref. 12, skin-depth turbulence theory⁴⁷ and electromagnetic drift-wave turbulence⁴⁸ are tested. It is concluded that the resistive ballooning modes¹⁷ and possibly microtearing modes⁴⁹ seem to provide the most consistent explanations of our results. Section 2.5 contains the conclusions of this work.

In Chap. III, we investigate the nonlinear evolution and saturation of neoclassical pressure-gradient-driven turbulence (NPGDT). Section 3.1 contains an introduction to this study. In Sec. 3.2, we summarize how the basic reduced equations of resistive MHD (Ohm's law, vorticity evolution, and pressure evolution) are modified by neoclassical parallel viscous stress effects. In Sec. 3.3, it is shown that the bootstrap current in Ohm's law and the neoclassical viscous damping of the vorticity acts to destabilize neoclassical pressure-gradient-driven instabilities.^{39,42,43} The resistive ballooning modes in the Pfirsch-Schlüter regime make a smooth transition to neoclassical pressure-gradient-driven instabilities in the banana-plateau regime, as neoclassical effects become predominant over the curvature drive. Due to the neoclassical correction to the resistivity, modes with poloidal wavelengths shorter than radial wavelengths (i.e., $m \gg 1$) are suppressed, in contradiction to the case of resistive interchange instabilities.¹³ In Sec. 3.4, nonlinear study of NPGDT is presented. Satur-

tion criteria are proposed. We use one-point DIA theory⁵⁰ to renormalize the $E \times B$ convective nonlinearities for the pressure and vorticity equations, yielding fluctuation-spectrum-dependent diffusivities. They are obtained as eigenvalues of the renormalized equations at saturation. The turbulent radial diffusivities, the level of turbulence, and radial scales of fluctuations are found to be enhanced significantly over mixing length estimates. In Sec. 3.5, χ_e due to NPGDT is re-examined. This may be the dominant heat loss channel in the L-mode, as shown in Chap. II. The bootstrap current contribution to magnetic fluctuations dominates over the Ohmic current contribution at saturation. The detailed structure of magnetic fluctuations should be considered when we determine *mixing length*. Proper analysis leads to results which significantly different from previous ones.²⁶ Section 3.6 contains a summary and conclusions of this work.

In Chap. IV, we investigate the nonlinear evolution of neoclassical resistivity gradient driven turbulence (NRGDT). Section 4.1 contains the introduction to this study. In Sec. 4.2, the theoretical model used in the study of NRGDT is presented. We describe how the classical Spitzer resistivity is modified to obtain the neoclassical resistivity. The structure of the neoclassical resistivity is investigated in detail. It is shown that the density coupling to the resistivity is greatest near $\nu_{*,e} \sim 1$. Since the couplings of the density and temperature

are different, the basic equations consist of Ohm's law, vorticity evolution, and temperature and density fluctuation evolutions. In Sec. 4.3, the linear stability results are presented. Eigenmodes have radially asymmetric structure because of the resistivity fluctuation, which is neglected in the study of NPGDT. Since the parallel equilibration of density fluctuations due to the neoclassical viscous damping has weaker stabilizing effects than the parallel thermal conduction, the density gradient free energy source dominates over that associated with the temperature gradient. Therefore, neoclassical rippling modes grow faster than usual rippling modes,²⁸ and the region where these modes are significantly excited extends to higher m -numbers. In Sec. 4.4, the nonlinear theory of NRGDT is presented. The same criteria for saturation as used in NPGDT are applied. The peculiar feature by which NRGDT at saturation can be distinguished from other saturated turbulence is current decoupling: the current fluctuation is negligible where other fluctuations are significant. Therefore, the vorticity evolution equation decouples from other basic equations. *Eigenvalue analysis* to obtain turbulent diffusivities is also utilized in this case. The density diffusivity is found to be larger than the temperature diffusivity. They differ from mixing length estimates not only quantitatively as in Chap. III, but also qualitatively. This is because the nonlinear decorrelation rate is completely different from the lin-

ear growth rate. The turbulence level is characterized by: $\tilde{T}_e/T_e < \tilde{n}/n_0$, and $e\tilde{\phi}/T_e \neq \tilde{n}/n_0$, consistent with experimental findings.³⁵ The magnetic fluctuation level due to NRGDT is too feeble to be significant. Section 4.5 contains conclusions of this work.

In Chap. V, we present a summary and conclusions of the thesis, and possible future applications. In Appendix A, it is shown that electrostatic turbulence cannot simultaneously explain the behavior of τ_E and τ_R on ASDEX, as noted to Chap. II. In Appendix B, we present a study of neoclassical tearing instabilities driven by Δ' . It is shown that these modes grow as: $\gamma \sim S_M^{-1} \tau_A^{-1}$. Therefore, dominant neoclassical instabilities are neoclassical resistivity-gradient-driven instabilities, neoclassical pressure-gradient-driven instabilities, and possibly neoclassical tearing modes driven by other than the current density gradient.

CHAPTER II

A STUDY OF RUNAWAY ELECTRON CONFINEMENT

2.1 Introduction

It is well known¹ that the electron thermal diffusivity in tokamaks is much larger than that predicted by neoclassical theory.² Magnetic microturbulence is often suggested as the cause of this anomalous transport,⁴ since even very small levels of magnetic flutter⁵ can destroy magnetic flux surfaces, thus leading to enhanced transport. The resulting electron thermal diffusivity, χ_e , due to stochastic magnetic fields has been calculated in various regimes,^{4,7,8} with the use of simple models for the structure of magnetic turbulence. However, the actual source and the structure of magnetic fluctuations are not well understood. Here, we report on the use of runaway electrons (REs) to elucidate the nature of magnetic turbulence. Such experiments are motivated by the high sensitivity of REs to magnetic flutter.^{10,11} It was shown in Ref. 10 that when RE drift effects were considered and a perpendicular correlation length was assumed, theoretical predictions for the RE confinement time (τ_R) and the global energy confinement time (τ_E) could be reconciled with the experimental results for moderate levels of magnetic turbulence. In this chapter, we report on the results of experiments

in the ASDEX tokamak which used REs as a probe to study the structure of magnetic turbulence that appears to be responsible for both τ_E and τ_R in L-mode confinement regimes. Using a simple, generalized expression for χ_e for the runaway and thermal electrons, we can determine the radial correlation length (W) of the magnetic turbulence from the experimentally determined ratio of τ_E/τ_R . This, in turn, is used to estimate magnetic turbulence levels.

In ASDEX discharges, REs evolve through three different phases: production, acceleration, and loss. First, during the initial discharge phase, when the breakdown voltage is 8 – 10 V, REs are produced throughout the plasma, since the electron temperature (T_e) and the density (n_e) profiles are flatter than those later in the discharge. The generation of REs greatly diminishes after 60 ms, since the loop voltage drops below 1.5V, so that E inside the plasma is less than 1/30 of the Dreicer electric field⁹ ($E_{Dreicer}$). The fact that there is no more significant RE production is further confirmed by sequential beam firing experiments (see Sec. II). In the second phase, during the current ramp-up (typically 600 – 800 ms), REs are no longer generated but are continuously accelerated. Finally, after about 1 second, the current plateau phase begins. This phase is characterized by a steady state RE distribution at a mean energy of about 1 MeV. In this phase, REs are continuously lost due to turbulent transport.

The measurements of thick target, hard X-ray bremsstrahlung⁵¹ (ϕ_x) are used to detect REs. A characteristic time for the exponential decrease of ϕ_x during the plateau phase can be interpreted as τ_R , since the population and the energy distribution of REs are invariant during this period. In ohmically heated plasmas (OH-mode), τ_R is generally a few hundred ms, while τ_E is 80–90 ms. It is worthwhile to note here that τ_R is strongly influenced by a change of magnetic field topology at the plasma periphery; a sharp degradation of τ_R , accompanied by strong modulation of ϕ_x by sawtooth activity, is observed when q_a is near 3, where q_a is the value of the safety factor at the edge. However, the bulk plasma is insensitive to such variations.

During neutral beam injection (NBI), ϕ_x surges upward and then decreases very sharply, corresponding to a deterioration in RE confinement. This deterioration is accompanied by a degradation in τ_E and in the particle confinement time (τ_P), even at low beam power. Unlike the OH-mode case, there is no additional drop in τ_R when a rational q_a value ($q_a = 3$) is passed through. This suggests that the quality of the magnetic field topology has deteriorated, so that the effects of additional perturbations are not so dramatic. Indeed, unlike in the OH-mode, sawteeth strongly modulate ϕ_x in the L-mode for *all* q_a values. However, because β_p is low (β_p is the ratio of the kinetic pressure to the poloidal

magnetic field pressure), the deterioration of τ_R cannot be trivially attributed to increased sawtooth activity. Furthermore, the behavior of ϕ_x remains same without sawteeth in both OH- and L-modes. At the transition from the L-mode to the H-mode,⁵² the confinement of REs sharply improves, along with τ_E and τ_P , while β_p also increases due to improved global confinement.

A clear correlation between the confinement properties of the bulk plasma and of the REs suggests that the degradation of τ_E and τ_P in the L-mode is perhaps due to magnetic turbulence, which is evidently also responsible for RE confinement. There is still doubt whether the OH confinement of the bulk plasma is controlled by magnetic turbulence, since the q_a dependences of τ_R and τ_E are uncorrelated in the OH-mode. However, it is clear that magnetic turbulence is not a trivial consequence of rising β , as predicted by drift wave theory,⁴⁸ because of the implication of what is observed at the L→H transition, where β and τ_R both increase.

In the present study, we analyse RE confinement data to probe the structure of magnetic microturbulence. Specifically, we determine the radial correlation length of the underlying magnetic turbulence using a simple model, explained in Sec.III, which clarifies and extends previous work.^{8,10,11} Because of the dominant ∇B drift effect, the coupling of REs to microturbulence is greatly

reduced, so that the effects⁷ of large RE velocity parallel to the equilibrium magnetic field (B_0) are weakened by cross-field drifts. This enables us to calculate W from the ratio of τ_E/τ_R , using the assumptions that energy is lost through the electron conduction channel and that the electron loss channel is controlled by magnetic turbulence in L-mode. Then, the relative amplitude of magnetic fluctuations ($b_0 = \tilde{B}_r/B_0$) necessary for the stochastic field-induced χ_e to match the experimentally deduced χ_e can also be determined if the spectrum-averaged poloidal mode number (\overline{m}) is known. The dependences of W and b_0 on basic plasma parameters, such as the toroidal magnetic field (B_T), the density, and the total input power (P), are determined semi-empirically from experimental scans of τ_E and τ_R with respect to those parameters. Having obtained the values and parametric dependences of W and b_0 , we then test the consistency of various microturbulence theories.

The remainder of this chapter is organized as follows. In Sec. 2.2, the experimental data is presented. The implications for χ_e and τ_R are discussed. A simple model for χ_e for both thermal and runaway electrons, including drift and finite Larmor radius effects, is derived in Sec. 2.3. In Sec. 2.4, the results obtained by using the model to analyze the data from ASDEX are compared with the predictions of various theoretical models. Finally, Sec. 2.5 contains a

summary and conclusions of this chapter.

2.2 Experimental Results

The measurements described below were performed on ASDEX, a diverted tokamak with major radius $R = 165$ cm and minor radius $a = 40$ cm. Discharges cover the parameter range of $B_T = 2.0 - 2.8$ T, plasma current $I_p = 200 - 400$ kA, loop voltage $V_L = 0.5 - 1.5$ V, and $n_e = (4 - 8) \times 10^{13} \text{ cm}^{-3}$.

The RE drift orbit is shifted outward with respect to the magnetic field lines⁵¹ (Fig. 2.1), because the guiding-center velocity of REs has both a poloidal (θ) component, due to the helical motion around the magnetic axis, given by

$$v_\theta = v_\parallel \frac{B_p}{B_T} \quad (2.1)$$

(where B_p is the poloidal magnetic field), and a vertical component, due to curvature and ∇B drifts, given by

$$v_D = \frac{1}{\Omega_e R} \left(v_\parallel^2 + \frac{1}{2} v_\perp^2 \right), \quad (2.2)$$

where $\Omega_e = eB_T/\gamma m_e c$ is the electron gyrofrequency and γ is the relativistic factor. The orbital displacement ΔR is determined by tracking v_θ and v_D .

When $a \gg \Delta R$, we have

$$\Delta R \simeq \frac{m_e c^2}{e B_T} \bar{q} \sqrt{\gamma^2 - 1}, \quad (2.3)$$

where \bar{q} is the average q value along the trajectory. Figure 2.1 shows the magnetic field topology of ASDEX with the nested surfaces (dashed curves).

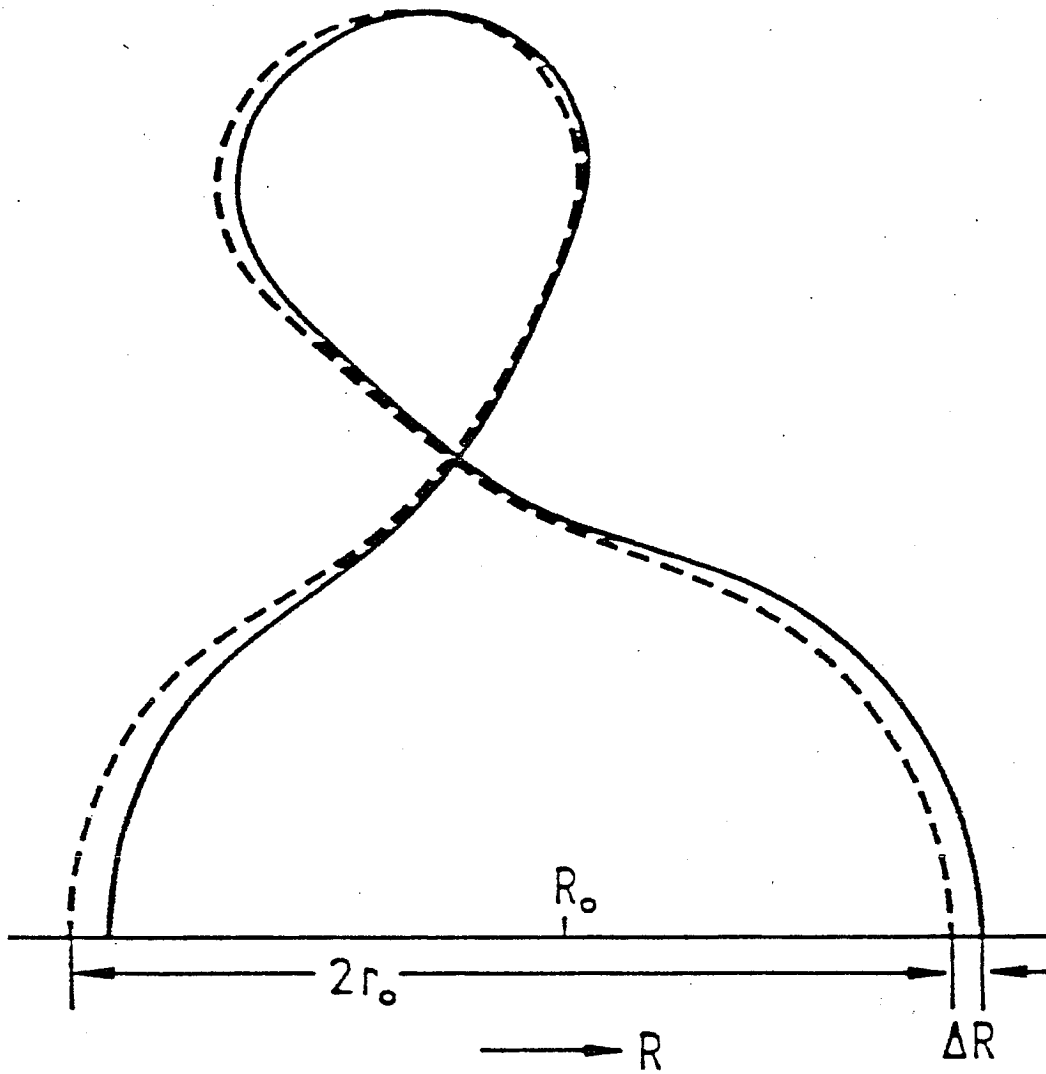


FIG. 2.1 Runaway electron drift orbit (solid line) shifted outward with respect to the magnetic separatrix (dashed line).

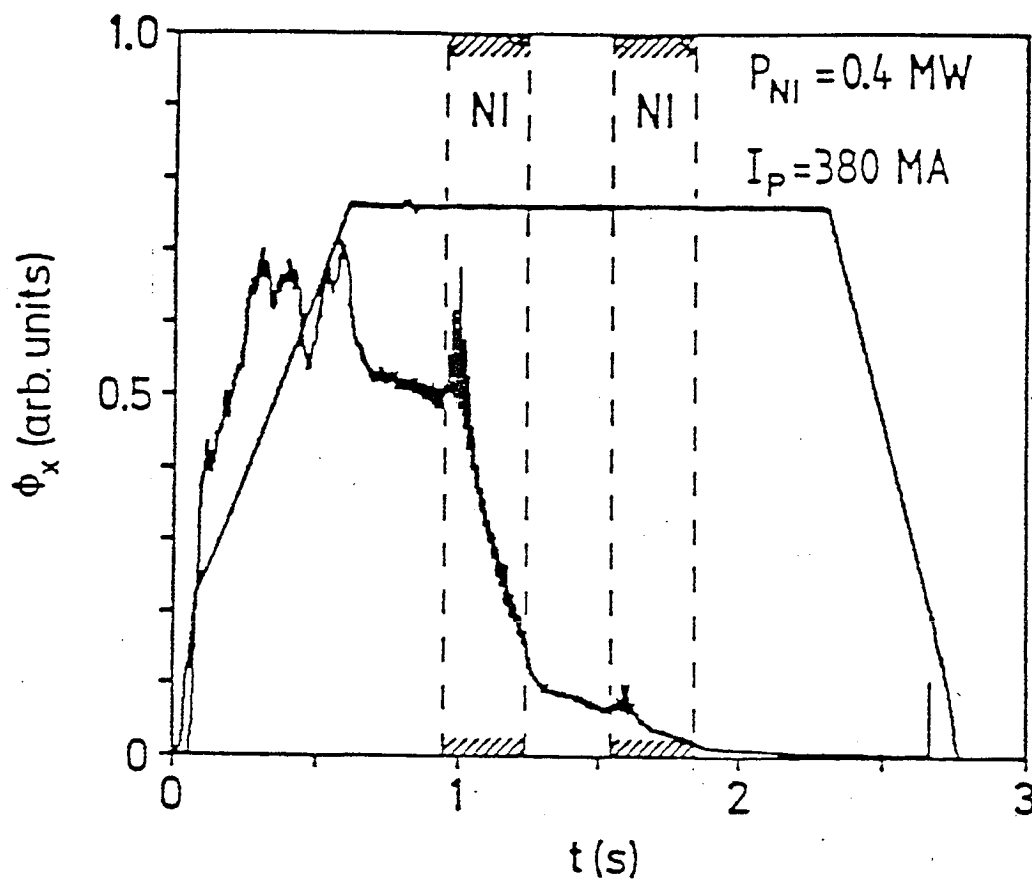


FIG. 2.2 Time evolution of hard X-ray signal ϕ_x during the OH-mode interrupted by two sequential neutral beam injection (NBI) pulses. NBI phases are indicated by hatched time intervals.

The RE drift surfaces for an energy of 5 MeV are shown as solid curves, both inside the plasma and at the separatrix. When this orbit intersects a target placed at the plasma midplane a few centimeters outside the separatrix on the low-field side, hard X-rays are emitted.⁵¹ The target is also shown in Fig. 2.1. Two targets are used, one out of molybdenum and the other out of tungsten. Both are movable radially outward from the separatrix, on a shot-to-shot basis.

In Fig. 2.2, ϕ_x is measured during the OH-mode interrupted by two sequential NBI pulses. During the first NBI phase, an initial increase of ϕ_x is followed by a sharp decrease, indicating that REs are quickly lost due to strong magnetic turbulence. The transient increase of ϕ_x at the OH→L transition (by a factor of the ratio of τ_R before NBI to τ_R after NBI) can be understood as a further confirmation of a reduction of τ_R during NBI. We note that V_L decreases as soon as NBI is applied. However, the second NBI pulse has little effect on ϕ_x because REs are already almost gone and there has been no significant generation since the first pulse. In order to confirm this situation on ASDEX in more detail, the loop voltage has been increased in the phase between the NBI pulses or after NBI (the plasma current also increases as a consequence). In spite of the phases of increased V_L , no REs are observed even in the phase of current termination. This result, along with the fact that the electric field inside the plasma is much

smaller than E_{Dreicer} , confirms the assumption that most REs are generated during the discharge initiation phase, especially before 60 ms. We note that ϕ_x during a discharge is solely determined by the filling conditions prior to the break-down.

Also, a steady-state energy distribution of REs seems to develop during the plateau phase, since the acceleration of high energy REs greatly diminishes compared to "free-fall" acceleration during this phase. At the three phases of an ohmic discharge, ϕ_x spectra have been investigated. In the plateau phase, steady conditions are achieved also for the RE distribution. A typical RE energy of 1 MeV is assumed in the analysis of Sec. 2.4. The detection system cuts off energies below 0.4 MeV. The viable probe position corresponded to RE energies in the range of 1–4 MeV. Because of the steep decrease of the RE flux towards higher energy (concluded from the ϕ_x radiation spectra), 1 MeV seems to be typical RE energy of the results presented here. Lower energy REs hit the target plates. REs of energy above 10 MeV intersect auxiliary limiters. Because of these characteristics and because the variation of ϕ_x is roughly exponential, the e-folding time of ϕ_x is a good measure of τ_R , even if there may be some corrections due to weak generation and acceleration processes.⁵³ It is worthwhile to note that these corrections have little effect on the results.

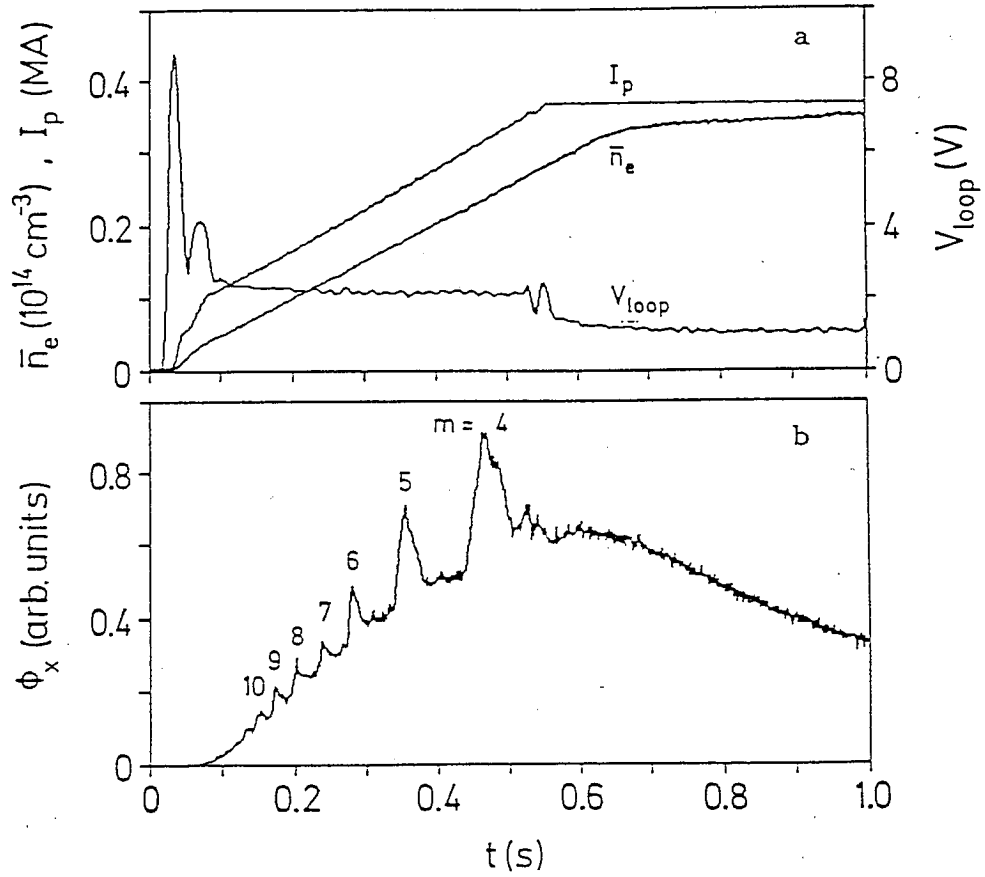


FIG. 2.3 Time evolution of (a) plasma current I_P , central chord-averaged electron density \bar{n}_e , loop voltage V_L , and (b) ϕ_x during the initial and current ramp-up phases.

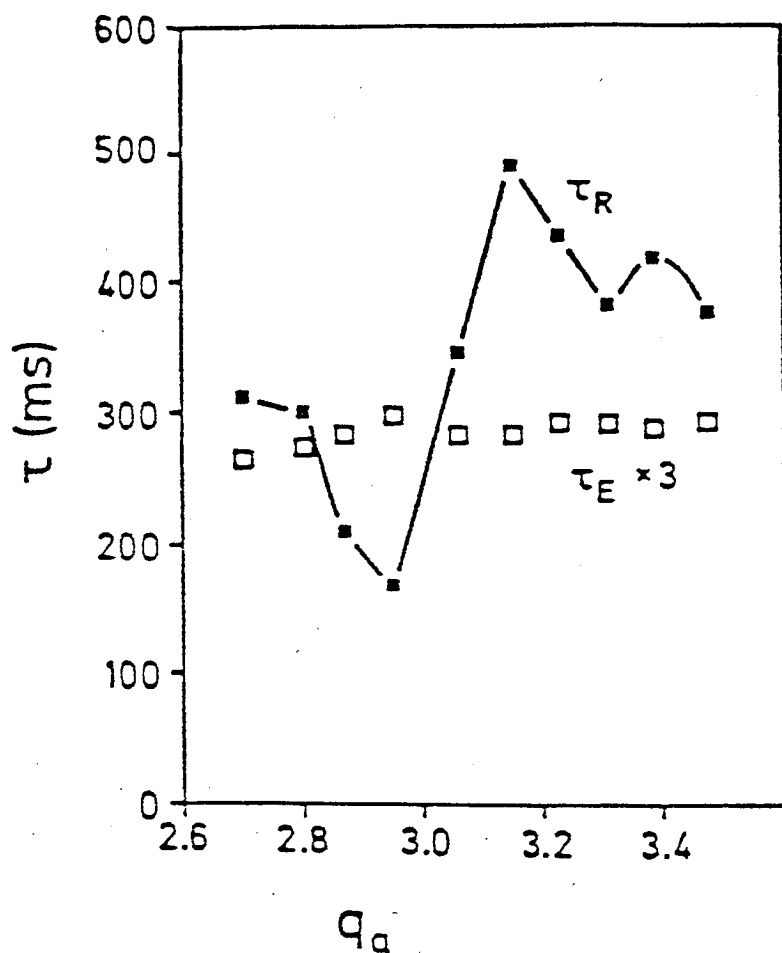


FIG. 2.4 Comparison of energy confinement time τ_E (open squares, measured kinetically and diamagnetically) and runaway electron confinement time τ_R (closed squares) in an ohmic B_T -scan.

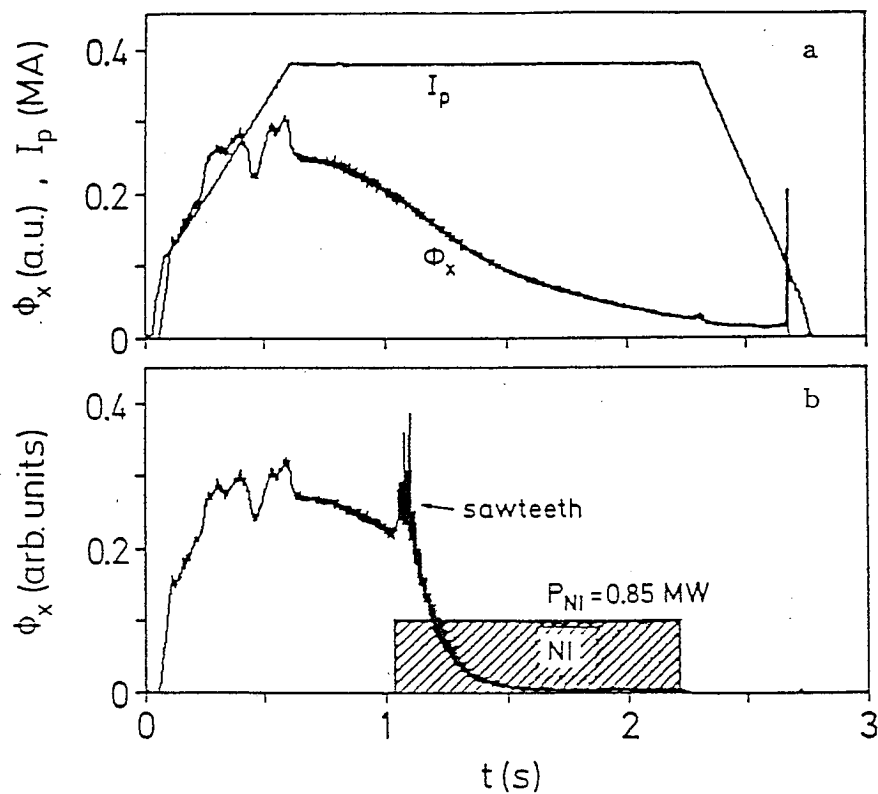


FIG. 2.5 Time evolution of (a) ϕ_x and I_p in the OH-mode and (b) ϕ_x in the L-mode. NBI phase is indicated by the hatched time interval.

Figure 2.3(a) shows I_p and the central chord-averaged electron density, \bar{n}_e , during the initial and current ramp-up phases. The corresponding ϕ_x is shown in Fig. 2.3(b). In the current ramp-up phase, ϕ_x increases, not because more REs are generated, but because REs continuously gain energy. The sequence of rational q surfaces moves from the interior across the separatrix as I_p is ramped up, with τ_R being degraded as each rational q_a crosses the separatrix. The quality of magnetic field configuration is not influenced by the presence of the separatrix, but rather by the cylindrical q_a value.

In ohmic discharges, RE confinement is strongly affected by q_a whereas bulk plasma confinement is not, as shown in the B_T scan of Fig. 2.4. A sharp degradation of τ_R is observed at $q_a \simeq 3$, where ϕ_x is strongly modulated by sawteeth. Away from $q_a \simeq 3$, little or no modulation of ϕ_x is observed. Other known global quantities, such as τ_E in Fig. 2.4, are almost completely insensitive to the destruction of the magnetic field topology at the plasma periphery.

NBI applied during the ohmic plateau phase causes a very sharp decrease in ϕ_x (Fig. 2.5(b)), as compared to the case without NBI (Fig. 2.5(a)). The variation of ϕ_x corresponds to a sharp reduction in τ_R , leading to almost full depletion of the RE population in a very short period of time.

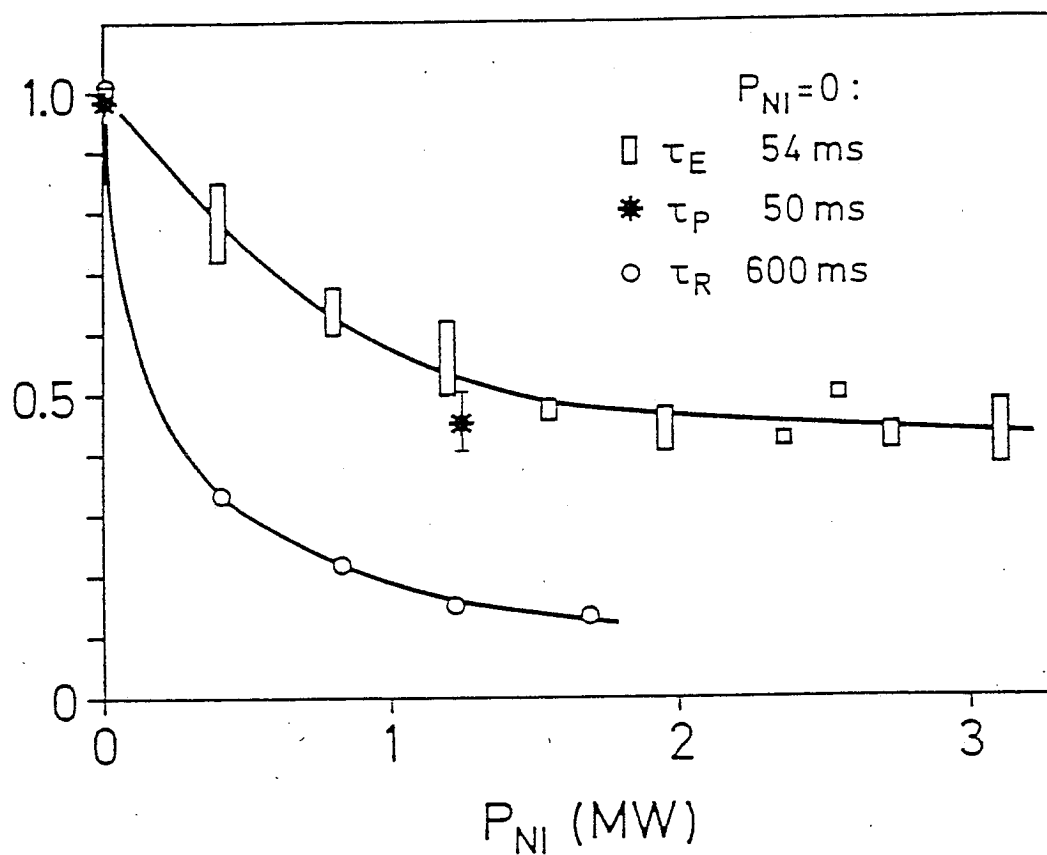


FIG. 2.6 Power dependence of τ_E (open rectangles), particle confinement time τ_P (asterisks, deduced from the particle balance; the recycling particle fluxes correspond to the backflow from the divertor chamber and is measured separately), and τ_R (open circles) normalized by their OH values.

In the L-mode, strong modulation of ϕ_x by sawteeth is observed for all q_a values (Fig. 2.5(b)), but in the OH-mode, only for rational q_a values. Sawteeth give rise to additional RE losses.⁵⁴ However, the dominant mechanism is the increased level of the magnetic turbulence. Also, in sawtooth-free injection phases, discharges display the same variation of ϕ_x with NBI as discharges with sawteeth. The turbulence that causes anomalous transport in the L-mode affects all three confinement properties (τ_E , τ_P , and τ_R) simultaneously (Fig. 2.6) and increases with higher neutral beam power (P_{NI}). Both τ_R and τ_E decrease monotonically from their values in the OH-mode with increasing P_{NI} and approach 100 ms and 20 ms, respectively, when P_{NI} reaches a few megawatts. In all cases, τ_R remains 5 – 10 times greater than τ_E . The sharp drop in τ_R at low P_{NI} indicates that a substantial degradation of magnetic field topology occurs at very low P_{NI} . It also indicates that sawtooth coupling does not play a significant role in τ_R . This suggests that in the case of ASDEX, at least, the L-mode is not a mere continuation of the OH-mode, but rather that a different mechanism is triggered by NBI. We note that the increase in P_{NI} is quantized in power steps of individual sources. The operation of a single source corresponds to a large step because the power input step is doubled.

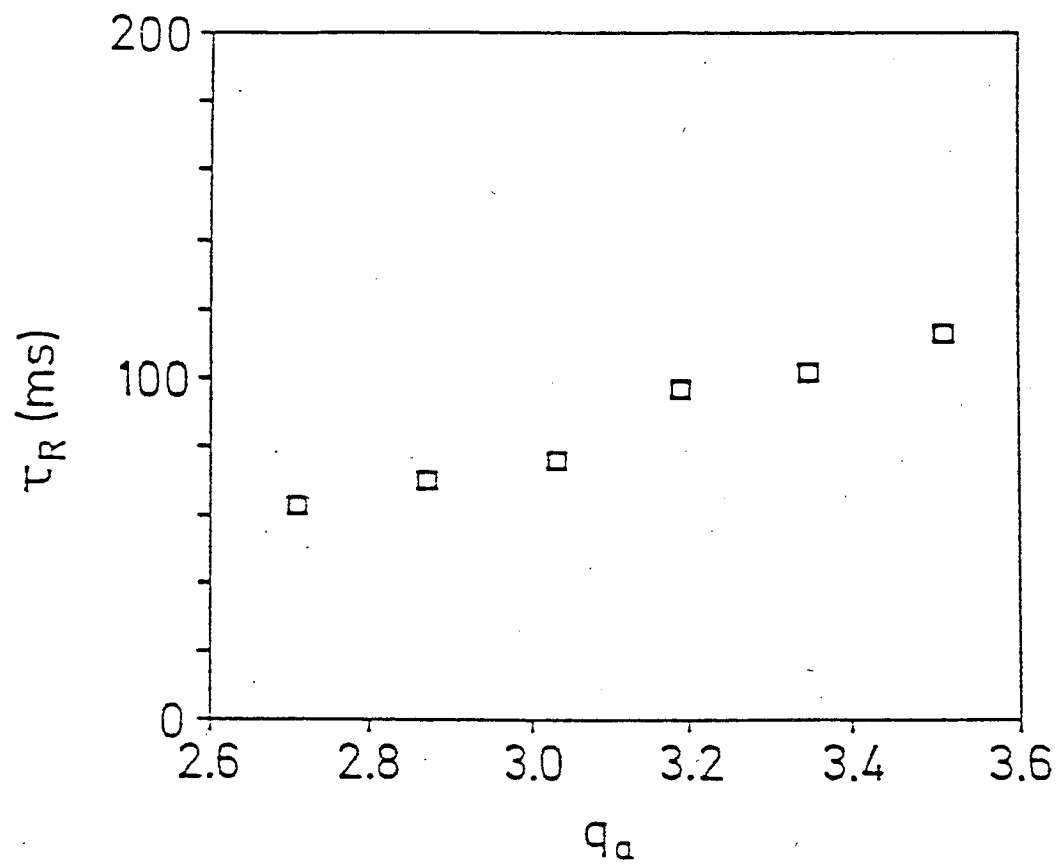


FIG. 2.7 τ_R in a q_a (or B_T) scan in the L-mode. τ_E is independent of q_a in this phase.

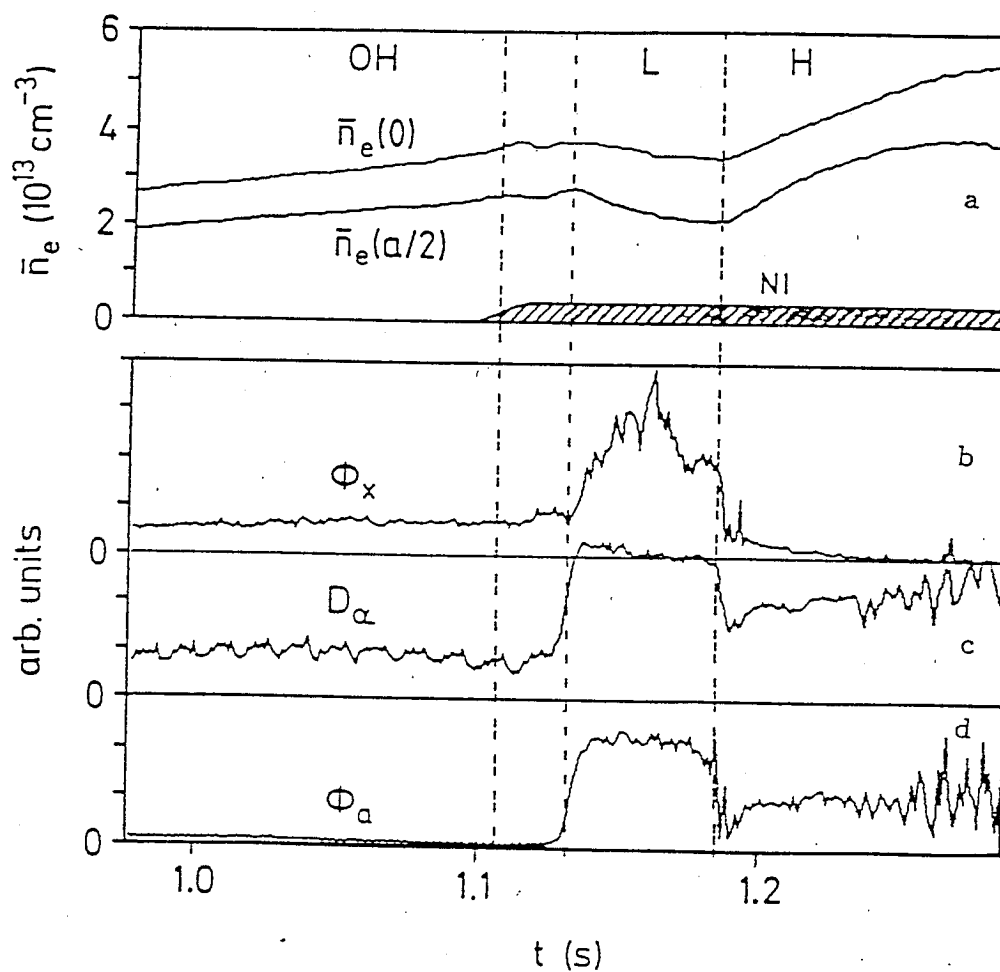


FIG. 2.8 Time evolution of (a) \bar{n}_e , (b) ϕ_x , (c) H_α -radiation, (d) back-reflected flux ϕ_a from the neutralized plate, in the OH-, L-, and H-modes. the transition from the L- to the H-mode is indicated by the dashed vertical line.

During NBI, τ_R increases monotonically with \dot{q}_a in a B_T scan (Fig. 2.7), unlike the case of the OH-mode, where sharp degradations at rational q_a values are observed (Fig. 2.4). The high sensitivity of REs to magnetic turbulence indicates that NBI degrades the quality of the magnetic field configuration to such an extent that the additional disturbance caused by a rational q_a surface is barely observable. The bulk plasma is insensitive to rational q_a values, as in the OH-mode.

Figure 2.8 shows sequential traces for ϕ_x , \bar{n}_e , H_α -radiation, and ϕ_a for OH-, L-, and H-modes. The H_α -radiation and ϕ_a are measures of the energy flux and the particle flux into the divertor, respectively. It is interesting to note that although the three signals (ϕ_x , H_α , and ϕ_a) are governed by different transport properties (i.e., RE, heat, and particle transport), they show simultaneous OH \rightarrow L and L \rightarrow H transitions. Especially at the L \rightarrow H transition, the rapid increase in τ_R , characterized by a sharp drop in ϕ_x (τ_R in the H-mode cannot be measured because fewer REs are left after the preceding L-phase), tracks the increase in τ_E and τ_P .

It is clear from correlations between the confinement properties of REs and the bulk plasma in the L-mode that the confinement properties of both may be governed by magnetic turbulence.

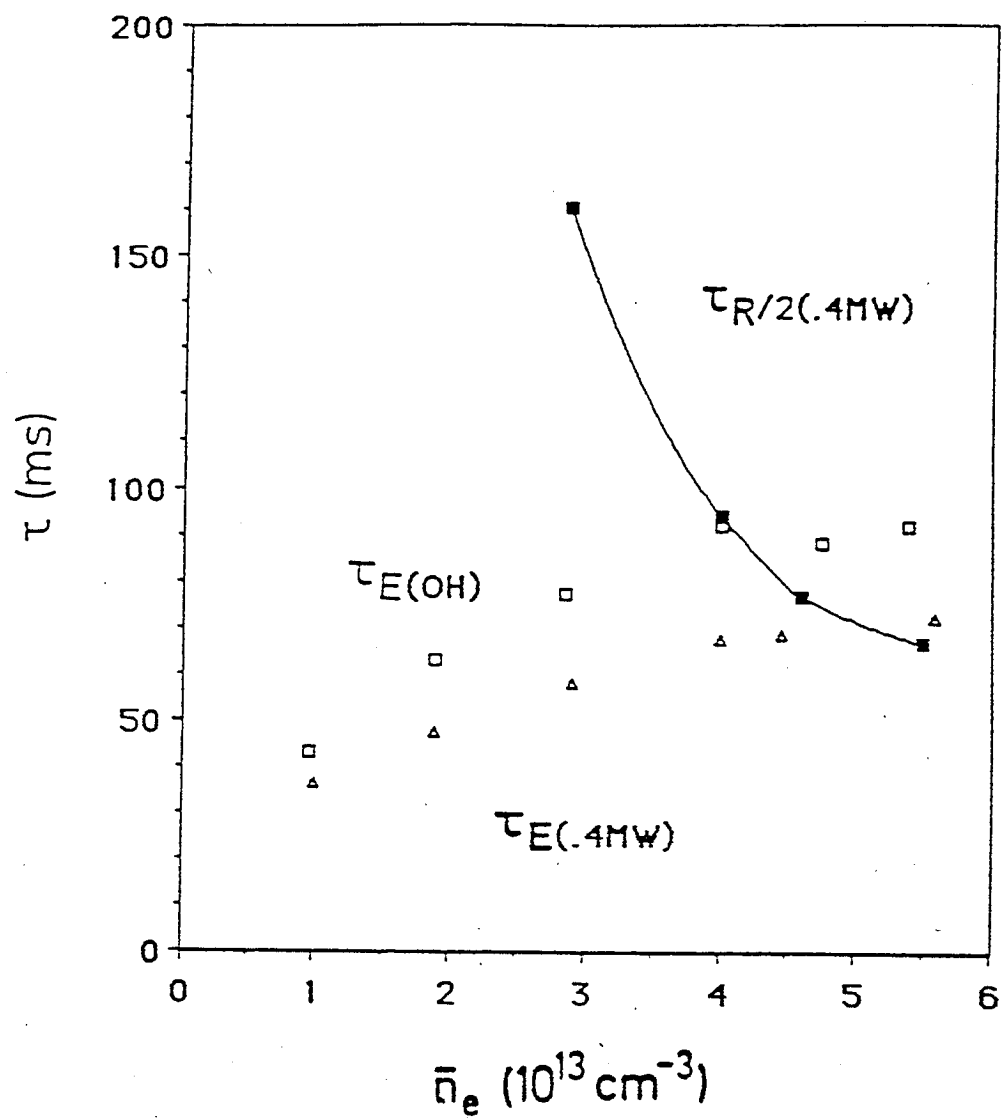


FIG. 2.9 n_e -dependence of τ_E in the OH-mode (open squares) and the L-mode (open triangles) and of τ_R in the L-mode (closed squares),

By analyzing data presented in this section, we can extract some useful information about the structure of magnetic microturbulence, mainly, W and b_0 . The scaling dependence of W and b_0 on P and q_a (or equivalently on B_T) can be determined by analyzing Figs. 2.6 and 2.7, respectively. The results of the scans of \bar{n}_e , which are used to determine the parametric dependence of τ_R and τ_E on \bar{n}_e in the OH- and L-modes, are presented in Fig. 2.9, where τ_E increases with \bar{n}_e , while τ_R decreases with \bar{n}_e for moderate beam power ($P_{NI} = 0.4MW$). We note that the density for L-mode power scans are kept below $3 \times 10^{13} \text{ cm}^{-3}$ to avoid H-transitions at a power level above 1.8 MW.

2.3 Generalized Theory of Electron Thermal Diffusivity

In this section, a simple model for χ_e due to stochastic magnetic field is set forth. An attempt is made to relate τ_E and τ_R , which are global quantities, to local values of χ_e that are determined from local estimates of microinstability-induced transport.

A. Electron Thermal Diffusivity

To derive an expression for χ_e that is applicable to REs as well as thermal electrons, the electron drift kinetic equation⁴⁵ is used:

$$-i(\omega - \omega_D - k_{\parallel}v_{\parallel})\tilde{g}_{\vec{k},\omega} + \sum_{\vec{k}',\omega'} v_{\parallel} \delta\vec{b}_{\vec{k}',\omega'} \cdot \nabla \tilde{g}_{\vec{k}-\vec{k}',\omega-\omega'} = -v_{\parallel} \tilde{b}_{r,\vec{k},\omega} \frac{\partial f_0}{\partial r} J_0(k_{\perp}\rho_e). \quad (2.4)$$

Here, $\tilde{g}_{\vec{k},\omega}$ is the nonadiabatic part of the fluctuating electron distribution function, ω is the mode frequency, k_{\parallel} is the wavenumber parallel to the magnetic field, $\delta\vec{b}$ is magnetic fluctuation normalized to B_0 , $\delta\vec{b} = \delta\vec{B}/B_0$, and f_0 is the equilibrium electron distribution function. Also, J_0 is the Bessel function of zeroth order, representing FLR effects, and ρ_e is the electron Larmor radius. A simple slab geometry is used to calculate the drift frequency, ω_D :

$$\omega_D = \frac{k_{\theta}}{\Omega_e R} \left(v_{\parallel}^2 + \frac{1}{2} v_{\perp}^2 \right), \quad (2.5)$$

where k_θ is the poloidal wavenumber. Note that the only nonlinear interaction of $\tilde{g}_{\vec{k},\omega}$ in Eq. (2.4) is with magnetic flutter, $\delta\vec{b}_{\vec{k},\omega}$. This nonlinear term is simplified as

$$\sum_{\vec{k}',\omega'} v_{\parallel} \delta\vec{b}_{\vec{k}',\omega'} \cdot \nabla \tilde{g}_{\vec{k}-\vec{k}',\omega-\omega'} = \frac{1}{\tau_{c\vec{k}}} \tilde{g}_{\vec{k},\omega}, \quad (2.6)$$

where $\tau_{c\vec{k}}$ is the nonlinear decorrelation time, which is an effective lifetime for eddies of scales of order $|\vec{k}|^{-1}$. The evolution of f_0 is described by

$$\frac{\partial f_0}{\partial t} = -\frac{\partial \Gamma_p}{\partial r}. \quad (2.7)$$

Here, Γ_p is the phase space flux, given by

$$\Gamma_p = v_{\parallel} \sum_{\vec{k},\omega} \tilde{b}_{r,-\vec{k},-\omega} J_0(k_{\perp}\rho_e) \tilde{g}_{\vec{k},\omega}. \quad (2.8)$$

It is easy to see that Eq. (2.7) is a diffusion equation with diffusion coefficient determined from Eqs. (2.4), (2.6), and (2.8) as

$$\chi_e = v_{\parallel}^2 \sum_{\vec{k},\omega} |\tilde{b}_{r,\vec{k},\omega}|^2 J_0^2(k_{\perp}\rho_e) \text{Re} \left[i \left(\omega - \omega_D - k_{\parallel} v_{\parallel} + \frac{i}{\tau_{c\vec{k}}} \right)^{-1} \right], \quad (2.9)$$

where $\text{Re}[\dots]$ denotes real part of $[\dots]$.

In the quasilinear approximation, where we neglect nonlinear mode coupling, Eq. (2.9) becomes

$$\chi_e = \pi v_{\parallel}^2 \sum_{\vec{k},\omega} |\tilde{b}_{r,\vec{k},\omega}|^2 J_0^2(k_{\perp}\rho_e) \delta(\omega - \omega_D - k_{\parallel} v_{\parallel}). \quad (2.10)$$

When the ballistic frequency, $k_{\parallel}v_{\parallel}$, is dominant over ω and ω_D and FLR effects are ignored, χ_e further reduces to

$$\chi_e = \pi|v_{\parallel}| \sum_{\bar{k}, \omega} |\tilde{b}_{r, \bar{k}, \omega}|^2 \delta(k_{\parallel}). \quad (2.11)$$

It is interesting to note that Eq. (2.11) is equivalent to the expression for χ_e derived in Ref. 7, since k_{\parallel} can be also written as $(n - m/q)/R$, where n and m are the toroidal and the poloidal mode numbers, respectively. However, this simple expression for χ_e leads to the conclusion that $\tau_R \ll \tau_E$ (because of the very large v_{\parallel} of REs), in contradiction with experimental results from ASDEX, for which $\tau_R \simeq (5 \sim 10)\tau_E$ (see Fig. 2.6), and elsewhere.¹⁰ This discrepancy can be resolved^{10,11} when the full expression for χ_e is considered.

B. Magnetic Fluctuation Spectrum

In this section, we specify the structure of the radial magnetic field fluctuations and make a few simplifications in order to evaluate the right-hand side of Eq. (2.9). The first simplification can be made if one notes that magnetic fluctuations that contribute to χ_e are due to microturbulence, excited near a rational surface and localized in radius. For a continuum of localized modes, we can write

$$\sum_{\bar{k}} = \sum_m \sum_n \simeq \int dm \frac{|q'|}{q^2} |m| \int dx, \quad (2.12)$$

where $q' = dq/dr$ and x is the radial displacement from the rational surface.

With this change, it is convenient to describe \tilde{b}_r in terms of m and x , i.e.,

$$|\tilde{b}_{r,\bar{k},\omega}|^2 = |\tilde{b}_{r,m,n,\omega}|^2 = C^M F(m) S_{\bar{k},\omega} \left(\frac{x}{W_m}, \omega \right). \quad (2.13)$$

Here, $F(m)$ is a poloidal mode number distribution function, W_m is the radial correlation length for mode m , and $S_{\bar{k},\omega}$ is a radial structure function. The constant C^M is chosen to give the mean-square amplitude of the magnetic fluctuation level, i.e.,

$$b_0^2 = \sum_{\bar{k},\omega} |\tilde{b}_{r,\bar{k},\omega}|^2, \quad (2.14)$$

and therefore

$$C^M = b_0^2 \left[\frac{|q'|}{q^2} \int dm |m| W_m F(m) \right]^{-1}. \quad (2.15)$$

Separating the frequency spectrum from $S_{\bar{k},\omega}$ in Eq. (2.13) yields

$$|\tilde{b}_{r,\bar{k},\omega}|^2 = \frac{b_0^2}{W_{mI} I} F(m) S_{\bar{k}} \left(\frac{x}{W_m} \right) \frac{\Delta\omega_{\bar{k}}}{\pi \{ (\omega - \omega_{\bar{k}})^2 + (\Delta\omega_{\bar{k}})^2 \}}. \quad (2.16)$$

Here, $\Delta\omega_{\bar{k}}$ is the line width of the frequency spectrum,

$$I = (|q'|/q^2) \int dm |m| F(m),$$

and W_{mI} normalizes $S_{\bar{k}}$ such that

$$\frac{1}{W_{mI}} \int dx S_{\bar{k}} \left(\frac{x}{W_m} \right) = 1, \quad (2.17)$$

with $S_{\vec{k}}(0) = 1$.

From Eqs. (2.12) and (2.17), one can easily evaluate the right-hand side of Eq. (2.11), which yields

$$\chi_e \simeq \frac{\pi |v_{\parallel}| L_s b_0^2}{\bar{k}_{\theta} \overline{W}_{mI}}, \quad (2.18)$$

where $L_s = Rq/\hat{s}$ is the shear length and $\hat{s} = rq'/q$ is the shear parameter. We have used $k_{\parallel} = k_{\theta}x/L_s$. Thus the effective connection length, denoted as D_{st} in Ref. 7, is identified as $\pi L_s b_0^2 / \bar{k}_{\theta} \overline{W}_{mI}$, where $(\overline{\dots})$ denotes the spectrum average. One can now experimentally estimate χ_e for the bulk plasma if b_0 , \overline{W}_{mI} , and \bar{k}_{θ} (or \bar{m}) are measured.

C. Basic Scales and Regimes

The estimation of χ_e is further simplified, without loss of generality, if χ_e is evaluated in two different regimes, separated according to different time scales. Autocorrelation times (τ_{ac}) are related to the natural randomization time of the spectrum. These are $|v_D \Delta \vec{k}|^{-1}$ (due to the spread in wavenumber, $\Delta \vec{k}$), $\Delta \omega_{\vec{k}}^{-1}$ (due to the spread in frequency spectrum), and $|k'_{\parallel} v_{\parallel} W_{\vec{k}}|^{-1}$ (the wave-electron decorrelation time). Usually, one can take

$$\tau_{ac} = (k'_{\parallel} |v_{\parallel} W_{\vec{k}}|)^{-1}, \quad (2.19)$$

since it is the fastest of the three time scales. The correlation time (τ_c) is the turbulent decorrelation time, determined under the assumptions that the

dominant length scale causing anomalous transport is $W_{\bar{k}}$ and that the dominant time scale is τ_c , i.e.,

$$\tau_c = \left(\frac{\chi_e}{W_{\bar{k}}^2} \right)^{-1}. \quad (2.20)$$

In the ‘strong’ turbulence regime, where $\tau_c < \tau_{ac}$, turbulence is fully developed and the nonlinear interaction between different modes becomes dominant. In the ‘weak’ turbulence regime, $\tau_{ac} < \tau_c$ and nonlinear interactions can be neglected.

D. Comparison of χ_e for Thermal and Runaway Electrons

In this section, we evaluate χ_e (Eq. (2.9)) for thermal and runaway electrons in both strong and weak turbulence regimes. These are compared in order to obtain W . The magnitude of b_0 can also be estimated so as to match the experimentally observed value of χ_e when \bar{m} is known.

For thermal electrons in the weak turbulence regime, χ_e is given by Eq. (2.18). For thermal electrons in the strong turbulence regime, χ_e can be calculated from Eqs. (2.9), (2.12), (2.16), (2.17), and (2.20) to yield

$$\chi_{e,th} = |v_{\parallel}|_{th} b_0 W, \quad (2.21)$$

where the subscript ‘th’ is added to indicate thermal electrons. Thus, in this regime the effective connection length for thermal electrons (D_{st}) is $b_0 W$. Comparing Eqs. (2.18) and (2.21), one can see that the integration constant \bar{W}_{mI} is

absent in Eq. (2.21) because $S_{\vec{k}}$ is radially averaged instead of being evaluated at a particular position (at $x = 0$ in Eq. (2.18)). It is interesting to note that because the dependence of χ_e on b_0 is different in the two regimes, one can experimentally determine the proper regime for thermal electron diffusion.

It is very likely that REs are in the weak turbulence regime because of their large parallel velocity. However, χ_e is not given by Eq. (2.18) since ω_D and $k_{\parallel}v_{\parallel}$ are comparable and the Doppler shift away from the $\vec{k} \cdot \vec{B} = 0$ resonance becomes significant for REs. Therefore, we have

$$\chi_{e,R} = \pi v_{\parallel,R}^2 \sum_{\vec{k}, \omega} |\tilde{b}_{r,\vec{k},\omega}|^2 J_0^2(k_{\perp} \rho_{e,R}) \delta(\omega_{D,R} - k_{\parallel} v_{\parallel,R}), \quad (2.22)$$

where the subscript 'R' denotes runaway electrons. Even for REs, the argument of J_0 is small enough for FLR effects to be ignored. Therefore, with our representation of the magnetic fluctuation spectrum, Eq. (2.22) yields

$$\chi_{e,R} = \pi |v_{\parallel}|_R \frac{L_s b_0^2}{k_{\theta} \overline{W}_{mI}} S_{\vec{k}} \left(\frac{\omega_{D,R}}{k_{\parallel} v_{\parallel,R} W} \right). \quad (2.23)$$

It is important to note the appearance of $S_{\vec{k}}$, representing the significance of radial excursion of the REs, as well as the appearance of \overline{W}_{mI} (instead of W). The X-ray spectrum is expected to cut off at very high energy because the radial excursion width of very high energy REs greatly exceeds W and the argument of $S_{\vec{k}}$ becomes so large that $\chi_{e,R}$ eventually vanishes.

Now, by comparing $\chi_{e,th}$ and $\chi_{e,R}$ and by using Fig. 2.6, we can calculate W . For simplicity, we assume that thermal electrons are also in the weak turbulence regime. This assumption is marginally satisfied for ASDEX parameters. From Eqs. (2.18) and (2.23), we obtain

$$\frac{\tau_E}{\tau_R} \simeq \frac{\chi_{e,R}}{\chi_{e,th}} = \frac{v_{\parallel,R}}{v_{\parallel,th}} S_{\bar{k}} \left(\frac{L_s v_{D,R}}{W v_{\parallel,R}} \right). \quad (2.24)$$

Without the $S_{\bar{k}}$ term, Eq. (2.24) would predict $\tau_R \ll \tau_E$, as in the simple theory.⁷ However, $S_{\bar{k}}$ evaluated at the radially shifted position for REs becomes smaller than the ratio of $v_{\parallel,R}/v_{\parallel,th}$, so that τ_R becomes longer than τ_E , consistent with experimental results.

To find W , we need to solve Eq. (2.24), which requires inversion of the $S_{\bar{k}}$ function. The structure of $S_{\bar{k}}$ could be understood in detail experimentally, if the τ_R spectrum of RE energy were measured. We consider a simple case here. If $S_{\bar{k}}$ is Gaussian, then Eq. (2.24) yields

$$W = L_s \frac{v_{D,R}}{v_{\parallel,R}} \ln^{-\frac{1}{2}} \left(\frac{v_{\parallel,R} \tau_R}{v_{\parallel,th} \tau_E} \right), \quad (2.25)$$

and from Eqs. (2.18) and (2.25), we find

$$b_0 = \pi^{-\frac{1}{4}} \left(\frac{\bar{k}_\theta \chi_{e,th} v_{D,R}}{v_{\parallel,th} v_{\parallel,R}} \right)^{\frac{1}{2}} \ln^{-\frac{1}{4}} \left(\frac{v_{\parallel,R} \tau_R}{v_{\parallel,th} \tau_E} \right). \quad (2.26)$$

Thus, only τ_E/τ_R and the average energy of the REs need to be measured to determine W . However, $\chi_{e,th}$ and \bar{k}_θ (or \bar{m}) must also be known in order to determine b_0 .

2.4 Analysis of Data

Having derived a simple generalized expression for χ_e for the REs and the bulk plasma, we now analyze experimental data from the ASDEX tokamak in order to find the magnitudes and scalings of W and b_0 . Noting that the τ_R and τ_E measurements are global, we calculate W and b_0 at the two different radial positions of plasma, that are believed to be related to the overall transport behavior, viz., at the $q = 2$ surface⁵⁵ and at the edge⁵⁶ of the plasma. The results are shown in Table 2.1. For the L-mode, a typical neutral beam injection power of 1 MW is chosen. It is worthwhile to note again that in the OH-mode, it is questionable whether the confinement of the bulk plasma is also governed by the magnetic turbulence, since the q_a dependences of τ_R and τ_E are uncorrelated. However, τ_R and τ_E cannot be simultaneously governed by electrostatic turbulence, as shown in the Appendix.

The magnitude of W is insensitive to the theoretical model for $S_{\bar{k}}$. Hence, detailed information about the structure of $S_{\bar{k}}$ (the τ_R spectrum in terms of the RE energy) is not very important for finding W and b_0 . As seen in Table 1, W is also insensitive to the confinement zones and is of order of 1 mm, consistent with the notion that W arises from *microturbulence*.

W (mm)			
OH-mode		L-mode	
$q = 2$	edge	$q = 2$	edge
1.3	1.1	1.3	1.2
$\delta B_r/B_0$ (10^{-4})			
OH-mode		L-mode	
$q = 2$	edge	$q = 2$	edge
0.48	0.87	1.1	1.8

TABLE 2.1 Values of the radial correlation length (W) and the radial magnetic fluctuation level ($\delta B_r/B_0$).

With the experimentally deduced radial profile⁵⁷ of χ_e and with the choice⁵⁸ $6 \leq \bar{m} \leq 10$, it is found that b_0 is larger at the edge than at the $q = 2$ surface, corresponding to radially increasing χ_e . The magnitude of b_0 is also larger in the L-mode than in the OH-mode, corresponding to confinement degradation during auxiliary heating. It is interesting to note that even very weak radial magnetic fluctuations ($b_0 \geq 10^{-4}$) can induce significant anomalous electron heat transport. Furthermore, this level suffices for magnetic field lines to become stochastic, which is a necessary condition for this theory to be valid.

The scalings of W with P (note that P denotes the total power, not just the neutral beam injection power) can be found by analysing Fig. 2.6. It should be noted here that the ratio of τ_R/τ_E is mostly influenced by W ; i.e., when W decreases, the RE drift effect is enhanced, leading to an increase in τ_R/τ_E and vice versa. Now, since Fig. 2.6 shows that the responses of τ_R and τ_E to changes in P are quite similar, it can be easily inferred that W is very weakly dependent on P .

However, τ_R and τ_E respond to changes in q_a (or B_T) differently; i.e., τ_R increases with q_a , while τ_E remains constant in the L-mode, making τ_R/τ_E increase with q_a as shown in Fig. 2.6. This indicates that W decreases as q_a increases, in that the Doppler effect of the REs due to their large radial excursion

becomes larger. The inverse scaling of $v_{D,R}$ with B_T makes this dependence even stronger. However, because τ_R/τ_E decreases as n_e increases as shown in Fig. 2.9, W increases as n_e increases, so that the RE drift effect is suppressed. The parameter scan results can be summarized as

$$W \sim n_e^{0.2} B_T^{-1.3} P^{0.05}. \quad (2.27)$$

Furthermore, a scaling study of b_0 can be similarly done, although simple inferences are not easily drawn from Figs. 2.6, 2.7, and 10 because of rather complicated dependences. The results is given by

$$b_0 \sim n_e^{-0.05} B_T^{-0.6} P^{0.6} \quad (2.28)$$

We next compare these results with predictions of various microturbulence theories. First, "skin-depth turbulence"⁴⁷ whose radial scale length is c/ω_{pe} , where ω_{pe} is the electron plasma oscillation frequency, is inconsistent with scaling result because c/ω_{pe} is proportional to $n_e^{-0.5}$ whereas W is proportional to $n_e^{0.2}$. It is also inconsistent with the B_T scaling result that W is strongly dependent on B_T , since c/ω_{pe} is independent of B_T .

In the usual theory of electromagnetic drift wave turbulence,⁴⁸ one has

$$W^{dw} \simeq 3\rho_s,$$

and

$$b_0^{dw} \simeq 3\beta \frac{\rho_s}{L_n}.$$

Here, the superscript "dw" denotes drift wave turbulence. Also, $\rho_s = c_s/\Omega_i$, $c_s = \sqrt{T_e/M_i}$, Ω_i is the ion gyrofrequency, M_i is the ion mass, $\beta = 8\pi p_o/B_T^2$, and $L_n = -[d \ln n_e/dr]^{-1}$. Although this theory correctly predicts the B_T scaling, b_0^{dw} is about 1/10 of b_0 . Also, because β is lower at the edge of the plasma, b_0^{dw} at the edge is smaller than b_0^{dw} at the $q = 2$ surface, in disagreement with the fact that b_0 must be larger at the edge in order to account for the radially increasing χ_e . Furthermore, τ_R and τ_E increase sharply at the onset of the H-mode (Fig. 2.8) while β_p also increases further, due to improved global confinement. This indicates that the high level of magnetic turbulence in the L-mode is not a trivial consequence of increasing β_p , in contradiction with the prediction of simple electromagnetic drift wave turbulence theory.

We now investigate the three resistive MHD instabilities.¹² Rippling modes,²⁸⁻³³ or current convective instabilities, are excited by a resistivity gradient and a parallel equilibrium current in Ohm's law and are stabilized by a large parallel thermal conductivity. A nonlinear study shows that

$$W^{ripp} = \left(c \frac{E_0 L_s}{B_0 L_\eta} \right)^{\frac{1}{3}} (\chi_{\parallel} \bar{k}_{\parallel}^2)^{-\frac{1}{3}}.$$

Here, the superscript “ripp” denotes rippling modes, E_0 is the equilibrium electric field, η is the resistivity, $L_\eta = [d \ln \eta / dr]^{-1}$, $k'_\parallel = k_\theta / L_s$, and χ_\parallel is the parallel thermal conductivity. One can then find b_0 by integrating Ohm’s law around the rational surface and using the constant- Ψ approximation,¹² which yields

$$b_0^{\text{ripp}} = \frac{2\pi}{c} \frac{E_0}{\eta B_0} \left(c \frac{E_0 L_s}{B_0 L_\eta} \right)^{\frac{2}{3}} (\chi_\parallel \bar{k}_\parallel^{-2})^{-\frac{2}{3}}.$$

Calculations show that W^{ripp} agrees with W , both in magnitude and in scalings. However, b_0^{ripp} is smaller than b_0 by a factor of 10^{-2} , which makes transport due to magnetic fluctuations induced by rippling modes insignificant.

Microtearing modes⁴⁹ are driven by an electron temperature gradient and the time-dependent thermal force. These modes have frequencies comparable to the diamagnetic drift frequency, ω_{*e} , and can be separated into two regimes according to the electron response: collisional for adiabatic electrons ($\omega \gg \chi_\parallel k_\parallel^2$), and semicollisional for isothermal electrons ($\omega \ll \chi_\parallel k_\parallel^2$). The width of the thermal conduction layer determines $W^{\mu t}$:

$$W^{\mu t} = \left(\frac{\nu_e L_s}{\Omega_e L_{T_e}} \right)^{\frac{1}{2}} (L_s \bar{k}_\theta^{-1})^{\frac{1}{2}}.$$

Here, the superscript “ μt ” denotes microtearing modes, ν_e is the electron collision rate, and $L_{T_e} = -[d \ln T_e / dr]^{-1}$. When $W^{\mu t}$ is comparable to the width of

the magnetic island, one finds

$$b_0^{\mu t} = \frac{\nu_e L_s}{\Omega_e L_{Te}}.$$

With ASDEX parameters, $W^{\mu t}$ is in agreement with W and is consistent with scaling results. This correctly predicts the radially increasing χ_e , since $b_0^{\mu t}$ at the edge is larger than $b_0^{\mu t}$ at the $q = 2$ surface, because of the low edge temperature. Its magnitude also agrees with b_0 as observed in the OH-mode. However, microtearing modes do not seem to be a viable candidate because the magnitude of $b_0^{\mu t}$ is about 1/10 that of b_0 in the L-mode.

Resistive-ballooning modes^{26,40} are excited by a pressure gradient in the bad curvature region, when β_p is large, in spite of the average minimum-B configuration of the tokamak. These are the toroidal analog of resistive interchange modes. Since field line bending is a dominant stabilizing force, one finds W^{rb} by balancing inertia with field line bending to obtain

$$W^{rb} = \frac{\bar{k}_{\theta} q}{\bar{s}} [\hat{s} n^2 \gamma_n \tau_A / S_M]^{\frac{1}{4}}.$$

Here, the superscript "rb" denotes resistive-ballooning modes and S_M is the ratio of the resistive time τ_r to the poloidal Alfvén time τ_A , with $\tau_A = Rq/v_A$ where v_A is the Alfvén speed. The growth rate, γ_n , is given by

$$\gamma_n = \left(\beta_p \epsilon \frac{r}{L_p} \right)^{\frac{2}{3}} \left(\frac{n^2}{S_M} \right)^{\frac{1}{3}} \tau_A^{-1}.$$

Here, ϵ is the inverse aspect ratio and $L_p = -[d \ln p / dr]^{-1}$, where p is the pressure. Using Ohm's law and Ampere's law, one finds

$$b_0 = \frac{4\pi}{c^2} \frac{\bar{k}_\theta}{\eta L_s} (W^{rb})^4 \gamma_n.$$

For ASDEX, W^{rb} agrees well with W in magnitude and scalings. Also, b_0^{rb} is consistent with radially increasing χ_e and the observed confinement degradation during NBI. Although the n_e and B_T dependence of b_0^{rb} is somewhat stronger than that indicated by the parameter scan, resistive-ballooning modes seem to offer the most plausible explanation of the results.

It is interesting to note that a recent study⁵⁹ of the effect of a diverted tokamak geometry shows that, because of increased shear near the separatrix, resistive MHD modes can be quenched, thus leading to a transport barrier⁶⁰ and a good confinement behavior in the H-mode. It is also interesting to note that because W^{rb} and b_0^{rb} are strongly dependent on m , an accurate measurement of \bar{m} may reveal that W^{rb} and b_0^{rb} are considerably larger or smaller than indicated by the present calculations. However, we note that scalings as well as relative magnitudes at different positions (i.e., b_0 at $q = 2$ must be smaller than b_0 at the edge to match with the radially increasing χ_e) and in different operational regimes (i.e., b_0 in the L-mode must be larger than b_0 in the OH-mode to be consistent with confinement degradation during auxiliary heating) are more

important than the magnitude itself in determining the consistency of theories.

Finally, Alfvénic microturbulence is also a plausible candidate since it has a characteristic radial scale length that is comparable to the Alfvén layer width, $x_A = \rho_s c_S L_S / L_n v_A$. Note that x_A is proportional to $n_e^{\frac{1}{2}} B_T^{-1}$, consistent with the n_e and B_T scan results. Further, detailed experimental results are needed to distinguish between the various possibilities.

2.5 Conclusions

We have derived a simple theory for χ_e , which enables us to calculate the radial correlation length, W , of the electromagnetic turbulence from the ratio of τ_R/τ_E . Then b_0 can also be determined by matching the experimentally deduced χ_e , if \bar{m} is known. This electromagnetic microturbulence seems to govern τ_R and τ_E simultaneously in the L-mode, as evidenced by the clear correlation in confinement properties. Scalings of W and b_0 are deduced from parameter scans. These properties of microturbulence are compared with various theoretical predictions in order to test the consistency of theories.

The principal results are as follows:

- (i) From the ratio of τ_R/τ_E , we calculate W to be about 1 mm, independent of assumptions about confinement zones or modelling.
- (ii) With the assumptions that \bar{m} is 6 – 10 and that the radial structure of the underlying magnetic turbulence is nearly Gaussian, b_0 is estimated to be about 2×10^{-4} at the edge of the typical L-mode plasma. This result is in agreement with the level which is experimentally deduced from measurements outside the separatrix.⁶¹
- (iii) From plasma parameter scanning results, we find

$$W \sim n_e^{0.2} B_T^{-1.3} P^{0.05} \quad \text{and} \quad b_0 \sim n_e^{-0.05} B_T^{-0.6} P^{0.6}.$$

(iv) Among various turbulence theories, the skin-depth turbulence theory⁴⁷ is in contradiction with our scan results, since c/ω_{pe} is proportional to $n_e^{-0.5}$. Rippling²⁸⁻³³ and microtearing⁴⁹ modes predict magnetic fluctuation levels that are too low to explain the observed χ_e in the L-mode. Resistive-ballooning modes^{26,40} seem to be the candidate which is most consistent, in both magnitude and scalings, with the data.

CHAPTER III

THEORY OF NEOCLASSICAL
PRESSURE-GRADIENT-DRIVEN TURBULENCE

3.1 Introduction

Resistive interchange-ballooning instabilities¹² have been successful in explaining experimentally observed anomalous heat transport in stellarators,¹³ reversed-field pinches,¹³ and the auxiliary heated high- β ISX-B tokamak.²⁶ However, these theories are based on a short mean free path description of the plasma, valid only in a Pfirsch-Schlüter regime where the collisional mean free path is much shorter than the parallel scale length (i.e., connection length). This makes the application of these models to present-day tokamak operational regimes rather dubious since the temperatures are so high that plasmas are in low-collisionality, banana-plateau regimes.

Recently, *neoclassical MHD* equations have been developed³⁹ to treat the low collisionality regime. It has been shown⁴² that these equations support interchange-like instabilities when $(dP/dr)(dq/dr) < 0$, where P and q are the pressure and the safety factor, respectively. In a related study,⁴³ a kinetic treatment of the dynamics of trapped particles reached similar conclusions. More-

over, these neoclassical MHD equations have well-known neoclassical properties such as: a bootstrap current⁴⁰ in Ohm's law as the consequence of the interaction of the pressure gradient with the radial excursion of trapped particles, an enhancement of the inertia⁴¹ (by a factor of B^2/B_θ^2) because of an additional polarization drift, neoclassical diffusion fluxes,² the Ware pinch,⁶² and the neoclassical correction to the resistivity.² Experimental evidence for the bootstrap current has been observed in TFTR⁶³ as well as in a toroidal multipole.⁶⁴ The neoclassical correction to the resistivity has important implications for the dynamics of resistivity-gradient-driven instabilities²⁸⁻³³ (rippling modes) since the neoclassical resistivity is a function of the density as well as the temperature. This will be discussed in Ch. IV.

In this chapter, we study the nonlinear saturation of neoclassical pressure-gradient-driven turbulence (NPGDT), evolving from linear interchange-like instabilities described by the neoclassical MHD equations. The structure of the neoclassical pressure-gradient-driven instabilities is similar to that of resistive interchange modes.¹³ However, it should be noted that neoclassical modes are somewhat more virulent, in that they are unstable for arbitrary β , S_M , etc. (β is the ratio of the kinetic pressure to the magnetic pressure and S_M is magnetic Reynolds number). Renormalized equations are derived. They are solved, yield-

ing the amplitude-dependent nonlinear viscosity (or diffusivity) as an eigenvalue. A similar treatment for resistive interchange modes¹³ led to the conclusion that although mixing-length estimates correctly predict the parameter scalings in leading order, they significantly underestimate the magnitude. Our study shows that the same result holds for NPGDT.

The remainder of the chapter is organized as follows. In Sec. 3.2, neoclassical MHD equations are summarized and corrections to the usual resistive MHD equations due to the inclusion of the parallel viscous stress tensor effects will be discussed. The parallel viscosity due to trapped particles leads to a bootstrap current and a neoclassical correction to the resistivity. The perpendicular component of the parallel viscous force (the cross viscosity) leads to additional viscous damping and a neoclassical enhancement of the polarization drift. Energetic trapped particle effects,⁶⁵ which are significant in experiments⁶⁶ with perpendicular neutral beam injection or resonant radio frequency heating, are also incorporated.

In Sec. 3.3, linear analysis reveals various branches of the neoclassical resistive interchange instability. Without neoclassical or hot trapped particle effects, resistive interchange modes¹³ become unstable due to the interaction of the pressure gradient with the average unfavorable curvature. These modes are

stable in tokamaks because of the minimum- B configuration. However, when the hot particle population trapped in the unfavorable curvature region becomes significant, energetic trapped-particle-driven resistive interchange modes⁶⁷ are unstable. When plasmas are in the banana-plateau regime of the collisionality, neoclassical effects are dominant and neoclassical pressure-gradient-driven modes^{42,43} (bootstrap current modes) become unstable. NPGDT evolves from these modes. In all cases, when the radial correlation length is much smaller than the poloidal correlation length, the growth rate scales like $\gamma \sim S_M^{-1/3} \tau_A^{-1}$ where τ_A is the poloidal Alfvén transit time. In the case of resistive interchange modes,¹³ it has been shown that when the poloidal correlation length becomes shorter than the radial mode width, one can recover *fast interchange* modes where the growth rate is independent of the resistivity. However, because of their rather unusual structure, bootstrap current modes are stabilized in the short poloidal wavelength limit. The neoclassical correction to the resistivity is responsible for suppressing small scale bootstrap current modes.

In Sec. 3.4, nonlinear study of NPGDT is presented. Nonlinear saturation occurs when the nonlinear energy cascade from linearly unstable, long wavelength modes to the short wavelength dissipation range balances the linear source. This cascade is mediated by $E \times B$ convective shearing. As to dominant

long wavelength modes, the saturation mechanism can be viewed as a radial diffusion, which balances the driving forces, naturally leading to the broadening of these modes. The amplitude-dependent turbulent diffusivity is obtained from the renormalized equations (i.e., as an eigenvalue of the renormalized eigenvalue problem at saturation) and is significantly larger than the mixing-length estimate. Other fluctuation quantities are also evaluated, showing significant enhancement over mixing-length estimates.

In Sec. 3.5, the problem of the electron heat transport due to stochastic magnetic fields driven by NPGDT is revisited. The radial structure of magnetic flutter⁵ associated with NPGDT is reconsidered. The bootstrap current contribution to anomalous transport, which is unique to NPGDT, is also included in the determination of magnetic fluctuation levels. Thus, a cross correlation between the pressure fluctuation and the electrostatic potential fluctuation appears. Results show both qualitative and quantitative differences from previous calculations²⁶ of χ_e (χ_e is the electron heat diffusivity). A recent study⁶⁸ of χ_e due to resistive interchange modes reached the same conclusion, as expected because of the similarity in the structure of the resistive interchange modes and NPGDT.

Finally, Sec. 3.6 contains a summary and conclusions.

3.2 Basic Equations

The neoclassical MHD equations³⁹ are employed in order to study the structure of neoclassical pressure-gradient-driven turbulence (NPGDT). They are valid in the long mean-free path (banana-plateau) regime. A comprehensive theory of the extension of resistive MHD equations, which are valid only in the short mean-free path (Pfirsch-Schlüter) regime, into a low collisionality regime can be found in Ref. 39. In this section, we summarize the results necessary for the nonlinear study of NPGDT, and discuss the differences between the two models.

The major correction to the momentum balance equation is the addition of a large parallel stress tensor due to the friction between trapped and circulating particles. The flux-surface averaged neoclassical parallel Ohm's law is then

$$E_{\parallel} = \frac{1}{c} \frac{\partial \psi}{\partial t} - \mathbf{b} \cdot \nabla \phi = \eta_{\text{sp}} \left(1 + \frac{\mu_e}{\alpha_e \nu_e} \right) J_{\parallel} + \eta_{\text{sp}} \frac{\mu_e}{\alpha_e \nu_e} \frac{c}{B_{\theta}} \frac{dP}{dr}. \quad (3.1)$$

Here, E_{\parallel} is the parallel electric field, $\mathbf{b} = \mathbf{B}/|\mathbf{B}_0|$, ψ is the parallel component of the magnetic potential, ϕ is the electrostatic potential, J_{\parallel} is the parallel current, and η_{sp} is the classical Spitzer resistivity (which is a function of the electron temperature only). For $Z_{\text{eff}} \simeq 1$, $\alpha_e \simeq 0.51$ and

$$\mu_e = \frac{2.3\sqrt{\epsilon} \nu_e}{1 + 1.02\nu_{*e}^{1/2} + 1.07\nu_{*e}}. \quad (3.2)$$

Here ϵ is the inverse aspect ratio, ν_e is the electron collision rate and $\nu_{*e} = \nu_e / \epsilon^{3/2} \omega_{be}$, ω_{be} being an electron bounce frequency. Recalling that the classical Ohm's law in resistive MHD is

$$E_{\parallel} = \eta_{\text{sp}} J_{\parallel},$$

it is easy to see that the Spitzer resistivity is replaced by the effective neoclassical resistivity,

$$\eta_{\text{neo}} = \eta_{\text{sp}} \left(1 + \frac{\mu_e}{\alpha_e \nu_e} \right). \quad (3.3)$$

It is interesting to note that since η_{neo} is a function of the density as well as the temperature, rippling modes²⁸⁻³³, which tap the free energy in the resistivity gradient, can now be driven by a density gradient. A nonlinear study, incorporating density dynamics in the evolution of resistivity-gradient-driven turbulence, indicates that the density gradient acts to enhance the turbulence level for normal tokamak profiles (i.e., $n_e' T_e' > 0$) where n_e and T_e are the electron density and the temperature, respectively, and $n_e' = dn_e/dr$, etc.. A detailed study of the neoclassical resistivity-gradient-driven turbulence will be presented in Ch. IV. The bootstrap current term in Eq. (3.1), $J_{\text{bt}} = (\mu_e / \alpha_e \nu_e) (c / B_{\theta}) dP/dr$, which does not have an analog in the classical Ohm's law should also be noted. The bootstrap current arises due to the fact that ion poloidal current vanishes

because of large ion viscous drag and electron viscous drag reduces electron poloidal current.

The vorticity evolution equation, derived from the charge neutrality condition, is

$$\frac{d}{dt} \left(1 + \frac{B^2}{B_\theta^2} \right) \nabla_\perp^2 \tilde{\phi} = \frac{B^2}{c^2 \rho} \nabla_\parallel \tilde{J}_\parallel + \frac{B}{c\rho} \frac{B}{B_\theta} \frac{d}{dr} \nabla_\parallel \tilde{P} + \frac{B}{c\rho} \mathbf{b} \times \mathbf{K} \cdot \nabla (2\tilde{P} + \tilde{P}_{\parallel,h} + \tilde{P}_{\perp,h}), \quad (3.4)$$

where $\mathbf{K} = \mathbf{b} \cdot \nabla \mathbf{b}$ is the magnetic curvature, the subscript 'h' denotes the hot particle component, and $d/dt = \partial/\partial t + (c/B)\mathbf{b} \times \nabla \phi \cdot \nabla$ denotes the total convective derivative. The left-hand-side of Eq. (3.4) denotes the parallel component of the vorticity, which arises from the polarization drift. Note that the inertia is enhanced by a factor of B^2/B_θ^2 . The first term in the right-hand-side of Eq. (3.4) represents field line diffusion (field line bending) and the second term represents viscous damping due to anisotropies in the perturbed pressure. The latter is an analog of the bootstrap current and should be kept pairwise with it. The interaction of these two terms is crucial in driving neoclassical pressure-gradient-driven instabilities.^{42,43} Finally, the third term denotes the interaction of the pressure with the magnetic curvature. Note that hot particles, treated separately from the core or warm particles, do not contribute to viscous damping because the collision rate for hot components is very small. Their contribution

to the bootstrap current is also negligible since $J_{bt,h} \sim -(c/B_\theta)dP_{\parallel,h}/dr$, so that in the present ordering scheme, $\epsilon^2 P \sim \epsilon P_{\perp,h} \sim P_{\parallel,h}$.

For the core plasma,

$$\frac{d\tilde{P}}{dt} \simeq \frac{\partial\tilde{P}}{\partial t} + \frac{c}{B}\mathbf{b} \times \nabla\tilde{\phi} \cdot \nabla P = 0, \quad (3.5)$$

i.e., the convective response to $E \times B$ flow is used. When hot particle effects and the curvature interaction are ignored, Eqs. (3.1), (3.4), and (3.5) constitute the basic equations for theoretical model of NPGDT. When the hot trapped particle population becomes significant, as in the perpendicular neutral beam injection experiment,⁶⁶ the perturbed distribution function is obtained from a drift kinetic description of hot particle dynamics. A complete description can be found elsewhere.⁶⁵ Taking a second moment of the nonadiabatic part of the perturbed distribution function of trapped particles yields the hot particle pressures:

$$\begin{pmatrix} \tilde{P}_{\perp,h} \\ \tilde{P}_{\parallel,h} \end{pmatrix} = -2^{\frac{5}{2}}\pi e_h B \int_{B_{\max}^{-1}}^{B_{\min}^{-1}} d\alpha (1 - \alpha B)^{1/2} \\ \times \int dE \left\{ \begin{matrix} \alpha B/2(1 - \alpha B) \\ 1 \end{matrix} \right\} \frac{E^{\frac{3}{2}} Q_h}{\omega - \bar{\omega}_{dh}} \left(\phi - \frac{v_{\parallel}}{c} \psi \right). \quad (3.6)$$

Here,

$$\begin{aligned}
 Q_h &= \left(\omega \frac{\partial}{\partial E} + \hat{\omega}_{*h} \right) F_{0h}, \\
 \hat{\omega}_{*h} &= -\frac{i}{\Omega_h} \mathbf{b} \cdot \times \nabla \ln F_{0h} \cdot \nabla, \\
 \omega_{dh} &= -i \frac{\mathbf{b} \times (v_{\perp}^2 \nabla \ln B + 2v_{\parallel}^2 \mathbf{K})}{2\Omega_h} \cdot \nabla,
 \end{aligned}$$

$\Omega_h = e_h B / m_h c$ is the cyclotron frequency, $\alpha = \mu / E$ is the pitch angle, $\mu = v_{\perp}^2 / 2B$ is the magnetic moment, $E = v^2 / 2$ is the energy per unit mass, F_{0h} is the unperturbed hot particle distribution function, and $\overline{(\dots)}$ denotes bounce averaging between turning points, i.e.,

$$\overline{(\dots)} = \frac{\int (dl / v_{\parallel}) (\dots)}{\int dl / v_{\parallel}}.$$

Also in a low- β approximation, $\nabla \ln B \simeq \mathbf{K}$. Now, Eqs. (3.1), (3.4), (3.5), and (3.6) constitute the basic equations for NPGDT with hot particle and curvature effects. The linear theory of this system will be studied in the next section.

3.3 Linear Theory

Having introduced the basic theoretical model, we study the linear stability of this model in this section. To render the theory analytically tractable, two important approximations are made. First, as a consequence of the electrostatic approximation, the neoclassical Ohm's law is simplified and \mathbf{b} reduces to the unit vector of the equilibrium magnetic field. Second, by neglecting the rippling effect ($\tilde{\eta}$ evolution), the density and the temperature evolutions need not be treated separately, and the model consists of evolution equations for $\tilde{\phi}$, \tilde{j}_{\parallel} , and \tilde{P} .

With these approximations, one finds two coupled equations for Φ and J_{\parallel} by solving for \tilde{P} , i.e.,

$$k_{\parallel}\Phi = i\eta J_{\parallel} + \delta_e \frac{c}{B_{\theta}} \frac{c\eta}{B\gamma} k_{\theta} \frac{dP}{dr} \frac{d\Phi}{dx}, \quad (3.7)$$

$$\begin{aligned} \rho\gamma^2 \left(1 + \frac{B^2}{B_{\theta}^2}\right) \nabla_{\perp}^2 \Phi = & i \frac{B^2 \gamma}{c^2} k_{\parallel} J_{\parallel} + \frac{B}{B_{\theta}} k_{\theta} \frac{dP}{dr} \frac{d}{dx} k_{\parallel} \Phi + 2k_{\theta}^2 \langle K_{\omega} \rangle \Phi \\ & - 2^{\frac{5}{2}} \pi e_h k_{\theta} \frac{B^2}{c} \int d\alpha \frac{K_{\omega} \alpha B}{2(1 - \alpha B)^{\frac{1}{2}}} \int dE \frac{\omega E^{\frac{3}{2}} Q_h}{\omega - \bar{\omega}_{dh}} \Phi. \end{aligned} \quad (3.8)$$

Here,

$$\delta_e = \frac{\mu_e}{\alpha_e \nu_e} \left/ \left(1 + \frac{\mu_e}{\alpha_e \nu_e}\right)\right.,$$

$\eta = \eta_{\text{neo}}$, K_ω is the total curvature, $\Phi = \langle \tilde{\phi} \rangle$, and $J_\parallel = \langle \tilde{j}_\parallel \rangle$ where $\langle (\dots) \rangle$ denotes flux surface averaging,

$$\langle (\dots) \rangle = \frac{\int (dl/B)(\dots)}{\int dl/B}.$$

Therefore, coefficients are also flux surface averaged. Also, perturbed quantities are Fourier analyzed according to:

$$\tilde{\phi} = \sum_{m,n} \tilde{\phi}(x) e^{i\omega t} \exp \left[i \left(n \frac{z}{R_0} - m\theta \right) \right],$$

where m and n are poloidal and toroidal mode numbers, respectively, R_0 is the major radius of tokamaks, z is the coordinate along the major axis, and $x = r - r_s$ is the displacement from the mode rational surface [where $q(r_s) = m/n$]. In Eqs. (3.7) and (3.8), the analysis assumes two different spatial scales: the longer parallel length scale, related to the connection length, and the shorter perpendicular length scale, related to the resistive layer width. Perturbed quantities are averaged over along the slowly varying parallel direction, such that the equations are in the fast variable x . This analysis is valid since these modes are extended along the magnetic field lines. Also, one can write $k_\parallel = k_\theta x / L_s$ where $L_s = Rq/\hat{s}$ is the shear length, and $\hat{s} = rq'/q$ is the shear parameter. If one further assumes that the radial variation is much faster than the poloidal variation, the approximation $\nabla_\perp^2 \simeq \partial^2/\partial x^2$ is possible. Then, solving Eqs. (3.7) and

(3.8) for Φ yields

$$I\gamma^2 \frac{d^2}{dx^2} \Phi - F_B \gamma x^2 \Phi + (N_V - F_{BB})x \frac{d}{dx} \Phi + (N_V - K + K_H)\Phi = 0. \quad (3.9)$$

Here,

$$\begin{aligned} I &= 1 + \frac{B^2}{B_\theta^2}, \\ F_B &= \frac{B^2 k_\theta^2}{c^2 \rho \eta L_s^2}, \\ N_V &= \frac{B k_\theta^2}{B_\theta \rho L_s} \left(-\frac{dP}{dr} \right), \\ F_{BB} &= \delta_e N_V, \\ K &= 2 \langle K_\omega \rangle \frac{k_\theta}{\rho} \left(-\frac{dP}{dr} \right). \end{aligned}$$

Physical interpretation for these terms is as follows: I represents the inertia of the fluid, F_B is the field-line bending, F_{BB} is an additional field-line bending due to the presence of the bootstrap current, and N_V is the neoclassical viscous damping which represents anisotropy in the perturbed pressure, which, in turn, drives NPGDT when combined with F_{BB} . Also, K denotes the interaction of the core plasma pressure gradient with the curvature, which drives the resistive interchange mode,¹³ important in stellarators. However, this has a stabilizing effect in tokamaks because of their average favorable curvature (minimum- B configuration). Finally, K_H represents the interaction of trapped hot particle pressure with the curvature, driving energetic trapped-particle-induced resistive

interchange modes.⁶⁷ The calculation of K_H is simplified when F_{0h} is approximated as slowing-down distribution, corresponding to a neutral beam injected at energy E_m ,

$$F_{0h} = \frac{C_0}{E_m} E^{-3/2} \delta(\alpha - \alpha_0),$$

for $E \leq E_m$, where α_0 is related to the injection angle. This choice of F_{0h} yields:

$$K_H = \frac{\hat{\omega}_{*h}}{\hat{\omega}_{dh}} \beta_{ph} \hat{I}_0(\omega). \quad (3.10)$$

Here, $\hat{\omega}_{dh} = \bar{\omega}_{dh}/E$, β_{ph} is the poloidal β for hot particles, and I_0 is a function of complete elliptic integrals. For modes growing faster than hot particle precessional time, K_H is independent of the growth rate.⁶⁷ Then, the general solution for Eq. (3.9) can be written as

$$\Phi(x) = \Phi_{0k} e^{-x^2/2W_k^2} H_l(ax).$$

Here, H_l is a Hermite polynomial, l is an integer,

$$a = \left(\frac{(N_V - F_{BB})^2}{4\gamma^4 I^2} + \frac{F_B}{\gamma I} \right)^{\frac{1}{4}},$$

$$W_k^{-2} = \left(\frac{(N_V - F_{BB})^2}{4\gamma^4 I^2} + \frac{F_B}{\gamma I} \right)^{\frac{1}{2}} + \frac{N_V - F_{BB}}{2\gamma^2 I}.$$

The eigenvalue condition is:

$$\frac{N_V + F_{BB} - K + K_H}{2\gamma^2} = (2l + 1) I^{1/2} \left(\frac{N_V - F_{BB}}{4\gamma^2} + \frac{F_B}{\gamma} \right)^{\frac{1}{2}}.$$

The $l = 0$ modes are centrally localized and

$$\Phi(x) = \Phi_{0k} e^{-x^2/2W_k^2}. \quad (3.11)$$

Now, Φ_{0k} is the magnitude of the electrostatic potential of the mode k , which cannot be determined from the linear theory, and W_k is the radial width of the mode. By substituting Eq. (3.11) into Eq. (3.9), one finds two coupled equations for γ and W_k , i.e.,

$$I \frac{\gamma^2}{W_k^4} = F_B \gamma + \frac{N_V - F_{BB}}{W_k^2}, \quad (3.12)$$

$$I \frac{\gamma^2}{W_k^2} = N_V + K_H - K. \quad (3.13)$$

These centrally localized modes are dominant, in that their growth rate exceeds that of higher modes due to field line-bending stabilization (of higher, broader modes). Various instability branches emerge immediately from these relations.

A. Resistive Interchange Modes

In the absence of neoclassical effects ($N_V = F_{BB} = 0$, $I = 1$) and trapped energetic particles ($K_H = 0$), resistive interchange modes, which might play an important role in anomalous thermal transport in stellarators¹³ and reversed-field pinches,¹⁴ are excited by the interaction of the pressure gradient with the average unfavorable curvature, where,

$$\gamma = (-K)^{2/3} / F_B^{1/3} \sim k_\theta^{2/3} S_M^{-1/3} \tau_A^{-1}. \quad (3.14)$$

Here, $S_M = \tau_R / \tau_A$ is magnetic Reynolds number, $\tau_R = r^2 / \eta c^2$ is the resistive time scale, and $\tau_A = Rq / v_A$ is the poloidal Alfvén transit time, v_A being the Alfvén speed. Instability of these modes requires $K \sim \langle K_w \rangle < 0$ which is not satisfied in tokamaks because of their minimum- B configuration. As a result, these modes are suppressed in tokamaks.

B. Energetic Trapped-Particle-Driven Resistive Interchange Modes

When neoclassical effects are ignored ($N_V = F_{BB} = 0$, $I = 1$), energetic trapped-particle-driven interchange modes⁶⁷ (due to hot particles trapped in the outside region for which $\omega_{*h}/\omega_{dh} > 0$) are excited even though tokamaks have average favorable curvature. The growth rate for these modes is

$$\gamma = \left(\frac{\hat{\omega}_{*h}}{\hat{\omega}_{dh}} \beta_{ph} \hat{I}_0 - K \right)^{2/3} / F_B^{1/3} \sim S_M^{-1/3} \tau_A^{-1}. \quad (3.15)$$

There is a threshold for these instabilities given by

$$\beta_{ph} > \frac{\hat{\omega}_{dh} K}{\hat{\omega}_{*h} \hat{I}_0}. \quad (3.16)$$

We have considered only the fluid limit here. These modes are purely growing in this limit and are not resonant with the precessional drift frequency of hot particles. Detailed results when these modes are resonant with the hot particle precession are described in Ref. 67.

C. Neoclassical Pressure-Gradient- Driven Modes

In the absence of curvature effects ($K = K_H = 0$), effects from bootstrap currents and neoclassical viscous damping, which are absent in a short mean free path description of the plasma, combine to destabilize the pressure-gradient-driven modes in the banana-plateau collisionality regime^{42,43} (bootstrap current instabilities) yielding:

$$\gamma = \left(\frac{N_V F_{BB}}{I F_B} \right)^{1/3} \sim k_\theta^{2/3} S_M^{-1/3} \tau_A^{-1}. \quad (3.17)$$

Interestingly, both the MHD description⁴² and the kinetic treatment⁴³ lead to the same result. Note that $I = B^2/B_\theta^2$ in this case. To be unstable, both N_V and F_{BB} are required to be positive. This is equivalent to $q'P' < 0$, as is satisfied in tokamaks. It is also interesting to note that γ is independent of \hat{s} , in contrast to previous cases where the shear has stabilizing effects. However, the effect of the shear here is to limit the radial width of the modes. These modes are of particular interest because they have fast growth rates, and they may play an important role in anomalous electron heat transport in tokamaks. NPGDT evolving from these modes and electron heat transport associated with magnetic fluctuations in the nonlinearly saturated state are the main topics of this chapter, and will be discussed later in Sec. 3.4 and in Sec. 3.5, respectively.

D. Complete Description

When we retain all of effects discussed earlier, we obtain

$$\gamma = (F_{BB} + K_H - K)^{1/3} (N_V + K_H - K)^{1/3} / (IF_B)^{1/3} \sim S_M^{-1/3} \tau_A^{-1}. \quad (3.18)$$

The instability condition is $F_{BB} + K_H > K$ and $N_V + K_H > K$. Bootstrap current interaction with viscous damping, as well as hot particles trapped in the unfavorable curvature region favors instability, while the core pressure gradient interaction with average curvature favors stability. Since the inequality, $N_V, F_{BB} > K, K_H$ is usually satisfied for the hot, core region of tokamaks, previously mentioned case C (bootstrap current modes) is of the greatest interest. It is worthwhile to note that all the modes treated here are of resistive interchange-ballooning family, in the sense that all growth rates scale as $\gamma \sim S_M^{-1/3} \tau_A^{-1}$.

Now, concentrating on neoclassical pressure gradient driven modes, one can rewrite Eq. (3.17) as

$$\begin{aligned} \gamma &= \left[\frac{c^2 \eta}{B^2 \rho} k_\theta^2 \delta_e \left| \frac{dP}{dr} \right|^2 \right]^{1/3} \\ &= \left(\frac{\delta_e}{16\pi} \right)^{1/3} \left(\frac{\epsilon}{q \beta_p} \right)^{2/3} \left(\frac{r^2 k_\theta}{L_P} \right)^{2/3} S_M^{-1/3} \tau_A^{-1}, \end{aligned} \quad (3.19)$$

where $L_P = -(d \ln P / dr)^{-1}$ is the pressure scale length. Then, from Eqs. (3.12)

and (3.13), the radial mode extent is

$$\begin{aligned}
 W_k &= \left(\frac{B}{B_\theta}\right)^{1/2} \delta_e^{1/3} \left[\frac{c^4 \rho \eta^2 L_s^3}{B^4 k_\theta^2} \left| \frac{dP}{dr} \right| \right]^{1/6} \\
 &= \sqrt{2} \left(\frac{\epsilon}{q} \beta_p\right)^{1/6} \left(\frac{\delta_e}{16\pi} \frac{r}{k_\theta L_P^2}\right)^{1/3} S_M^{-1/3} (L_s L_P)^{1/2}. \quad (3.20)
 \end{aligned}$$

It is important to note that we recover the *slow interchange* regime, where γ is proportional to $\eta^{1/3}$, in the limit where $\nabla_\perp^2 \simeq \partial^2/\partial x^2$. This is satisfied only for low- m modes, i.e., $W_k^2 \ll k_\theta^{-2}$. In Ref. 13, it was found that there are also *fast interchange* regime where γ is independent of η , for very large m . However, since the structure of neoclassical pressure gradient modes is somewhat different from resistive interchange modes (i.e., both bootstrap current and viscous damping contribute to the former, while the pressure gradient in bad curvature is the only source for the latter), one finds that there are no instabilities for large m , where $k_\theta \ll \partial^2/\partial x^2$. This is due to the fact that $\delta_e > 1$, which leads to an unphysical situation of radially increasing eigenfunction for growing modes.

3.4 Nonlinear Theory

In this section, we investigate nonlinear evolution and saturation of NPGDT evolving from linear neoclassical pressure gradient driven instabilities. Dominant $E \times B$ drift convective nonlinearities are replaced by spectrum-dependent turbulent diffusion coefficients using standard one-point renormalization theory.⁵⁰ The renormalized equations are solved as an eigenvalue problem to determine transport coefficients at saturation. The pressure diffusivity and fluctuation levels are found to exceed mixing-length estimates by powers of an enhancement factor obtained from the eigenvalue analysis.

Before describing the nonlinear closure scheme, we define two energy-like quantities. By eliminating \tilde{J}_{\parallel} , we obtain two coupled equations for Φ and $\Pi = \langle \tilde{P} \rangle$:

$$\rho \frac{B^2}{B_{\theta}^2} \frac{d}{dt} \nabla_{\perp}^2 \Phi = -\frac{B^2}{c^2 \eta} \nabla_{\parallel}^2 \Phi - \delta_e \frac{B^2}{c B_{\theta}} \nabla_{\parallel} \frac{d}{dr} \Pi + \frac{B^2}{c \rho B_{\theta}} \frac{d}{dr} \nabla_{\parallel} \Pi + \rho \mu \nabla_{\perp}^2 \nabla_{\perp}^2 \Phi, \quad (3.21)$$

$$\frac{d}{dt} \Pi = \frac{c}{B} \frac{dP}{dr} \mathbf{b} \times \hat{\mathbf{r}} \cdot \nabla \Phi + \chi_{\perp} \nabla_{\perp}^2 \Pi. \quad (3.22)$$

Here, μ and χ_{\perp} are added to provide energy sinks at small scales for $\nabla_{\perp}^2 \Phi$ and Π , respectively. They serve as short-wavelength dissipation to allow a nonlinearly saturated, turbulent state. However, they do not affect the growth of large scale modes. As usual, we define E_K and E_P as

$$E_K = \frac{1}{2} \int d^3x \rho |\nabla_{\perp} \Phi|^2,$$

$$E_P = \frac{1}{2} \int d^3x \Pi^2.$$

The evolution of these quantities is determined by:

$$\begin{aligned} \frac{d}{dt} E_K = & - \int d^3x \frac{B_\theta^2}{c^2 \eta} |\nabla_{\parallel} \Phi|^2 + \int d^3x \frac{B_\theta}{c} \delta_e \Phi \nabla_{\parallel} \frac{d}{dr} \Phi \\ & - \int d^3x \frac{B_\theta}{c} \Phi \frac{d}{dr} \nabla_{\parallel} \Phi - \int d^3x \rho \mu \frac{B_\theta^2}{B^2} |\nabla_{\perp}^2 \Phi|^2, \end{aligned} \quad (3.23)$$

$$\frac{d}{dt} E_P = - \int d^3x \frac{c}{B} \frac{dP}{dr} \Pi \mathbf{b} \times \hat{\mathbf{r}} \cdot \nabla \Phi - \int d^3x \chi_{\perp} |\nabla_{\perp} \Pi|^2. \quad (3.24)$$

The interaction of bootstrap currents with neoclassical viscous damping drives the kinetic energy (E_K), part of which is dissipated by viscosity (μ) and part of which is transformed into magnetic energy which, in turn, is dissipated by magnetic field diffusion (i.e., resistivity). The averaged pressure fluctuation (E_P) is driven by relaxation of equilibrium pressure gradients and damped by small scale dissipation due to χ_{\perp} . A saturated state is attained when there is energy transfer, mediated by nonlinear three wave couplings, from the low- m energy source to the high- m dissipation region. To build a complete picture of the saturated state, two point theory, which allows the calculation of the fluctuation spectrum, must be utilized. However, in this chapter, we study the saturation mechanism of low- m modes using the standard one-point theory where nonlinear interactions are renormalized to yield spectrum-dependent turbulent diffusivities. The saturation condition ($\gamma = 0$) then determines these diffusivities.

Since detailed treatment of the standard one-point theory can be found elsewhere,¹³ we only summarize basic steps here. Noting that the dominant nonlinearity comes from $E \times B$ convection, one can write the nonlinearity for the field A_k (in our case, A_k denotes $\nabla_{\perp}^2 \Phi_k$ or Π_k) as:

$$N(A_k) = i \frac{c}{B} \frac{\partial}{\partial r} \left[\sum_{k'} k'_{\theta} (\Phi_{-k'} A_{k''} - \Phi_{k''} A_{-k'}) \right] + i \frac{c}{B} k_{\theta} \sum_{k'} \left(A_{k''} \frac{\partial \Phi_{-k'}}{\partial r} - \Phi_{k''} \frac{\partial A_{-k'}}{\partial r} \right), \quad (3.25)$$

where $k'' = k + k'$. Now, the total convective derivative can be written as

$$\frac{d}{dt} A_k = \frac{\partial}{\partial t} A_k + N(A_k). \quad (3.26)$$

We renormalize $N(A_k)$ by iteratively substituting the nonlinearly driven fluctuations ($A_{k''}^{(2)}$ and $\Phi_{k''}^{(2)}$) resulting from the direct beat interaction of test modes ($\Phi_k^{(1)}$ and $A_k^{(1)}$) with background modes ($\Phi_{k'}^{(1)}$ and $A_{k'}^{(1)}$) to extract the piece which is phase coherent with test modes. Here, the superscripts “(1)” and “(2)” denote first and second order in perturbed quantities, respectively. The renormalization can be simplified when one notes that $\Phi_{k''}^{(2)}$ is spatially smoother than $\nabla_{\perp}^2 \Phi_{k''}^{(2)}$ or $\Pi_{k''}^{(2)}$. The smoothness is because $\Phi_{k''}^{(2)}$ is obtained from the inversion of the eigenmode operator, involving complicated spatial convolutions. By neglecting $\Phi_{k''}^{(2)}$, we can write equations for the driven fields as:

$$A_{k''}^{(2)} = \left(k_\theta \Phi_k^{(1)} \frac{\partial A_{k'}^{(1)}}{\partial r} + k'_\theta \Phi_{k'}^{(1)} \frac{\partial A_k^{(1)}}{\partial r} - k'_\theta A_{k'}^{(1)} \frac{\partial \Phi_k^{(1)}}{\partial r} - k_\theta A_k^{(1)} \frac{\partial \Phi_{k'}^{(1)}}{\partial r} \right) \times i \frac{c}{B} \Gamma^{-1}(A_{k''}) \quad (3.27)$$

where $\Gamma^{-1}(A_{k''})$ is the propagator for $A_{k''}$,

$$\Gamma(\nabla_\perp^2 \Phi_{k''}) = \gamma_{k''} + \Delta\omega(\nabla_\perp^2 \Phi_{k''}) - \mu \nabla_\perp^2, \quad (3.28)$$

$$\Gamma(\Pi_{k''}) = \gamma_{k''} + \Delta\omega(\Pi_{k''}) - \chi_\perp \nabla_\perp^2. \quad (3.29)$$

Here, $\gamma_{k''}$ is the growth rate, which vanishes at saturation. Also, $\Delta\omega(A_{k''})$ is the nonlinear decorrelation rate which effectively limits the coherence time of nonlinear interactions. Since Π is not straightforwardly related to Φ , Π is convected by Φ and it is easy to calculate $N(\Pi_k)$ as:

$$N(\Pi_k) = -\frac{\partial}{\partial x} D_k^{xx} \frac{\partial}{\partial x} \Pi_k + k_\theta^2 D_k^{yy} \Pi_k, \quad (3.30)$$

where

$$D_k^{xx} = \frac{c^2}{B^2} \sum_{k'} |k'_\theta \Phi_{k'}|^2 / \Gamma(\Pi_{k''}),$$

$$D_k^{yy} = \frac{c^2}{B^2} \sum_{k'} \left| \frac{\partial \Phi_{k'}}{\partial r} \right|^2 / \Gamma(\Pi_{k''}). \quad (3.31)$$

Here, terms such as $\sum_{k'} \Phi_{-k'} (\partial \Phi_{k'} / \partial r)$, etc. have been eliminated by symmetry arguments. Physically, D_k^{xx} and D_k^{yy} are interpreted as turbulent radial and poloidal pressure diffusivities, respectively.

To calculate $N(\nabla_{\perp}^2 \Phi)$, one cannot simply neglect $\Phi_{\mathbf{k}''}^{(2)}$ in Eq. (3.25) because the vorticity is directly related to Φ . Equivalently, the vorticity is not simply convected by Φ , so that its back-reaction on Φ must be considered, as well. To simplify this consideration, we note that for a continuum of localized modes, one can replace the sum in \mathbf{k} -space by $\int dm' |m'q'/q^2| \int dx'$, where $q' = dq/dr$. Then, $N(\nabla_{\perp}^2 \Phi_{\mathbf{k}})$ can be written as

$$N(\nabla_{\perp}^2 \Phi_{\mathbf{k}}) \simeq i \frac{c}{B} \frac{\partial}{\partial x} \sum_{\mathbf{k}'} k'_{\theta} \frac{m^2 + 2mm'}{m''^2} \Phi_{-\mathbf{k}'}^{(1)} \nabla_{\perp}^2 \Phi_{\mathbf{k}''}^{(2)} + i \frac{c}{B} k_{\theta} \sum_{\mathbf{k}'} \frac{m^2 + 2mm'}{m''^2} \frac{\partial \Phi_{-\mathbf{k}'}^{(1)}}{\partial r} \nabla_{\perp}^2 \Phi_{\mathbf{k}''}^{(2)}. \quad (3.32)$$

We have used $dx''/dx' = m''/m'$, near the mode rational surface of \mathbf{k} . By substituting Eq. (3.27) into Eq. (3.32), we get

$$N(\nabla_{\perp}^2 \Phi_{\mathbf{k}}) = -\frac{\partial}{\partial x} \mu_{\mathbf{k}}^{xx} \frac{\partial}{\partial x} \nabla_{\perp}^2 \Phi_{\mathbf{k}} + k_{\theta}^2 \mu_{\mathbf{k}}^{yy} \nabla_{\perp}^2 \Phi_{\mathbf{k}} - \frac{\partial}{\partial x} C_{\mathbf{k}}^{xx} \frac{\partial}{\partial x} \Phi_{\mathbf{k}} + k_{\theta}^2 C_{\mathbf{k}}^{yy} \Phi_{\mathbf{k}}, \quad (3.33)$$

where

$$\begin{aligned} \mu_{\mathbf{k}}^{xx} &= \frac{c^2}{B^2} \sum_{\mathbf{k}'} \frac{m^2}{m''^2} |\Phi_{\mathbf{k}'}|^2 / \Gamma(\nabla_{\perp}^2 \Phi_{\mathbf{k}''}), \\ \mu_{\mathbf{k}}^{yy} &= \frac{c^2}{B^2} \sum_{\mathbf{k}'} \frac{m^2}{m''^2} \left| \frac{\partial \Phi_{\mathbf{k}'}}{\partial r} \right|^2 / \Gamma(\nabla_{\perp}^2 \Phi_{\mathbf{k}''}), \\ C_{\mathbf{k}}^{xx} &= \frac{c^2}{B^2} \sum_{\mathbf{k}'} \frac{m^2}{m''^2} k'_{\theta} |\nabla_{\perp} \Phi_{\mathbf{k}'}|^2 / \Gamma(\nabla_{\perp}^2 \Phi_{\mathbf{k}''}), \\ C_{\mathbf{k}}^{yy} &= \frac{c^2}{B^2} \sum_{\mathbf{k}'} \frac{m^2}{m''^2} \left| \nabla_{\perp} \frac{\partial \Phi_{\mathbf{k}'}}{\partial r} \right| / \Gamma(\nabla_{\perp}^2 \Phi_{\mathbf{k}''}). \end{aligned} \quad (3.34)$$

Here, odd moments in x' as well as in k_θ -space vanish because of symmetry considerations. The factor of m^2/m''^2 (in comparison to Eq. (3.31)) represents the effect of the back-reaction of the vorticity on the convecting fluid. Physical interpretations of these coefficients are as follows. μ_k^{xx} and μ_k^{yy} are nonlinear radial and poloidal diffusivities of the vorticity, respectively, and act as effective sinks for E_K . C_k^{xx} and C_k^{yy} are their kinetic energy-conserving counterpart, and act as destabilizing energy sources.

Now, we determine how much energy outflow from long wavelength modes due to nonlinear multiple-helicity interactions is needed to balance the growth of these modes. When low- m modes dominate in the energy spectrum, turbulent radial diffusions are most effective stabilizing effects. Thus at saturation, the low- m modes satisfy:

$$\frac{\partial}{\partial x} \mu_k^{xx} \frac{\partial}{\partial x} \nabla_\perp^2 \Phi_k - \frac{B_\theta^2}{c^2 \rho \eta} \nabla_\parallel^2 \Phi_k - \frac{B_\theta}{c \rho} \delta_e \nabla_\parallel \frac{d}{dr} \Pi_k + \frac{B_\theta}{c \rho} \frac{d}{dr} \nabla_\parallel \Pi_k = 0, \quad (3.35)$$

$$\frac{\partial}{\partial x} D_k^{xx} \frac{\partial}{\partial x} \Pi_k + ik_\theta \frac{c}{B} \frac{dP}{dr} \Phi_k = 0. \quad (3.36)$$

By solving these eigenmode equations, we obtain D_k^{xx} and μ_k^{xx} as x -independent eigenvalues, required for the saturation of low- m modes. The level of turbulence is then determined from D_k^{xx} and μ_k^{xx} . In this treatment, nonlinear multiple-helicity interactions and significant overlap between different helicity modes are

crucial. We solve this eigenvalue problem by Fourier transforming, i.e.,

$$\Phi(u) = (2\pi)^{-1/2} \int dx \Phi_k(x) e^{iux}, \text{ etc..}$$

Then, from Eqs. (3.35) and (3.36),

$$F_B u^2 \frac{d^2}{du^2} \Phi(u) + \frac{F_{BB} - N_V}{D_k^{xx}} u \frac{d}{du} \Phi(u) + \left(\frac{2N_V - F_{BB}}{D_k^{xx}} - \mu_k^{xx} I u^6 \right) \Phi(u) = 0. \quad (3.37)$$

Here, $\nabla_{\perp}^2 \simeq \partial/\partial x^2$ is used again. The solutions are Bessel functions of integer order,⁶⁹

$$\Phi(u) = u^b Z_{\nu}(\lambda u^3),$$

where

$$1 - 2b = \frac{F_{BB} - N_V}{F_B D_k^{xx}}.$$

For localized modes $\nu = 0$, and an eigenvalue condition for this case is

$$b^2 = (2N_V - F_{BB})/F_B D_k^{xx},$$

or

$$1 + \left(\frac{F_{BB} - N_V}{F_B D_k^{xx}} \right)^2 + 2 \frac{F_{BB} - 3N_V}{F_B D_k^{xx}} = 0 \quad (3.38)$$

Note that $\gamma W_k^2 = F_{BB}/F_B$ is the mixing length estimate of D_k^{xx} obtained by balancing the linear growth rate and the turbulent diffusion (D_k/W_k^2). Thus, if we put

$$D_k^{xx} = \Lambda^2 \frac{F_{BB}}{F_B}, \quad (3.39)$$

we can interpret Λ as a nonlinear diffusion enhancement factor. Equation (3.37) is thus an eigenvalue equation for Λ :

$$\Lambda^2 = 3\delta_e^{-1} - 1 + 2 [\delta_e^{-1} (2\delta_e^{-1} - 1)]^{1/2}. \quad (3.40)$$

We have chosen the + sign to eliminate the unphysical situation of zero diffusion as $\mu_e/\alpha_e\nu_e \rightarrow \infty$. Thus, $\Lambda^2 \geq 4$ is always satisfied. It is interesting to note that nonlinear interactions always act to enhance the pressure diffusivity over the mixing length estimate ($\Lambda > 1$). This is consistent with the notion that the stabilizing mechanism for low- m modes is turbulent radial diffusion, thus leading to broadening of the modes. Also, although $\Lambda^2 \rightarrow \infty$ at very high temperature ($\mu_e/\alpha_e\nu_e \rightarrow 0$), the pressure diffusivity remains finite.

From Eq. (3.39), we can evaluate saturation levels of perturbed quantities. We follow the standard procedure¹³ by approximating $\Gamma(\nabla_{\perp}^2 \Phi_k) \simeq \mu_k^{xx}/\Delta_{\Phi}^2$ and $\Gamma(\Pi_k) \simeq D_k^{xx}/\Delta_{\Pi}^2$, where Δ_{Φ} and Δ_{Π} are nonlinear mode widths of Φ and Π , respectively. We thus find

$$\mu_k^{xx} \simeq \frac{m^2}{\bar{m}^2} \frac{\overline{\Delta_{\Phi}}}{\Delta_{\Pi}} D_k^{xx}, \quad (3.41)$$

$$\overline{V_r^2} \simeq \frac{(D_k^{xx})^2}{\langle \Delta_{\Pi}^2 \rangle_{\text{rms}}}. \quad (3.42)$$

Here, $\overline{(\dots)}$ denotes spectrum-averaged value of (\dots) , i.e.,

$$\overline{\Delta_{\Phi}^2} = \sum_{\mathbf{k}} |x\Phi_{\mathbf{k}}|^2 / \sum_{\mathbf{k}} |\Phi_{\mathbf{k}}|^2, \text{ etc.}$$

Also, $V_r = ck_\theta\Phi/B$ is the radial $E \times B$ velocity. Then, asymptotically balancing nonlinear viscosity with field-line bending yields:

$$\Delta_\Phi^6 = \mu_k^{xx} \frac{c^2 \rho \eta L_s^2}{B_\theta k_\theta^2}, \quad (3.43)$$

while balancing nonlinear pressure diffusion with the source (the pressure gradient) gives:

$$D_k^{xx} \frac{\bar{\Pi}}{\Delta_\Pi^2} = \bar{V}_r \left| \frac{dP}{dr} \right|. \quad (3.44)$$

It is interesting to note that by combining Eqs. (3.42) and (3.44), one finds

$$\frac{\bar{\Pi}}{P} = \frac{\bar{\Delta}_\Pi}{L_P},$$

which is just the mixing-length estimate of the pressure fluctuation. However, since Δ_Π is different from its linear value, W_k , due to mode broadening, this relation should be understood in its nonlinear sense. Finally, balancing nonlinear viscosity with destabilizing neoclassical viscosity near the rational surface gives:

$$\mu_k^{xx} \frac{\langle V_r^2 \rangle_{\text{rms}}^{1/2}}{\langle \Delta_\Phi^4 \rangle_{\text{rms}}} = \frac{B_\theta k_\theta^2}{B_\rho L_s} \langle \Pi^2 \rangle_{\text{rms}}^{1/2}. \quad (3.45)$$

Equations (3.39) - (3.45) completely determine levels and radial scales of turbulence, i.e.,:

$$\bar{\Delta}_\Phi = \bar{W}_k \Lambda^{1/6},$$

$$\begin{aligned}
\Delta_{\Pi} &= W_k \Lambda^{7/6}, \\
\bar{V}_r &= \bar{\gamma} \bar{W}_k \Lambda^{5/3}, \\
\bar{\Pi} &= \frac{P}{L_P} \bar{W}_k \Lambda^{7/6}, \\
D_k^{xx} &= \bar{\gamma} \bar{W}_k^2 \Lambda^2 \\
&= \Lambda^2 \frac{1}{8\pi} \frac{\epsilon}{q} \beta_p c^2 \eta \delta_e \frac{L_s}{L_P}, \\
\mu_k^{xx} &= \frac{m^2}{\bar{m}^2} \bar{\gamma} \bar{W}_k^2 \Lambda. \tag{3.46}
\end{aligned}$$

Our results are quite similar to those in Ref. 13. This is as expected, because of similarities in the structure of basic equations. It is shown there that analytic results agree well with nonlinear multiple-helicity simulations. It is interesting to note that in the nonlinearly saturated state, $\Delta_{\Pi} > \Delta_{\Phi}$, which is a consequence of the direct dependence of the vorticity on the convecting $E \times B$ velocity ($D^{xx} > \mu^{xx}$). Also, because Λ is only weakly dependent of plasma parameters, nonlinear results have the same parameter dependences as the mixing-length results, but show considerable enhancement in the magnitude.

3.5 Electron Heat Transport

In this section, we evaluate electron heat diffusivity due to stochastic magnetic fields⁷ in saturated NPGDT. Magnetic fluctuations in NPGDT are coupled to electrostatic modes through the parallel Ohm's law.

From the electron drift kinetic equation⁴⁵ with magnetic flutter nonlinearity, one can calculate χ_e yielding:

$$\chi_e = \sum_{\mathbf{k}} v_{\parallel}^2 |\tilde{b}_{r,\mathbf{k}}|^2 \text{Re} \left[i \left(\omega - \omega_D - k_{\parallel} v_{\parallel} + \frac{i}{\tau_{ck}} \right)^{-1} \right]. \quad (3.47)$$

Here, χ_e is electron heat diffusivity, ω is the mode frequency, ω_D is the drift frequency, $\tilde{b}_{r,\mathbf{k}} = \tilde{B}_{r,\mathbf{k}}/B_0$, and τ_{ck} is the nonlinear decorrelation time, representing the nonlinear interaction term. Also, $\text{Re}[(\dots)]$ denotes the real part of (\dots) . In the quasilinear approximation, where $1/\tau_{ck}$ is neglected, Eq. (3.47) reduces to the χ_e of Ref. 7. In the more relevant so-called *strong turbulence* regime, where nonlinear mode couplings become dominant, we can approximate Eq. (3.47) to yield

$$\chi_e = \sum_{\mathbf{k}} v_{\parallel}^2 |\tilde{b}_{r,\mathbf{k}}|^2 \tau_{ck}. \quad (3.48)$$

To find $\tilde{b}_{r,\mathbf{k}}$, we use the neoclassical Ohm's law and Ampere's law;

$$\tilde{b}_{r,\mathbf{k}} = \frac{\mathbf{b} \times \hat{\mathbf{r}}}{B} \cdot \nabla \tilde{\psi}_{\mathbf{k}}, \quad (3.49)$$

where,

$$\tilde{\psi}_{\mathbf{k}} = \frac{4\pi}{c\eta} \nabla_{\perp}^{-2} \nabla_{\parallel} \Phi_{\mathbf{k}} + \frac{4\pi}{B_{\theta}} \delta_e \nabla_{\perp}^{-2} \frac{d}{dr} \Pi_{\mathbf{k}}. \quad (3.50)$$

By Fourier transforming, we can approximate $\tau_{\mathbf{ck}}$ by

$$\tau_{\mathbf{ck}}^{-1} = \chi_e \bar{u}^2, \quad (3.51)$$

where

$$\bar{u} \equiv \left(\frac{\sum_{\mathbf{k}} u^2 |\tilde{\psi}_{\mathbf{k}}|^2}{\sum_{\mathbf{k}} |\tilde{\psi}_{\mathbf{k}}|^2} \right)^{1/2}. \quad (3.52)$$

To evaluate \bar{u}^2 , we note that

$$\sum_{\mathbf{k}} = \int dm' \left| \frac{m' q'}{q^2} \right| \int dx' = \frac{Rr}{L_s} \int dk_{\theta} |k_{\theta}| \int dx, \quad (3.53)$$

where R is the major radius of the tokamak. By assuming that nonlinear interactions change the radial correlation lengths without significant deformation of the linear eigenfunctions, we can write

$$\begin{aligned} \Phi(u) &= \Delta_{\Phi} \left[C_{\Phi} \bar{\Phi}^2 S_{\Phi}(k_{\theta}) \right]^{1/2} \exp\left(-\frac{1}{2} \Delta_{\Phi}^2 u^2\right), \\ \Pi(u) &= i \Delta_{\Pi} \left[C_{\Pi} \bar{\Pi}^2 S_{\Pi}(k_{\theta}) \right]^{1/2} \exp\left(-\frac{1}{2} \Delta_{\Pi}^2 u^2\right). \end{aligned} \quad (3.54)$$

Here, S_{Φ} and S_{Π} represent k_{θ} -spectrum of Φ and Π , respectively. Also, C_{Φ} and C_{Π} satisfy spectrum-averaged fluctuation level normalization conditions,

$$\begin{aligned} \sum_{\mathbf{k}} |\Phi_{\mathbf{k}}|^2 &= \bar{\Phi}^2, \\ \sum_{\mathbf{k}} |\Pi_{\mathbf{k}}|^2 &= \bar{\Pi}^2, \end{aligned}$$

to yield

$$\begin{aligned} C_{\Phi} &= \left[\pi^{1/2} r R \int dk_{\theta} \frac{|k_{\theta}|}{L_s} S_{\Phi}(k_{\theta}) \Delta_{\Phi} \right]^{-1}, \\ C_{\Pi} &= \left[\pi^{1/2} r R \int dk_{\theta} \frac{|k_{\theta}|}{L_s} S_{\Pi}(k_{\theta}) \Delta_{\Pi} \right]^{-1}. \end{aligned} \quad (3.55)$$

From Eqs. (3.50), (3.53)-(3.55), we obtain

$$\bar{u}^2 = \frac{I_1}{I_2}. \quad (3.56)$$

Here,

$$\begin{aligned} I_1 &= \left(\frac{4\pi}{c\eta L_s} \right)^2 C_{\Phi} \bar{\Phi}^2 \frac{Rr}{L_s} \int dk_{\theta} |k_{\theta}|^3 S_{\Phi}(k_{\theta}) \Delta_{\Phi}^5 I_1^{\Phi\Phi} \\ &+ \left(\frac{4\pi}{B_{\theta}} \delta_e \right)^2 C_{\Pi} \bar{\Pi}^2 \frac{Rr}{L_s} \int dk_{\theta} |k_{\theta}| S_{\Pi}(k_{\theta}) \Delta_{\Pi} I_1^{\Pi\Pi} \\ &- 2(4\pi)^2 \delta_e \frac{(C_{\Phi} C_{\Pi})^{1/2} \bar{\Phi} \bar{\Pi}}{cB_{\theta} \eta L_s} \frac{Rr}{L_s} \int dk_{\theta} |k_{\theta}|^2 S_{\Phi}^{1/2} S_{\Pi}^{1/2} \Delta_{\Phi}^3 \Delta_{\Pi} I_1^{\Phi\Pi}, \quad (57) \\ I_2 &= \left(\frac{4\pi}{c\eta L_s} \right)^2 C_{\Phi} \bar{\Phi}^2 \frac{Rr}{L_s} \int dk_{\theta} |k_{\theta}|^3 S_{\Phi}(k_{\theta}) \Delta_{\Phi}^7 I_2^{\Phi\Phi} \\ &+ \left(\frac{4\pi}{B_{\theta}} \delta_e \right)^2 C_{\Pi} \bar{\Pi}^2 \frac{Rr}{L_s} \int dk_{\theta} |k_{\theta}| S_{\Pi}(k_{\theta}) \Delta_{\Pi}^3 I_2^{\Pi\Pi} \\ &- 2(4\pi)^2 \delta_e \frac{(C_{\Phi} C_{\Pi})^{1/2} \bar{\Phi} \bar{\Pi}}{cB_{\theta} \eta L_s} \frac{Rr}{L_s} \int dk_{\theta} |k_{\theta}|^2 S_{\Phi}^{1/2} S_{\Pi}^{1/2} \Delta_{\Phi}^3 \Delta_{\Pi}^2 I_2^{\Phi\Pi}, \quad (3.58) \end{aligned}$$

where

$$\begin{aligned} I_1^{\Phi\Phi} &= \int_{-\infty}^{+\infty} d\alpha \frac{\alpha^4 e^{-\alpha^2}}{(\alpha^2 + k_{\theta}^2 \Delta_{\Phi}^2)^2}, \\ I_1^{\Pi\Pi} &= \int_{-\infty}^{+\infty} d\alpha \frac{\alpha^4 e^{-\alpha^2}}{(\alpha + k_{\theta}^2 \Delta_{\Pi}^2)^2}, \end{aligned}$$

$$\begin{aligned}
I_1^{\Phi\Pi} &= \int_{-\infty}^{+\infty} d\alpha \frac{\alpha^4 \exp[-\alpha^2 (1 + \Delta_\Phi^2/\Delta_\Pi^2)/2]}{(\alpha^2 + k_\theta^2 \Delta_\Pi^2)^2}, \\
I_2^{\Phi\Phi} &= \int_{-\infty}^{+\infty} d\alpha \frac{\alpha^2 e^{-\alpha^2}}{(\alpha^2 + k_\theta^2 \Delta_\Phi^2)^2}, \\
I_2^{\Pi\Pi} &= \int_{-\infty}^{+\infty} d\alpha \frac{\alpha^2 e^{-\alpha^2}}{(\alpha^2 + k_\theta^2 \Delta_\Pi^2)^2}, \\
I_2^{\Phi\Pi} &= \int_{-\infty}^{+\infty} d\alpha \frac{\alpha^2 \exp[-\alpha^2 (1 + \Delta_\Phi^2/\Delta_\Pi^2)/2]}{(\alpha^2 + k_\theta^2 \Delta_\Pi^2)^2}.
\end{aligned} \tag{3.59}$$

These integrals can be evaluated analytically, yielding:

$$\begin{aligned}
\int_{-\infty}^{+\infty} d\alpha \frac{\alpha^4 e^{-\mu^2 \alpha^2}}{(\alpha^2 + \nu^2)^2} &= \frac{\sqrt{\pi}}{\mu} (1 + \mu^2 \nu^2) - \frac{\pi}{2} \nu (3 + 2\mu^2 \nu^2) e^{\mu^2 \nu^2} [1 - \text{Erf}(\mu\nu)], \\
\int_{-\infty}^{+\infty} d\alpha \frac{\alpha^2 e^{-\mu^2 \alpha^2}}{(\alpha^2 + \nu^2)^2} &= \frac{\pi}{2\nu} (1 + 2\mu^2 \nu^2) e^{\mu^2 \nu^2} [1 - \text{Erf}(\mu\nu)] - \mu\sqrt{\pi},
\end{aligned}$$

where $\text{Erf}(\mu\nu)$ is an error function,

$$\text{Erf}(\mu\nu) = \frac{2\nu}{\sqrt{\pi}} \int_0^\mu d\alpha e^{-\nu^2 \alpha^2}.$$

In the limit where low- m modes are dominant, we obtain

$$\begin{aligned}
I_1 &= \left(\frac{4\pi \bar{k}_\theta}{c\eta L_s} \right)^2 \bar{\Delta}_\Phi^4 \bar{\Phi}^2 + \left(\frac{4\pi}{B_\theta} \delta_e \right)^2 \bar{\Pi}^2 \\
&\quad - 2 \frac{(4\pi)^2 \bar{k}_\theta}{cB_\theta \eta L_s} (\bar{\Delta}_\Phi^5 \bar{\Delta}_\Pi^{-1})^{1/2} \bar{\Phi} \bar{\Pi}^2 \left[2 \left(1 + \frac{\bar{\Delta}_\Phi^2}{\bar{\Delta}_\Pi^2} \right)^{-1} \right]^{1/2}, \\
I_2 &= \frac{8\pi^{5/2}}{c^2 \bar{k}_\theta} \left[\frac{\bar{k}_\theta}{\eta L_s} \bar{\Delta}_\Phi^{-5/2} \bar{\Phi} - \frac{c}{B_\theta} \delta_e \bar{\Delta}_\Pi^{-1/2} \bar{\Pi} \right]^2.
\end{aligned} \tag{3.60}$$

A simple mixing length would suggest²⁶ $\bar{u}^2 \sim \bar{W}_k^{-2}$. This approximation would be relevant if NPGDT has a tearing parity or if magnetic fluctuations have Gaussian structure. However, NPGDT has a twisting parity, or negligible magnetic

fluctuations near $x = 0$. By using the turbulence level determined in Sec. 3.4, we find $\bar{u}^2 \sim \bar{k}_\theta / \bar{W}_k$, when Λ is large. Therefore, the radial structure of magnetic fluctuations plays an important role when we apply the mixing length principle.

By substituting Eqs. (3.49)-(3.53), and (3.56) into Eq. (3.48), we obtain

$$\begin{aligned} \chi_e^2 &= v_{\parallel}^2 \bar{u}^2 \sum_{\mathbf{k}} \left| i \frac{4\pi}{Bc\eta L_s} \frac{k_\theta^2}{(u^2 + k_\theta^2)} \frac{d}{du} \Phi(u) + \frac{4\pi}{BB_\theta} \delta_e \frac{uk_\theta}{(u^2 + k_\theta^2)} \Pi(u) \right|^2 \\ &= \left(\frac{v_{\parallel} \bar{k}_\theta}{B} \right)^2 \frac{(I_2)^2}{I_1}. \end{aligned} \quad (3.61)$$

During the linearly growing stage, χ_e due to magnetic fluctuations is negligible because contributions from Φ and Π fluctuations are almost equal in magnitude but opposite in sign (i.e., $I_2 \simeq 0$). However, in the nonlinearly saturated state, the contribution from the bootstrap current becomes dominant over that from the inductive current because of different power dependences on Λ . When Λ is large, χ_e can thus be written as

$$\chi_e = 4.6 \times 10^{-2} |v_{\parallel}| L_s \left(\frac{\epsilon}{q\beta_p} \right)^{4/3} \delta_e^{5/3} \left(\frac{r}{\bar{k}_\theta L_P^2} \right)^{2/3} S_M^{-2/3} \Lambda^{7/3}. \quad (3.62)$$

Parameter scalings of χ_e are

$$\chi_e \sim \hat{s}^{-1} S_M^{-2/3} \beta^{4/3} L_P^{-4/3} T_e^{1/2}. \quad (3.63)$$

It is interesting to compare these results with those of Ref. 26. There, the mixing length theory is used, thereby neglecting the contribution from integrals

due to the radial structure of magnetic fluctuations. If the same approximation is applied to NPGDT, one finds that the scaling of χ_e would be

$$\chi_e \sim \hat{s}^{-3/2} S_M^{-1} \beta^{3/2} L_P^{-3/2} T_e^{1/2}.$$

Hence, both quantitative and qualitative differences are apparent. Note that because of the similarity in the structure of NPGDT and resistive-interchange modes,¹³ the same procedure can be applied to resistive-interchange modes. Recent study⁶⁸ of the electron heat transport due to resistive-interchange modes reached conclusions similar to the present study.

Finally, the magnitudes of the radial and the poloidal magnetic fluctuation levels are given by

$$\begin{aligned} \frac{\overline{\tilde{B}_r}}{B} &= 0.11 \left(\frac{\epsilon}{q} \beta_p \right)^{5/6} \delta_e^{3/2} \left(\frac{r^2 L_s^3}{L_P^5} \right)^{1/4} S_M^{-1/2} \Lambda^{7/4}, \\ \frac{\overline{\tilde{B}_\theta}}{B} &= 9.6 \times 10^{-2} \left(\frac{\epsilon}{q} \beta_p \right)^{7/6} \delta_e^{4/3} \left(\frac{r^2 L_s^3}{\bar{k}_\theta^2 L_P^7} \right)^{1/6} S_M^{-1/3} \Lambda^{7/6}. \end{aligned}$$

Thus, magnetic fluctuation levels and associated electron thermal conduction are enhanced by increasing β_p and a sharper pressure gradient, but are suppressed by strong shear.

3.6 Summary

From neoclassical resistive MHD equations³⁹ including hot, trapped particle effects, we have identified various branches of instability: stable resistive-interchange modes,¹³ which are due to the average unfavorable curvature in the absence of neoclassical effects; energetic trapped-particle-driven resistive-interchange modes,⁶⁷ destabilized when there is a sufficient population of hot trapped particles; and neoclassical pressure-gradient-driven modes^{42,43} (bootstrap current modes), which become important when neoclassical effects are dominant. The linear study of NPGDT shows that small scale bootstrap current modes are stabilized.

Nonlinear saturation of NPGDT is achieved via nonlinear coupling of unstable, long-wavelength modes to stable, short-wavelength modes, thus balancing the linear free energy source with its ultimate sink, the viscosity and χ_{\perp} . Renormalized equations are obtained. The turbulence level is determined from nonlinear steady state condition. The principal results are as follows:

- (i) The pressure diffusivity is obtained as an eigenvalue of renormalized equations at saturation, yielding:

$$D_p = \frac{1}{8\pi} \frac{\epsilon}{q} \beta_p c^2 \eta \delta_e \frac{L_s}{L_P} \Lambda^2.$$

This value is larger than the mixing length estimate of D_P by a factor

of Λ^2 (Λ is always greater than 1; see Eq. (3.40)).

- (ii) At saturation, the radial scale of pressure fluctuations differ from that of electrostatic potential fluctuations, i.e.,

$$\Delta_{\Pi} = \sqrt{2} \left(\frac{\epsilon}{q} \beta_p \right)^{1/6} \left(\frac{1}{16\pi} \frac{\delta_e r}{k_{\theta} L_P^2} \right)^{1/3} S_M^{-1/3} (L_s L_P)^{1/2} \Lambda^{7/6},$$

$$\Delta_{\Phi} = \sqrt{2} \left(\frac{\epsilon}{q} \beta_p \right)^{1/6} \left(\frac{1}{16\pi} \frac{\delta_e r}{k_{\theta} L_P^2} \right)^{1/3} S_M^{-1/3} (L_s L_P)^{1/2} \Lambda^{1/6}.$$

- (iii) The levels of turbulence are determined from the diffusivities, i.e.:

$$\frac{e\tilde{\phi}}{T_e} = \sqrt{2} \left(\frac{\delta_e}{16\pi} \right)^{2/3} \left(\frac{\epsilon}{q} \beta_p \right)^{5/6} \left(\frac{r^5 \bar{k}_{\theta}}{L_P} \right)^{1/3} S_M^{-2/3} \frac{(L_s L_P)^{1/2}}{\rho_s} \frac{\tau_A}{\bar{k}_{\theta} c_s} \Lambda^{5/6},$$

$$\frac{\tilde{P}}{P} = \sqrt{2} \left(\frac{\epsilon}{q} \beta_p \right)^{1/6} \left(\frac{\delta_e r}{16\pi \bar{k}_{\theta} L_P^2} \right)^{1/3} \left(\frac{L_s}{L_P} \right)^{1/2} S_M^{-1/3} \Lambda^{7/6}.$$

- (iv) Electron heat transport due to stochastic magnetic fields induced by NPGDT has been estimated. The radial structure of magnetic fluctuations has been taken into account, yielding:

$$\chi_e = 4.6 \times 10^{-2} |v_{\parallel}| L_s \left(\frac{r}{\bar{k}_{\theta} L_P^2} \right)^{2/3} S_M^{-2/3} \Lambda^{7/3}.$$

- (v) Magnetic fluctuation levels are also determined:

$$\frac{\tilde{B}_r}{B} = 0.11 \left(\frac{\epsilon}{q} \beta_p \right)^{5/6} \delta_e^{3/2} \left(\frac{r^2 L_s^3}{L_P^5} \right)^{1/4} S_M^{-1/2} \Lambda^{7/4},$$

$$\frac{\tilde{B}_{\theta}}{B} = 9.6 \times 10^{-2} \left(\frac{\epsilon}{q} \beta_p \right)^{7/6} \delta_e^{4/3} \left(\frac{r^2 L_s^3}{\bar{k}_{\theta}^2 L_P^7} \right)^{1/6} S_M^{-1/3} \Lambda^{7/6}.$$

We note that while the resistive MHD turbulence¹² is relevant only in the cold edge of the plasma, the region where NPGDT can be applied is

extended over wide zone between the center and the edge of the plasma. Also, as the pressure is increased with additional heating, NPGDT becomes aggravated. Therefore, NPGDT may have some bearings on confinement degradation during the L-mode.¹ Furthermore, since NPGDT shows similar behavior⁵⁹ to resistive turbulence under the influence of strong shear, it can be suppressed at the edge of an H-mode discharge,⁵² thus providing improved confinement behavior.

So far, we have investigated the turbulence evolving from instabilities with the twisting parity. Neoclassical tearing instabilities driven by current density gradient will be studied in Appendix B.

CHAPTER IV
THEORY OF NEOCLASSICAL
RESISTIVITY-GRADIENT-DRIVEN TURBULENCE

4.1 Introduction

Resistivity-gradient-driven turbulence²⁸ (RGDT) has been successful in explaining many characteristics³⁵ of tokamak edge plasmas: large fluctuation levels, radially increasing large diffusivities, and the breakdown of Boltzmann relation. Consideration of impurity density fluctuation dynamics^{32,33} and radiation effects³⁴ has made RGDT an even more realistic tokamak edge turbulence model. Recently, it has been argued²⁹ that these attractive features are ill-founded from the conventional standpoint of linear stability. Indeed, RGDT evolves from unstable rippling modes,^{12,30,31} and detailed linear analyses²⁹ indicate that the linear rippling modes tend to be quenched at moderate temperature due to stabilizing effects of large parallel thermal conduction and finite electron diamagnetism. However, both theoretical and computational analyses^{28,33} have demonstrated that the nonlinear evolution of RGDT is characterized by the nonlinear broadening of an asymmetric mode structure, so that the resistivity and potential fluctuations move away from the rational surface and decouple from

the current perturbation. This current decoupling drastically modifies the usual linear structure¹² of the perturbations, and renders the stabilizing influence of field line bending ineffective. Therefore, RGDT is nonlinearly robust. It is also crucial to note that the tokamak edge is rarely quiescent,³⁵ due to the presence of impurities, plasma-wall interaction, etc.. Therefore, the conventional picture of linear instability developing from a quiescent plasma at equilibrium is not necessarily appropriate. Hence, the tokamak edge fluctuations can only be understood by nonlinear theory. All afore-mentioned RGDT models^{28,33,34} are based on a reduced, resistive MHD description³⁸ of a plasma, and consists of Ohm's law and the vorticity and resistivity evolutions. However, this model is valid only in the Pfirsch-Schlüter collisionality regime.³⁷

Recently, neoclassical MHD equations³⁹ have been derived which are valid in the experimentally relevant banana-plateau collisionality regimes. The most significant modification in RGDT due to neoclassical effects is that the neoclassical resistivity^{2,39} is now a function of the density as well as the temperature, while the classical Spitzer resistivity³⁶ depends on the temperature only. Therefore, rippling modes²⁸⁻³³ can couple to the density gradient, and the density fluctuation dynamics becomes significant in determining the evolution of neoclassical rippling modes. Main purpose of this chapter is to investigate

neoclassical resistivity-gradient-driven turbulence (NRGDT) evolving from neoclassical rippling modes, to incorporate density fluctuation dynamics, and to extend the validity regime of RGDT further into high temperature, low collisionality regimes of tokamaks. The resulting particle diffusivity increases as temperature decreases, allowing a possibility of explaining the radially increasing profile of particle diffusivity from experimental measurements.^{35,46} We note that drift wave instabilities⁶⁷ are unable to account for this experimental result.

Linear stability analysis shows that without neoclassical coupling to the density gradient, the large parallel thermal conduction has a strong stabilizing effect for small scale modes, and that the growth rate decreases with the poloidal mode number, m , for large m . In a small- m limit, parallel conduction is less efficient, and the growth rate increases with m . Therefore, conventional rippling modes are most unstable (linearly) for moderate m -values. When the density gradient is included, the equilibration of density fluctuations along flux surfaces is affected by parallel stress tensor effects (due to collisions between trapped and untrapped particles). This has a much weaker stabilizing effect than thermal conduction. Therefore, the unstable region extends both in distance from the edge (i.e., into regions of higher temperature) and in m -values.

The radial asymmetry in the mode structure develops further during

the nonlinear evolution, resulting in negligible current fluctuation in the region of interest. This leads to the decoupling of the vorticity evolution equation from the other basic equations, so that the system consists of Ohm's law and the temperature and density evolution equations. Nonlinear saturation is attained when parallel dissipations, enhanced by nonlinear mode broadening, balance linear instability sources. The mode broadening results from nonlinear mode couplings mediated via $E \times B$ convection. Convective nonlinearity is renormalized to yield spectrum-dependent turbulent diffusivities. The turbulent temperature and density diffusivities are obtained as eigenvalues of the stationary renormalized eigenmode equations at saturation. Their values are much larger than naive mixing length estimates, based upon linear growth rates and mode widths. The dominant effect of the inclusion of the density dynamics is the considerable increase in the level of turbulence, in comparison to the case with only the temperature gradient.

Levels of electrostatic potential, temperature, and density fluctuations are determined. The level of density fluctuation is higher than that of temperature fluctuation as a consequence of larger radial scale-length of density fluctuation, and is different from the level of electrostatic fluctuation. The magnetic fluctuation level is shown to be too low to induce any significant heat

transport along perturbed magnetic field lines.

The remainder of this chapter is organized as follows: In Sec. 4.2, the theoretical model for NRGDT is presented. The structure of the neoclassical resistivity is investigated in detail. In Sec. 4.3, the linear stability results are presented. In Sec. 4.4, the nonlinear saturation mechanism is identified and the level of turbulence is determined. A discussion of the theory in the context of edge localized modes (ELMs) in DIII-D H-mode⁷⁰ plasmas is also presented. Finally, Sec. 4.5 contains a summary and conclusions.

4.2 Neoclassical Resistivity-Gradient-Driven Turbulence Model

In this section, we present the basic neoclassical resistivity-gradient-driven model which is derived from the simplified neoclassical MHD equations.³⁹ The simplification is due to the omission of perpendicular flow. The neoclassical correction^{2,39} to the Spitzer resistivity is most relevant to the evolution of NRGDT, and is discussed in detail.

The simplified neoclassical Ohm's law in the electrostatic approximation can be written as:

$$\tilde{E}_{\parallel} = -\nabla_{\parallel}\tilde{\phi} = \eta_{\text{nc}}\tilde{J}_{\parallel} + \tilde{\eta}_{\text{nc}}J_{\parallel} - \frac{1}{e}\nabla_{\parallel}\left(T_e\frac{\tilde{n}}{n_0} + \tilde{T}_e\right). \quad (4.1)$$

Here, E_{\parallel} is the parallel electric field, ϕ is the electrostatic potential, J_{\parallel} is the parallel current, T_e is the electron temperature, and n_0 is the density. Also, (\dots) denotes the perturbed quantity and the η_{nc} is the neoclassical resistivity, the expression for which will be given later. The origin of Eq. (4.1) can be easily seen by considering the electron momentum balance equation,

$$m_e\frac{dv_{\parallel}}{dt} = -eE_{\parallel} - \frac{1}{n_0}\mathbf{b}\cdot\nabla P_e + \frac{1}{n_0}\mathbf{b}\cdot\nabla\cdot\Pi_{\parallel e} + e\eta_{\text{sp}}J_{\parallel}. \quad (4.2)$$

Here, P_e is the electron pressure, m_e is the electron mass, Π_{\parallel} is the parallel stress tensor, and $\mathbf{b} = \mathbf{B}/B$. Also, the Spitzer resistivity,³⁶ η_{sp} is given by

$$\eta_{\text{sp}} = K_{\parallel}\frac{m_e}{n_0e^2}\nu_e,$$

where $K_{\parallel} \simeq 0.51$ for $Z_{\text{eff}} = 1$ plasma, and the electron collision rate, ν_e , is

$$\nu_e = \frac{4}{3} \sqrt{2\pi} \frac{n_0 e^4}{m_e^{1/2} T_e^{3/2}} \ln \Lambda.$$

The parallel viscous drag due to collisions with trapped particles is given approximately by:

$$\mathbf{b} \cdot \nabla \cdot \Pi_{\parallel e} \simeq m_e n_0 \mu_e v_{\parallel}. \quad (4.3)$$

Here,

$$\mu_e \simeq \frac{2.3 \epsilon^{1/2} \nu_e}{1 + 1.02 \nu_{*e}^{1/2} + 1.07 \nu_{*e}}, \quad (4.4)$$

where ϵ is the inverse aspect ratio, $\nu_{*e} = \nu_e / \omega_{be} \epsilon^{3/2}$; $\omega_{be} = v_{th,e} / R_0 q$, R_0 is the major radius, and q is the safety factor. The poloidal component of the first order electron perpendicular flow, leading to the bootstrap current^{2,39} is omitted for simplicity. From Eqs. (4.2) and (4.3), Ohm's law becomes

$$E_{\parallel} = \eta_{\text{sp}} \left(1 + \frac{4.51 \epsilon^{1/2}}{1 + 1.02 \nu_{*e}^{1/2} + 1.07 \nu_{*e}} \right) J_{\parallel} - \frac{1}{en_0} \mathbf{b} \cdot \nabla P_e. \quad (4.5)$$

Thus, the neoclassical resistivity^{2,39} can be written as

$$\eta_{\text{nc}} = \eta_{\text{sp}} \left(1 + \frac{4.51 \epsilon^{1/2}}{1 + 1.02 \nu_{*e}^{1/2} + 1.07 \nu_{*e}} \right).$$

Note that η_{nc} now depends on the density as well, through the density dependence of ν_{*e} , while the Spitzer resistivity is a function of T_e only, i.e.,

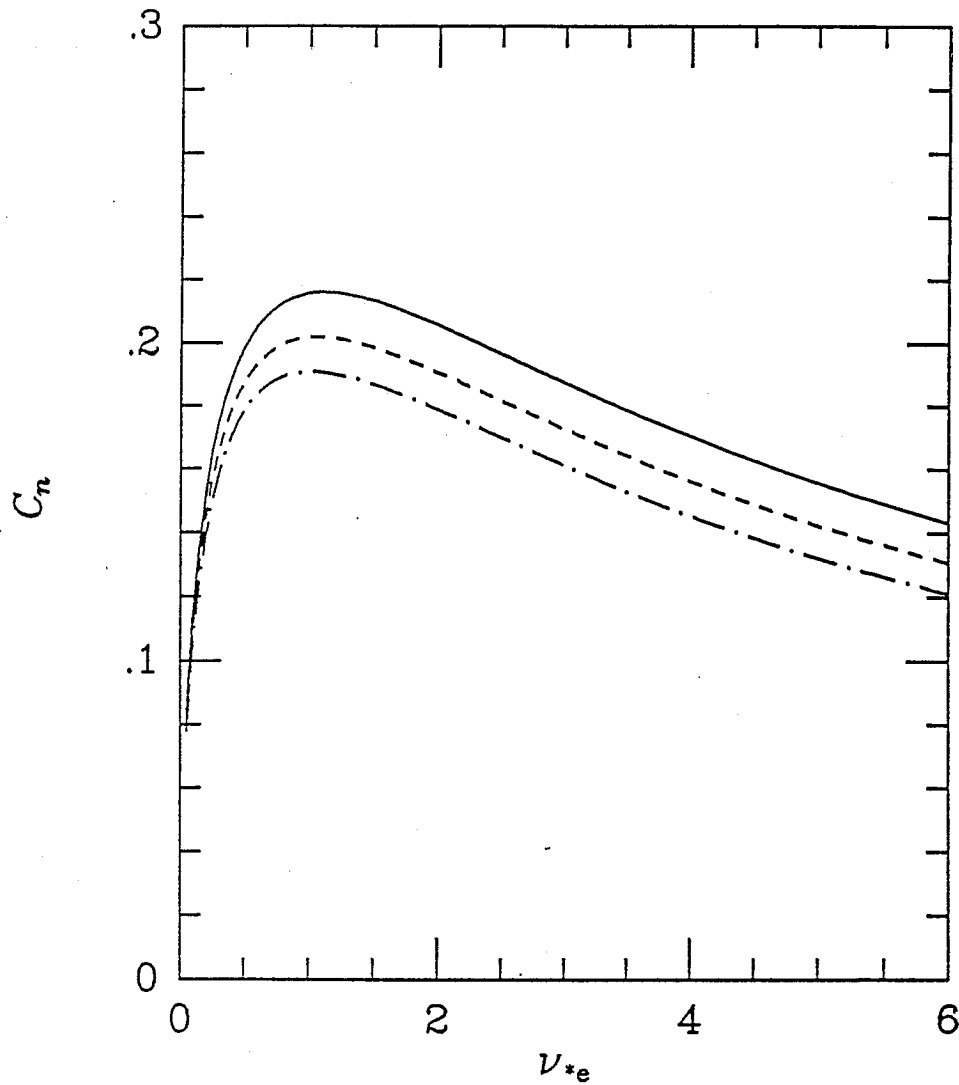


FIG. 4.1 Plot of the density coupling coefficient to the neoclassical resistivity ($C_n = -\partial \ln \eta_{nc} / \partial \ln n_e$), in terms of ν_{*e} for (i) $\epsilon=1/4$ (solid line), (ii) $\epsilon=1/5$ (dashed line), and (iii) $\epsilon=1/6$ (dash-dotted line).

$\eta_{sp} \propto T_e^{-3/2}$. Therefore, in the neoclassical theory, resistivity-gradient-driven turbulence²⁸ is modified by, and depends on density fluctuation dynamics as well as temperature fluctuation dynamics. Exploring the consequence of this novel feature is the motivation of the present work.

The structure of the neoclassical resistivity fluctuation can be written as

$$\frac{\tilde{\eta}_{nc}}{\eta_{nc}} = -C_t \frac{\tilde{T}_e}{T_e} - C_n \frac{\tilde{n}}{n_0}, \quad (4.6)$$

where

$$C_n = -\frac{\partial \ln \eta_{nc}}{\partial \ln n_0} = \frac{4.51\epsilon^{1/2}(0.51\nu_{*e}^{1/2} + 1.07\nu_{*e})}{(1 + 1.02\nu_{*e}^{1/2} + 1.07\nu_{*e})^2} \left(1 + \frac{4.51\epsilon^{1/2}}{1 + 1.02\nu_{*e}^{1/2} + 1.07\nu_{*e}} \right)^{-1}, \quad (4.7)$$

$$C_t = -\frac{\partial \ln \eta_{nc}}{\partial \ln T_e} = \frac{3}{2} - 2C_n. \quad (4.8)$$

Since C_n vanishes in both limits ($\nu_{*e} \rightarrow 0$ and $\nu_{*e} \rightarrow \infty$), the density gradient effect on rippling modes also vanishes for values of ν_{*e} far from the unity. For moderate values of ϵ , C_n has a maximum value of about 0.2 around $\nu_{*e} \sim 1$ and decreases slowly as ν_{*e} increases, as seen in Fig. 4.1. Also, note that C_n and C_t are always positive.

The vorticity evolution equation can be derived from the charge neutrality condition:

$$\rho \frac{d}{dt} \nabla_{\perp}^2 \tilde{\phi} = \frac{B^2}{c^2} \nabla_{\parallel} \tilde{J}_{\parallel}, \quad (4.9)$$

where ρ is the mass density. We have neglected the neoclassical enhancement of the inertia (arising from an additional polarization drift) and the neoclassical cross viscosity^{39,42} (arising from an anisotropy in the perturbed pressure) in Eq. (4.9). The neoclassical cross viscosity, along with the bootstrap current which is also neglected in Eq. (4.1), act as destabilizing sources for the neoclassical pressure-gradient-driven instabilities.^{42,43} The neoclassical enhancement of the inertia as well as the ion diamagnetism acts to reduce the growth rate. However, in lowest order, these are irrelevant to the evolution of NRGDT due to current decoupling. The heating due to the bootstrap current is also neglected for simplicity.

The density equation is determined from the continuity equation:

$$\frac{d\tilde{n}}{dt} = -\frac{c}{B} \mathbf{b} \times \nabla \tilde{\phi} \cdot \nabla n_0 + \frac{1}{e} \nabla_{\parallel} \tilde{J}_{\parallel} - n_0 \nabla_{\parallel} \tilde{u}_{\parallel}. \quad (4.10)$$

The center-of-mass velocity \tilde{u}_{\parallel} evolves as

$$\frac{d\tilde{u}_{\parallel}}{dt} = -\frac{c_s^2}{n_0} \nabla_{\parallel} \tilde{n} - \frac{1}{M} \nabla_{\parallel} \tilde{T}_e - \mu_i \tilde{u}_{\parallel}. \quad (4.11)$$

Here, ion temperature fluctuations are neglected, M is the ion mass,

$$c_s^2 = \frac{1}{M}(T_e + T_i),$$

$$\mu_i = \frac{0.66\epsilon^{1/2}\nu_i}{1 + 1.03\nu_{*i}^{1/2} + 0.31\nu_{*i}},$$

where ν_i is the ion collision rate and $\nu_{*i} = \nu_{*e \rightarrow i}$. The term involving μ_i comes from the ion neoclassical parallel viscous force due to collisions with trapped ions. The first-order ion perpendicular flow component has been omitted, consistently with previous simplifications. In the regime where modes grow slower than the effective neoclassical collision time ($d/dt \ll \mu_i$), Eq. (4.10) simplifies to:

$$\frac{d\tilde{n}}{dt} - \chi_n \nabla_{\parallel}^2 \tilde{n} - \frac{n_0}{\mu_i M} \nabla_{\parallel}^2 \tilde{T}_e = -\frac{c}{B} \mathbf{b} \times \nabla \tilde{\phi} \cdot \nabla n_0 + \frac{1}{e} \nabla_{\parallel} \tilde{J}_{\parallel}, \quad (4.12)$$

where $\chi_n = c_s^2/\mu_i$. Note that χ_n , combined with the shear, cuts off sound wave propagation. Also, note that up to additional couplings to \tilde{T}_e and \tilde{J}_{\parallel} dynamics, density fluctuation dynamics is similar to impurity fluctuation dynamics,^{32,33} with neoclassical viscosity replacing effective parallel diffusion χ_z . Therefore, results structurally similar to those of Ref. 33 are expected.

The temperature evolution equation is

$$\frac{d\tilde{T}_e}{dt} - \chi_{\parallel} \nabla_{\parallel}^2 \tilde{T}_e = -\frac{c}{B} \mathbf{b} \times \nabla \tilde{\phi} \cdot \nabla T_e, \quad (4.13)$$

where χ_{\parallel} is the parallel electron thermal conductivity. The large value of χ_{\parallel} tends to localize classical rippling modes around the mode rational surface, and

thus has a strong stabilizing effect. We have neglected impurity radiation cooling effects,³⁴ for simplicity.

Equations (4.1), (4.9), (4.12), and (4.13) constitute the basic NRGDT model to be studied analytically.

4.3 Linear Theory

We study the linear instability described by the basic NRGDT model by Fourier analyzing perturbations as:

$$\tilde{\phi} = \sum_{m,n} \Phi_{mn}(x) \exp[i(m\theta - n\frac{z}{R}) + \gamma t],$$

where m and n are poloidal and toroidal mode numbers, respectively, R is the major radius, z is the coordinate along the major axis, and $x = r - r_s$ is the distance from the singular surface, r_s , at which $q(r_s) = m/n$. Then, the eigenmode equation becomes

$$\begin{aligned} \frac{d^2}{dX^2} \Phi - \left[\frac{1}{4} X^2 - \frac{\delta_t X}{1 + b_t X^2} - \frac{\delta_n X}{1 + b_n X^2} \left(1 - \frac{d_t X^2}{1 + b_t X^2} \right) \right] \Phi \\ - i \left[\frac{\alpha_t X^2}{1 + b_t X^2} + \frac{\alpha_n X^2}{1 + b_n X^2} \left(1 - \frac{d_t X^2}{1 + b_t X^2} \right) \right] \Phi = 0. \end{aligned} \quad (14)$$

Here,

$$X = x/x_R,$$

$$x_R^4 = \frac{1}{4} \eta_{nc} \gamma \rho \left(\frac{cL_s}{Bk_\theta} \right)^2,$$

$$\delta_t = \frac{cC_t E_{\parallel} L_s}{4B\gamma L_t x_R},$$

$$b_t = \frac{\chi_{\parallel}}{\gamma} \left(\frac{k_\theta x_R}{L_s} \right)^2,$$

$$\delta_n = \frac{C_n \delta_t}{C_t \eta_e},$$

$$d_t = \frac{\eta_e T_e}{\gamma \mu_i M} \left(\frac{k_\theta x_R}{L_s} \right)^2,$$

$$b_n = \frac{\chi_n}{\gamma} \left(\frac{k_\theta x_R}{L_s} \right)^2,$$

$$\alpha_t = \frac{T_e c k_\theta}{4 L_t e \gamma B},$$

$$\alpha_n = \alpha_t / \eta_e.$$

We have used $\nabla_\perp^2 \simeq d^2/dx^2 \gg k_\theta^2$, $\nabla_\theta = ik_\theta = im/r_s$, and $\nabla_\parallel = ik_\parallel = -ik_\theta x/L_s$. Also, $L_s = Rq^2/rq'$ is the shear length, $L_t = -[d \ln T_e/dr]^{-1}$ is the temperature scale length, $L_n = -[d \ln n_0/dr]^{-1}$ is the density scale length, and $\eta_e = L_n/L_t$. The first term in Eq. (4.14) represents the inertia and the second represents field line bending which has a stabilizing effect. The third and the fourth represent drive due to the temperature gradient (δ_t) and the density gradient (δ_n), respectively, through temperature and density dependences of the neoclassical resistivity. The drive is limited to small regions by b_t and b_n . Also, the d_t factor represents the coupling of temperature evolution to density evolution. Finally, the imaginary part of Eq. (4.14) represents the electron diamagnetic effect, which gives rise to finite real frequency. It is crucial to note that the eigenmode equation is not symmetric in x , with the consequence that Φ is asymmetrically skewed about the rational surface. The resistivity fluctuation breaks the parity of Ohm's law to localize Φ at the high resistivity side around the rational surface. This is because the destabilizing part of $\tilde{\mathbf{J}} \times \mathbf{B}$ force (proportional to $\tilde{\eta}$) changes sign as the rational surface is crossed.^{12,32}

Equation (4.14) can be solved approximately³¹ by using the WKB method, by ignoring the subdominant imaginary part. Eigenvalues are determined from the condition:

$$\int_0^{X_0} dX \left[\frac{\delta_t X}{1 + b_t X^2} + \frac{\delta_n X}{1 + b_n X^2} \left(1 - \frac{d_t X^2}{1 + b_t X^2} \right) - \frac{X^2}{4} \right]^{1/2} = \frac{\pi}{2}(2l + 1), \quad (4.15)$$

where l is an integer, and X_0 is a turning point, other than 0.

First, we consider the limit where $\delta_n = 0$, corresponding to the flat density profile, where the density coupling to the resistivity is neglected. In the limit of small electron parallel thermal conduction ($b_t = 0$), exact solutions can be found:

$$\Phi(X) = \Phi(0) \exp \left[-\frac{1}{4}(X - 2\delta_t)^2 \right] H_l \left[2^{1/2}(X - 2\delta_t) \right], \quad (4.16)$$

where H_l is a Hermite polynomial. The eigenvalue condition is $2\delta_t^2 = 2l + 1$. Note that the center of modes are located $2\delta_t$ outside the rational surface. Most dominant modes are the localized $l = 0$ modes, for which

$$\gamma_t = \left(\frac{\pi}{4} \right)^{1/5} \left(\frac{Rr^3 q k_\theta L_s C_t^2 J_\parallel^2}{c^2 B^2 L_t^2} \right)^{2/5} S_M^{-3/5} \tau_A^{-1}. \quad (4.17)$$

Here, $S_M = \tau_R/\tau_A$ is the local magnetic Reynolds number, $\tau_R = r^2/\eta c^2$ is the resistive time scale, $\tau_A = Rq/v_A$ is the poloidal Alfvén transit time, and

$v_A = B/(4\pi\rho)^{1/2}$ is the Alfvén speed. In the limit of large χ_{\parallel} (b_t), the dominant mode has

$$\gamma_t = 0.78 \left(\frac{cE_{\parallel} C_t L_s}{BL_t \chi_{\parallel}} \right)^{4/3} \left(\frac{L_s}{k_{\theta}} \right)^{2/3} \frac{R^2 q^2}{r^2} S_M \tau_A^{-1}. \quad (4.18)$$

Except for the extreme edge region of tokamaks, the approximation given by Eq. (4.18) is more appropriate. The radial scale length, W , is also greatly reduced compared to the small χ_{\parallel} limit, and is given by

$$W_t \sim \left(\frac{cE_{\parallel} C_t}{BL_t \chi_{\parallel} k_{\theta}^2} \right)^{1/3} L_s. \quad (4.19)$$

The naive mixing length ‘principle’, based on linear mode widths and growth rates, thus predicts a thermal diffusivity:

$$D_t^{\text{ML}} \sim \left(\frac{cE_{\parallel} C_t L_s R q}{BL_t \chi_{\parallel} k_{\theta} r} \right)^2 S_M \frac{L_s^2}{\tau_A}, \quad (4.20)$$

which is small, due to strong dependence on χ_{\parallel} . This is qualitatively different from the nonlinear prediction of D^t , as we will see later in Sec. 4.4. This is because the character of the nonlinear evolution of NRGDT differs significantly from its linear antecedent, because of current decoupling.

It is interesting to note that the growth rate for a small b_t scales as $\gamma_t \propto m^{2/5}$. The nonlinear saturation mechanism requires that the energy cascades to small scale modes where it is eventually dissipated. Therefore, additional sinks at small scales would be necessary to achieve nonlinearly saturated state in a

small b_t limit. However, for a large b_t , $\gamma_t \propto m^{-2/3}$, and nonlinear saturation is attained without additional sinks.

Next, we consider the isothermal limit ($\delta_t = 0$), while retaining the density dependence of the resistivity ($\delta_n \neq 0$). The mathematical structure is same as when $\delta_n = 0$, since $b_t \gg d_t$. When b_n is small,

$$\gamma_n = \left(\frac{\pi}{4}\right)^{1/5} \left(\frac{Rr^3 q k_\theta L_s C_n^2 J_\parallel^2}{c^2 B^2 L_n^2}\right)^{2/5} S_M^{-3/5} \tau_A^{-1}. \quad (4.21)$$

When $b_n \rightarrow \infty$,

$$\gamma_n = 0.78 \left(\frac{cE_\parallel C_n L_s}{BL_n \chi_n}\right)^{4/3} \left(\frac{L_s}{k_\theta}\right)^{2/3} \frac{R^2 q^2}{r^2} S_M \tau_A^{-1}, \quad (4.22)$$

$$W_n \sim \left(\frac{cE_\parallel C_n}{BL_n \chi_n k_\theta^2}\right)^{1/3} L_s, \quad (4.23)$$

$$D_n^{\text{ML}} \sim \left(\frac{cE_\parallel C_n L_s R q}{BL_n \chi_n k_\theta r}\right)^2 \frac{L_s^2}{\tau_A}. \quad (4.24)$$

Since $b_n/b_t \sim O(m_e/M)$, these modes cannot be neglected ($\gamma_n \gg \gamma_t$), even in a relatively high temperature region.

In general, tokamaks operate in the regime where L_t and L_n are comparable and same in sign. Therefore, both driving terms contribute to the instability. In the limit of $b_t = b_n = 0$,

$$\gamma^{5/4} = \gamma_t^{5/4} + \gamma_n^{5/4},$$

i.e., the density gradient acts to enhance the growth rate. In a more relevant, large b_t and b_n limit, γ is expected to be slightly bigger than γ_n (Eq. (4.22)),

since $b_t \gg b_n$. When two gradients have different sign, these modes will grow more slowly.

4.4 Nonlinear Theory

Having discussed the linear properties of the basic NRGDT model, we investigate the nonlinear evolution and saturation of NRGDT evolving from linearly unstable neoclassical rippling modes. Energy-like quantities (E_K , E_t , and E_n) are defined. These are required to be stationary at saturation. The condition $\partial E_K / \partial t = 0$ leads to the current decoupling, an important feature common to turbulence^{28,33,34} evolving from the linear rippling instabilities.²⁸⁻³² Two remaining conditions determine the level of the turbulence. We use the standard one-point DIA theory⁵⁰ to iteratively renormalize the dominant $E \times B$ convective nonlinearities. This procedure shows that amplitude-dependent radial diffusions are induced by convective nonlinearities. The spectrum-dependent radial diffusion broadens radial scales of modes. This, in turn, facilitates coupling to $\chi_{||}$ and χ_n dissipation as a means for saturation. This saturation mechanism persists without, and dominates over, the quasilinear flattening of the background gradients.

To study the nonlinear dynamics of fluctuations, it is customary to de-

fine energy-like integrals which are quadratic in fluctuation quantities as follows:

$$E_K = \frac{1}{2} \int d\tau |\nabla_{\perp} \tilde{\phi}|^2,$$

$$E_t = \frac{1}{2} \int d\tau |\tilde{T}_e|^2,$$

$$E_n = \frac{1}{2} \int d\tau |\tilde{n}|^2.$$

These will evolve as:

$$\frac{\partial E_K}{\partial t} = - \int d\tau \frac{B^2}{\rho c^2} \tilde{\phi}^* \nabla_{\parallel} \tilde{J}_{\parallel}, \quad (4.25)$$

$$\frac{\partial E_t}{\partial t} = - \int d\tau \left[\frac{c}{B} \tilde{T}_e^* \mathbf{b} \times \nabla \tilde{\phi} \cdot \nabla T_e + \chi_{\parallel} |\nabla_{\parallel} \tilde{T}_e|^2 \right], \quad (4.26)$$

$$\frac{\partial E_n}{\partial t} = - \int d\tau \left[\frac{c}{B} \tilde{n}^* \mathbf{b} \times \nabla \tilde{\phi} \cdot \nabla n_0 + \chi_n |\nabla_{\parallel} \tilde{n}|^2 - \frac{1}{e} \tilde{n}^* \nabla_{\parallel} \tilde{J}_{\parallel} - \frac{n_0}{\mu_i M} \tilde{n}^* \nabla_{\parallel}^2 \tilde{T}_e \right]. \quad (4.27)$$

Nonlinear mode coupling terms do not appear explicitly the spectrum-summed energy evolution since they only represent energy transfer between fluctuations at different scales. Destabilizing sources are the resistivity perturbations produced by the relaxation of the background temperature and density gradients. The magnetic field line bending, thermal conduction, and viscous drags are stabilizing. We note that the current decoupling approximation (\tilde{J}_{\parallel} is negligible where $\tilde{\phi}$ is significant) is a sufficient condition for $\partial E_t / \partial t = 0$. Also, the simulation results^{28,33} support this condition showing that $\tilde{\phi}$, \tilde{T}_e , and \tilde{n} (equivalent to \tilde{Z}_{eff} in Ref. 33) are sharply skewed off the rational surface where \tilde{J}_{\parallel} is peaked.

Therefore, we can neglect \tilde{J}_{\parallel} in the region of interest. This condition (current decoupling) greatly simplifies the governing equations because it renders the vorticity evolution equation irrelevant. This decoupled system is also referred to as the *current convective instability*.³⁰ Indeed, in the nonlinear regime, RGDT reverts from its manifestation as a rippling mode to that of a current convective instability. This is accomplished by the fact that nonlinear effects resolve singularities at the mode rational surface. We study the nonlinear evolution of NRGDT for this case.

We use a standard one-point DIA theory^{28,33,50} to describe the nonlinear evolution of NRGDT. The driven fields, $(\tilde{n}_{k''}^{(2)}$ and $\tilde{T}_{e,k''}^{(2)})$, which are 'second order' in fluctuations, are calculated from Eqs. (4.12) and (4.13). These are produced by the direct beating between the test (k) and the background (k') modes where $k'' = k + k'$. Subdominant contributions from other driven fields are neglected. The driven fields are then substituted into the $\mathbf{E} \times \mathbf{B}$ convective nonlinearity to yield amplitude-dependent diffusivities. The coupled, renormalized equations are

$$\begin{aligned} \frac{\partial}{\partial t} \tilde{T}_{e,k} - \chi_{\parallel} \nabla_{\parallel}^2 \tilde{T}_{e,k} - \frac{\partial}{\partial x} D_{\mathbf{k}}^t \frac{\partial}{\partial x} \tilde{T}_{e,k} &= \frac{cE_{\parallel}}{B} \frac{k_{\theta} T_e}{k_{\parallel} L_t} \left(C_t \frac{\tilde{T}_{e,k}}{T_e} + C_n \frac{\tilde{n}_{\mathbf{k}}}{n_0} \right) \\ &\quad - i\omega_{*e}^t T_e \left(\frac{\tilde{T}_{e,k}}{T_e} + \frac{\tilde{n}_{\mathbf{k}}}{n_0} \right), \end{aligned} \quad (4.28)$$

$$\begin{aligned} \frac{\partial}{\partial t} \tilde{n}_k - \chi_n \nabla_{\parallel}^2 \tilde{n}_k - \frac{\partial}{\partial x} D_k^n \frac{\partial}{\partial x} \tilde{n}_k - \frac{n_0}{\mu_i M} \nabla_{\parallel}^2 \tilde{T}_{e,k} = \frac{c E_{\parallel}}{B} \frac{k_{\theta} n_0}{k_{\parallel} L_n} \left(C_t \frac{\tilde{T}_{e,bfk}}{T_e} + C_n \frac{\tilde{n}_k}{n_0} \right) \\ - i \omega_{*e}^n n_0 \left(\frac{\tilde{T}_{e,k}}{T_e} + \frac{\tilde{n}_k}{n_0} \right). \end{aligned} \quad (4.29)$$

Here,

$$\omega_{*e}^t = k_{\theta} c T_e / e B L_t,$$

$$\omega_{*e}^n = k_{\theta} c T_e / e B L_n,$$

$$D_k^t = \sum_{k'} (\Gamma_{k''}^t)^{-1} \left| \frac{c}{B} k'_{\theta} \tilde{\phi}_{k'} \right|^2, \quad (4.30)$$

$$D_k^n = \sum_{k'} (\Gamma_{k''}^n)^{-1} \left| \frac{c}{B} k'_{\theta} \tilde{\phi}_{k'} \right|^2. \quad (4.31)$$

The propagators are

$$(\Gamma_{k''}^t)^{-1} = \text{Re} \left[\gamma_{k''} + \Delta \omega_{k''}^t - \chi_{\parallel} \nabla_{\parallel}^2 + i \omega_{*e}^t(k'') \right]^{-1}, \quad (4.32)$$

$$(\Gamma_{k''}^n)^{-1} = \text{Re} \left[\gamma_{k''} + \Delta \omega_{k''}^n - \chi_n \nabla_{\parallel}^2 + i \omega_{*e}^n(k'') \right]^{-1}. \quad (4.33)$$

Here, $\text{Re}[(\dots)]$ denotes the real part of (\dots) , and $\Delta \omega_{k''}$ is the nonlinear decorrelation rate, which effectively limits the coherence time of nonlinear interaction.

It is interesting to note that one-point DIA theory generically does not conserve the total energy. However, in energy spectrum evolution,⁷¹ incoherent emission as well as coherent damping act to conserve energy. Indeed, the local (in k) competition of these two effects yields a spectrum flow rate comparable

to the damping rate predicted by one-point theory. This feature underlies the validity of one-point theory here. It is worthwhile to draw analogy between the propagator in energy-conserving two-point theory and the propagator in one-point theory. By neglecting \tilde{n} for simplicity, one can write for \tilde{T}_e :

$$\frac{\partial \tilde{T}_{e,k}}{\partial t} + i\Omega_k \tilde{T}_{e,k} = \sum_{k=k'+k''} \Lambda_{k',k''} \tilde{\phi}_{k'} \tilde{T}_{e,k''}, \quad (4.34)$$

where,

$$\Omega_k = \omega_{*e}^t - i \left(\chi_{\parallel} k_{\parallel}^2 - \frac{C_t k_{\theta} \eta J_{\parallel}}{k_{\parallel} B L_t} \right),$$

$$\Lambda_{k',k''} = \frac{c}{B} k' \times k''.$$

Nonlinear terms conserve energy since $\int d\tau \tilde{T}_e \mathbf{b} \times \nabla \tilde{\phi} \cdot \nabla \tilde{T}_e = 0$. By multiplying $\tilde{T}_{e,k}^*$ to Eq. (4.34), one finds the evolution of the energy spectrum:

$$\begin{aligned} & \frac{\partial}{\partial t} \langle \tilde{T}_e^2 \rangle_k - 2 \text{Im}(\Omega_k) \langle \tilde{T}_e^2 \rangle_k \\ &= \text{Re} \sum_{k=k'+k''} \Lambda_{k',k''} \langle \tilde{T}_{e,k}^* \tilde{\phi}_{k'} \tilde{T}_{e,k''} \rangle \\ &\simeq \text{Re} \sum_{k=k'+k''} \Lambda_{k',k''} \left(\langle \tilde{T}_{e,k}^{*(2)} \tilde{\phi}_{k'} \tilde{T}_{e,k''} \rangle + \langle \tilde{T}_{e,k}^* \tilde{\phi}_{k'} \tilde{T}_{e,k''}^{(2)} \rangle \right). \end{aligned} \quad (4.35)$$

Here, $\langle \langle \dots \rangle \rangle$ denotes ensemble-average. The first term in the right-hand-side of Eq. (4.35) denotes the incoherent emission and the second term denotes the coherent damping. The contributions from $\langle \tilde{T}_{e,k}^* \tilde{\phi}_{k'}^{(2)} \tilde{T}_{e,k''} \rangle$ are similar to the second term, and are neglected for simplicity. From Eq. (4.34), $\tilde{T}_{e,k}^{*(2)}$ satisfies:

$$\tilde{T}_{e,k}^{*(2)} = \int^t dt' e^{-(i\Omega_k^* + \Delta\omega_k)(t-t')} \Lambda_{k',k''}^* \tilde{\phi}_{k'}^*(t') \tilde{T}_{e,k''}^*(t').$$

Here, $\Delta\omega_k$ reflects nonlinear scrambling due to interaction with modes other than k' and k'' . We further assume that the spectrum evolution time-scale is much larger than the nonlinear scrambling time-scale to approximate:

$$\langle \tilde{\phi}_{k'}^*(t') \tilde{\phi}_{k'}(t) \rangle = \langle \tilde{\phi}^2(t) \rangle_{k'} e^{-i(\Omega_{k'} + \Delta\omega_{k'})(t-t')}.$$

Therefore, Eq. (4.35) can be written as

$$\begin{aligned} & \frac{\partial}{\partial t} \langle \tilde{T}_e^2 \rangle_k - 2 \text{Im}(\Omega_k) \langle \tilde{T}_e^2 \rangle_k \\ & \simeq \text{Re} \sum_{k=k'+k''} \int^t dt' e^{-\{i(\Omega_k^* + \Omega_{k'} + \Omega_{k''}) + \Delta\omega_k + \Delta\omega_{k'} + \Delta\omega_{k''}\}(t-t')} \\ & \quad \times \Lambda_{k',k''} \left[\Lambda_{k',k''}^* \langle \tilde{\phi}^2(t) \rangle_{k'} \langle \tilde{T}_e^2(t) \rangle_{k''} + \Lambda_{-k',k} \langle \tilde{\phi}^2(t) \rangle_{k'} \langle \tilde{T}_e^2(t) \rangle_k \right] \\ & \simeq \text{Re} \sum_{k=k'+k''} \Lambda_{k',k''} \frac{\Lambda_{k',k''}^* \langle \tilde{\phi}^2 \rangle_{k'} \langle \tilde{T}_e^2 \rangle_{k''} + \Lambda_{-k',k} \langle \tilde{\phi}^2 \rangle_{k'} \langle \tilde{T}_e^2 \rangle_k}{i(\Omega_k^* + \Omega_{k'} + \Omega_{k''}) + \Delta\omega_k + \Delta\omega_{k'} + \Delta\omega_{k''}}. \end{aligned} \quad (4.36)$$

Note that the terms on the right hand side of Eq. (4.36) are comparable as noted above. Also, the nonlinear decorrelation rate can be recursively defined as

$$\Delta\omega_k \simeq \text{Re} \sum_{k=k'+k''} \frac{\Lambda_{k',k''} \Lambda_{-k',k} \langle \tilde{\phi}^2(t) \rangle_{k'}}{i(\Omega_k^* + \Omega_{k'} + \Omega_{k''}) + \Delta\omega_k + \Delta\omega_{k'} + \Delta\omega_{k''}}.$$

Therefore, the propagator can be written as:

$$(\Gamma_{k'}^t)^{-1} = \text{Re} [i(\Omega_k^* + \Omega_{k'} + \Omega_{k''}) + \Delta\omega_k + \Delta\omega_{k'} + \Delta\omega_{k''}]^{-1}. \quad (4.37)$$

When nonlinear interactions are negligible, the interaction time becomes infinite, and we recover the *weak turbulence* limit. However, since rippling modes are

nondispersive ($\omega_{\mathbf{k}''} \simeq \omega_{\mathbf{k}} + \omega_{\mathbf{k}'}$), NRGDT is always in the *strong turbulence* regime, and the real frequency and ω_{*e} effects play no role. Also, the radial diffusivities can be written as:

$$D_{\mathbf{k}}^t = \frac{L_s^2 \langle \tilde{V}_r^2 \rangle}{\chi_{\parallel} \bar{k}_{\theta}^2 (\Delta^t)^2}, \quad (4.38)$$

$$D_{\mathbf{k}}^n = \frac{L_s^2 \langle \tilde{V}_r^2 \rangle}{\chi_n \bar{k}_{\theta}^2 (\Delta^n)^2}. \quad (4.39)$$

Here,

$$\tilde{V}_r^2 = \sum_{\mathbf{k}} \left| \frac{c}{B} k_{\theta} \tilde{\phi}_{\mathbf{k}} \right|^2, \quad (4.40)$$

and \bar{k}_{θ} is the spectrum-averaged mean poloidal wavenumber. Also, Δ^t and Δ^n are the nonlinear radial scale lengths for the temperature and the density fluctuations, respectively, evaluated at \bar{k}_{θ} .

We now determine the level of the turbulence which mediates the energy cascade from the dominant large scale modes to small scale modes, thus leading to the saturation of NRGDT. To find the dependences of Δ^t and Δ^n on the level of turbulence, we asymptotically balance (at large x) the radial turbulent diffusions with parallel conduction terms, yielding:

$$(\Delta_{\mathbf{k}}^t)^4 = \frac{L_s^2 D_{\mathbf{k}}^t}{\chi_{\parallel} k_{\theta}^2}, \quad (4.41)$$

$$(\Delta_{\mathbf{k}}^n)^4 = \frac{L_s^2 D_{\mathbf{k}}^n}{\chi_n k_{\theta}^2}. \quad (4.42)$$

We note that Δ^t and Δ^n increase as the level of the turbulence increases. When the turbulence level reaches the point where the dissipation sink ($\chi_{\parallel} \nabla_{\parallel}^2$ and $\chi_n \nabla_{\parallel}^2$) balances the linear instability source, the saturated state can be attained.

Following Ref. 33, we multiply $\int d\tau \tilde{n}^*$ to Eqs. (4.28) and (4.29), yielding:

$$\langle \tilde{n} | L_1 | \tilde{T}_e \rangle \langle \tilde{n} | \tilde{T}_e \rangle + \langle \tilde{n} | L_2 | \tilde{n} \rangle \langle \tilde{n} | \tilde{n} \rangle = 0, \quad (4.43)$$

$$\langle \tilde{n} | L_3 | \tilde{T}_e \rangle \langle \tilde{n} | \tilde{T}_e \rangle + \langle \tilde{n} | L_4 | \tilde{n} \rangle \langle \tilde{n} | \tilde{n} \rangle = 0. \quad (4.44)$$

Here,

$$\langle \tilde{n} | L | \tilde{T}_e \rangle = \frac{\int d\tau \tilde{n}^* L \tilde{T}_e}{\langle \tilde{n} | \tilde{T}_e \rangle},$$

$$\langle \tilde{n} | \tilde{T}_e \rangle = \int d\tau \tilde{n}^* \tilde{T}_e,$$

$$L_1 = \chi_{\parallel} \frac{k_{\theta}^2}{L_s^2} x^2 - D_k^t \frac{\partial^2}{\partial x^2} - C_t \frac{cE_{\parallel} L_s}{BL_t} \frac{1}{x},$$

$$L_2 = -\frac{T_e}{n_0} C_n \frac{cE_{\parallel} L_s}{BL_n} \frac{1}{x},$$

$$L_3 = \frac{n_0 k_{\theta}^2}{\mu_i M L_s^2} x^2 - \frac{n_0}{T_e} C_t \frac{cE_{\parallel} L_s}{BL_t} \frac{1}{x},$$

$$L_4 = \chi_n \frac{k_{\theta}^2}{L_s^2} x^2 - D_k^n \frac{\partial^2}{\partial x^2} - C_n \frac{cE_{\parallel} L_s}{BL_n} \frac{1}{x},$$

where we have required $\partial/\partial t = 0$ for saturation. We note that \tilde{T}_e and \tilde{n} are skewed about the rational surface, and that they are negligible at $x = 0$. Therefore, integrations involving $1/x$ remains finite. Also, when cross products are involved in integration, Δ^t should be taken as the characteristic width, since

$\Delta^t < \Delta^n$. For Eqs. (4.43) and (4.44) to have a nontrivial solution, the determinant should vanish, i.e.,

$$\begin{vmatrix} \tilde{V}_r - C_t c E_{\parallel} L_s / B L_t & -C_n c E_{\parallel} L_s / B L_n \\ T_e \tilde{V}_r / \chi_{\parallel} \mu_i M - C_t c E_{\parallel} L_s / B L_t & \tilde{V}_r - C_n c E_{\parallel} L_s / B L_n \end{vmatrix} = 0. \quad (4.45)$$

The solution is

$$\tilde{V}_r = \frac{c E_{\parallel} L_s}{B L_n} \left[C_n \left(1 + \frac{T_e}{\chi_{\parallel} \mu_i M} \right) + C_t \eta_e \right]. \quad (4.46)$$

As expected, the density gradient acts to enhance the turbulence level, in comparison to the case with only the temperature gradient.²⁸ However, the way the gradient drives combine $[(C_n/L_n) + (C_t/L_t)]$, is interesting because one may naively expect the temperature gradient drive contribution to be suppressed, due to the large parallel thermal conduction.

From Eqs. (4.38)-(4.42), and (4.46), we obtain

$$\Delta^t = \left[\frac{c E_{\parallel} L_s}{B L_n} (C_n + C_t \eta_e) \right]^{\frac{1}{3}} \left(\chi_{\parallel} \frac{\bar{k}_{\theta}^2}{L_s^2} \right)^{-\frac{1}{3}}, \quad (4.47)$$

$$\Delta^n = \left[\frac{c E_{\parallel} L_s}{B L_n} (C_n + C_t \eta_e) \right]^{\frac{1}{3}} \left(\chi_n \frac{\bar{k}_{\theta}^2}{L_s^2} \right)^{-\frac{1}{3}}. \quad (4.48)$$

We have used $\chi_{\parallel} \gg T_e / \mu_i M$. Turbulent radial diffusivities are then given by

$$D^t = \left[\frac{c E_{\parallel} L_s}{B L_n} (C_n + C_t \eta_e) \right]^{\frac{4}{3}} \left(\chi_{\parallel} \frac{\bar{k}_{\theta}^2}{L_s^2} \right)^{-\frac{1}{3}}, \quad (4.49)$$

$$D^n = \left[\frac{c E_{\parallel} L_s}{B L_n} (C_n + C_t \eta_e) \right]^{\frac{4}{3}} \left(\chi_n \frac{\bar{k}_{\theta}^2}{L_s^2} \right)^{-\frac{1}{3}}. \quad (4.50)$$

Since $\Delta^n \gg \Delta^t$, and Δ^n controls the particle flux, the thermal flux due to NRGDT is dominated by convection ($D^n \gg D^t$). By comparing Eq. (4.49) for $L_n \rightarrow \infty$ (or $C_n = 0$) with Eq. (4.20), we find that the prediction of D_t^{ML} according to the mixing length principle differs substantially from the more consistent nonlinear result. The same can be said when Eq. (4.50) for $L_t \rightarrow \infty$ is compared with Eq. (4.24). However, Δ^t and Δ^n compare well with W^t and W^n , respectively, in limiting cases. Therefore, we conclude that the nonlinear decorrelation time-scale decouples from the linear growth time-scale, in contradiction to the mixing length prediction. Also, since L_n has the same sign as L_t in tokamak discharges, the density gradient acts to enhance the turbulence level. The density gradient drive is most relevant near $\nu_{*e} \sim 1$, where C_n has a maximum, and C_t has a minimum. The density gradient drive becomes also important for a steep density profile ($\eta_e \ll 1$). Thus, the region where resistivity-gradient-driven turbulence is significantly excited broadens inward from the edge of the plasma. The particle diffusivity in Eq. (4.50) has an interesting scaling which may offer further insights into understanding of confinement properties in H-mode²⁸ tokamak edge, in particular, ELMs in DIII-D tokamak.⁷⁰ The confinement improvement in the H-mode after L→H transition is due to the formation of a transport barrier just inside the separatrix flux surface.⁶⁰ It has been also

suggested⁵⁹ that the strong global shear near separatrix region is responsible for the reduction of turbulent transport due to resistive MHD type of modes and the creation of a transport barrier. This favorable role of global shear is also supported by the limiter H-mode results in JFT-2M,⁷² where the quality of H-mode is better for higher elongation. After L→H transition, the plasma density at the edge rises continuously. In DIII-D, the electron density profile changes dramatically, and becomes very flat (sometimes even hollow) with a sharp gradient at transport barrier region. It is interesting to note that T_e at the edge remains relatively low, implying a higher value of ν_{*e} for H-mode compared to L-mode. This unique feature of DIII-D H-mode profiles at the edge (sharp L_n , high n_0 , $\nu_{*e} > 1$, modest T_e) is usually destroyed by ELMs, resulting in a large outward particle flux. Interestingly, from Eq. (4.50), we have

$$D^n \propto \frac{n_0^{1/3}}{T_e^{5/6}} \left[\frac{C_n(\nu_{*e})}{L_n} + \frac{C_t(\nu_{*e})}{L_t} \right]^{4/3},$$

which indicates a rapid increase in turbulent particle flux as the density and density gradient are increased as ν_{*e} passes through unity from below. To this end, it should be noted that recent experiments have established that the ideal ballooning stability limits edge pressure gradients but have not identified the physical mechanism of the giant ELMs. Indeed, it should be mentioned that resistive ballooning modes^{26,40} are also a candidate for explaining ELM activity.

Now, we derive the saturation amplitude of various fluctuations. Balancing the destabilizing gradient with the stabilizing parallel conduction (this is *effective* mixing length theory in that the nonlinear mode width is used) yields:

$$\frac{\tilde{T}_e}{T_e} = \frac{L_s^2 \tilde{V}_r}{\chi_{\parallel} \bar{k}_{\theta}^2 (\Delta^t)^2 L_t}, \quad (4.51)$$

$$\frac{\tilde{n}}{n_0} = \frac{L_s^2 \tilde{V}_r}{\chi_n \bar{k}_{\theta}^2 (\Delta^n)^2 L_n}. \quad (4.52)$$

By combining Eqs. (4.51) and (4.52) with Eqs. (4.47) and (4.48), we obtain the temperature and density fluctuation levels:

$$\frac{\tilde{T}_e}{T_e} = \frac{\Delta^t}{L_t} = \frac{1}{L_t} \left[\frac{cE_{\parallel} L_s}{BL_n} (C_n + C_t \eta_e) \right]^{\frac{1}{3}} \left(\chi_{\parallel} \frac{\bar{k}_{\theta}^2}{L_s^2} \right)^{-\frac{1}{3}}, \quad (4.53)$$

$$\frac{\tilde{n}}{n_0} = \frac{\Delta^n}{L_n} = \frac{1}{L_n} \left[\frac{cE_{\parallel} L_s}{BL_n} (C_n + C_t \eta_e) \right]^{\frac{1}{3}} \left(\chi_n \frac{\bar{k}_{\theta}^2}{L_s^2} \right)^{-\frac{1}{3}}. \quad (4.54)$$

Usually, since $\Delta^n \gg \Delta^t$,

$$\left(\frac{\tilde{T}_e}{T_e} \right) / \left(\frac{\tilde{n}}{n_0} \right) = \eta_e \left(\frac{\chi_n}{\chi_{\parallel}} \right)^{\frac{1}{3}} < 1,$$

as experimentally observed in tokamaks.³⁵ The electrostatic potential fluctuation level is given by

$$\frac{e\tilde{\phi}}{T_e} = \frac{eE_{\parallel} L_s}{T_e \bar{k}_{\theta} L_n} (C_n + C_t \eta_e). \quad (4.55)$$

We note that unlike drift wave turbulence,⁴⁸ the Boltzmann relation, $e\tilde{\phi}/T_e = \tilde{n}/n_0$, does not hold in NRGDT, which is also consistent with experimental results.³⁵

Unlike \tilde{T}_e and \tilde{n} , \tilde{J}_\parallel has nonvanishing components near the rational surface:

$$\frac{\tilde{J}_\parallel}{J_\parallel} \simeq C_t \frac{\tilde{T}_e}{T_e} + C_n \frac{\tilde{n}}{n_0}. \quad (4.56)$$

Therefore, magnetic fluctuations can be induced in NRGDT. Then, by integrating Eq. (4.56) using the constant- ψ approximation,¹² we obtain

$$\Delta' \tilde{\psi} = \frac{4\pi}{c} J_\parallel \left(C_t \Delta^t \frac{\tilde{T}_e}{T_e} + C_n \Delta^n \frac{\tilde{n}}{n_0} \right),$$

where ψ is the parallel component of the vector potential. For large poloidal mode numbers, $\Delta' \simeq -2k_\theta$, and therefore,

$$\frac{\tilde{B}_r}{B} = \frac{2\pi J_\parallel}{cBL_n} \left[\frac{cE_\parallel L_s}{BL_n} (C_n + C_t \eta_e) \right]^{\frac{2}{3}} \left(\chi_n \frac{\bar{k}_\theta^2}{L_s^2} \right)^{-\frac{2}{3}} \left[C_n + C_t \eta_e \left(\frac{\chi_n}{\chi_\parallel} \right)^{\frac{2}{3}} \right]. \quad (4.57)$$

This magnetic fluctuation level is too feeble to induce any significant electron heat transport due to stochastic magnetic fields.⁷ The electron heat transport according to NRGDT is mainly due to thermal convection.

4.5 Summary and Conclusions

We have incorporated the effects of the neoclassical correction to the resistivity^{2,39} into the evolution of rippling modes.²⁸⁻³³ Through the density dependence of the neoclassical resistivity, rippling modes can tap the density gradient free energy source as well as the usual temperature gradient free energy source. The density coupling (C_n) to the neoclassical resistivity is strong when $\nu_{*,e} \sim 1$. Although C_n is smaller than C_t , the density gradient is much more effective free energy source, since conduction of density fluctuations along flux surfaces provided by neoclassical viscous force is less efficient than the parallel thermal conduction. Thus, the region where the neoclassical rippling modes are significantly unstable (linearly) extends further inside from the edge. The growth rate and the linear mode width are calculated in limiting cases.

The nonlinearly saturated state is characterized by current decoupling: asymmetry further develops to make other fluctuations skewed around the singular surface where \tilde{J}_{\parallel} is localized. Mathematically, this is a sufficient condition for a stationary E_K . Two remaining stationary conditions determine the level of turbulence. The saturation mechanism is nonlinear mode coupling between long wavelength modes and stable short wavelength modes. It is shown that NRGDT is always in the *strong turbulence* regime, and that ω and ω_{*e} do not

play important roles in nonlinear evolution. In one-point DIA theory,⁵⁰ the nonlinear damping is expressed in terms of fluctuation-spectrum-dependent radial diffusion, acting to broaden the radial scale of modes, thus leading to more effective parallel dissipation of fluctuations. The renormalized coupled equations are solved by treating the turbulent diffusivities as eigenvalues. The principal results are as follows:

- (i) The density gradient enhances the turbulence level in comparison to the case with only temperature gradient,²⁸ as expected from the linear theory.
- (ii) The density fluctuation becomes much broader than the temperature fluctuation.
- (iii) Turbulent radial diffusivities (D^t and D^n) are different from mixing length estimates ($\gamma^t(W^t)^2$ and $\gamma^n(W^n)^2$) both qualitatively and quantitatively, i.e.,:

$$D^t = \left[\frac{cE_{\parallel}L_s}{BL_n}(C_n + C_t\eta_e) \right]^{\frac{4}{3}} \left(\chi_{\parallel} \frac{\overline{k_{\theta}^{-2}}}{L_s^2} \right)^{-\frac{1}{3}},$$

$$D^n = \left[\frac{cE_{\parallel}L_s}{BL_n}(C_n + C_t\eta_e) \right]^{\frac{4}{3}} \left(\chi_n \frac{\overline{k_{\theta}^{-2}}}{L_s^2} \right)^{-\frac{1}{3}}.$$

We note that the recent nonlinear study of resistive interchange modes¹³ and neoclassical pressure-gradient-driven turbulence (Ch. III) revealed only quantitative difference between nonlinear results and estimates from

mixing length principle. Here, current decoupling, a novel feature which modifies the mode structure drastically in NRGDT, is responsible for this more significant discrepancy.

- (iv) The density fluctuation level is higher than the temperature fluctuation level and the Boltzmann relation does not hold:

$$\begin{aligned}\frac{\tilde{n}}{n_0} &= \frac{1}{L_n} \left[\frac{cE_{\parallel}L_s}{BL_n} (C_n + C_t\eta_e) \right]^{\frac{1}{3}} \left(\chi_n \frac{\bar{k}_{\theta}^2}{L_s^2} \right)^{-\frac{1}{3}}, \\ \frac{\tilde{T}_e}{T_e} &= \frac{1}{L_t} \left[\frac{cE_{\parallel}L_s}{BL_n} (C_n + C_t\eta_e) \right]^{\frac{1}{3}} \left(\chi_{\parallel} \frac{\bar{k}_{\theta}^2}{L_s^2} \right)^{-\frac{1}{3}}, \\ \frac{e\tilde{\phi}}{T_e} &= \frac{eE_{\parallel}L_s}{T_e\bar{k}_{\theta}L_n} (C_n + C_t\eta_e).\end{aligned}$$

- (v) The magnetic component of NRGDT is calculated to be too feeble to be significant.
- (vi) The region where RGDТ applies is extended into $\nu_{*,e} \leq 1$ regimes. Real frequency and ω_* effects do not play a significant role in the nonlinear evolution.
- (vii) Some speculations into ELMs in DIII-D H-mode plasmas⁷⁰ are developed in the context of this model.

Other potentially important neoclassical corrections which we neglected in this study due to the omission of the poloidal component of the first order perpendicular flows are the bootstrap current^{2,39} in Ohm's law and neoclassical

viscous damping in the vorticity equation. These effects combine to excite neoclassical pressure-gradient-driven instabilities^{42,43}. These instabilities are significant when β (β is the ratio of the kinetic pressure to the magnetic pressure) is large, while the present study is limited to a low- β case. Study of turbulence evolving from neoclassical pressure-gradient-driven instabilities is reported in Ch. III. Modification of the current decoupling in presence of these neoclassical corrections will be studied later.

CHAPTER V

CONCLUSIONS

In this thesis, we have investigated several aspects of runaway electron confinement and neoclassical MHD turbulence in tokamaks. The study of runaway electron confinement was motivated by high sensitivity of runaway electrons to the structure of magnetic fluctuations and the experiments on ASDEX, which revealed strong correlation in the behavior of particle, heat, and runaway electron confinement during L-mode and at the transitions of OH→L→H. The motivation behind the study of neoclassical MHD turbulence is to extend the validity of resistive MHD theories, which have been successful in explaining many phenomena in tokamaks, into more experimentally relevant, low collisionality regimes. The results provide us with reasonable criteria to check consistency of theoretical models and reasonable explanations for experimentally observed particle diffusion, heat transport, and levels of turbulence. Furthermore, the method developed here can be applied to other systems, thus leading to a better understanding of turbulence. In this section, we summarize our understandings and offer some suggestions for future work.

In Chap. II, we have shown that the radial correlation length (W) of the electromagnetic turbulence underlying both runaway and thermal transport

can be determined from τ_R/τ_E , when the ∇B drift of runaway electrons across magnetic surfaces is considered in the analysis. The magnetic fluctuation level (\tilde{B}_r/B_0) is then determined to match the experimentally determined electron thermal diffusivity. We can also determine the scalings of W and \tilde{B}_r/B_0 from parameter scan experiments. These results can be used as criteria to test the consistency of theoretical models. We have concluded that the resistive ballooning modes provide the most plausible explanation of the results. However, detailed experimental results (average poloidal mode number and magnetic fluctuation level inside the plasma, τ_R spectrum, etc.) are necessary to further distinguish between the various possibilities. Theoretically, it is interesting to investigate how small generation and acceleration of runaway electrons during the current plateau phase modify runaway electron transport. This analysis is expected to involve a time-dependent transport coefficient. Further, self-consistent correction of magnetic fluctuations due to the motion of electrons, though extremely hard to account for, is a very interesting, generic theoretical problem.

In Chap. III, we have studied the turbulence evolving from neoclassical pressure-gradient-driven instabilities. Neoclassical MHD equations, which are valid in experimentally relevant, low-collisionality regimes, have been used in the study. Neoclassical pressure-gradient-driven instabilities can be catago-

rized as the interchange and ballooning type instabilities, in that their growth rate scale as $\gamma \propto S_M^{-1/3}$ and that the pressure gradient acts as the free energy source. However, the bootstrap current and neoclassical viscous damping of the vorticity are crucial to the instability. Linear analyses with curvature and hot trapped particle effects have revealed many branches of instabilities which can be described in this context. In the case of neoclassical pressure-gradient-driven instabilities, modes with poloidal wavelengths shorter than radial mode width are shown to be suppressed. Nonlinear saturation conditions determine the turbulent radial pressure diffusivity as an eigenvalue of the renormalized conditions. The pressure diffusivity, as well as levels of fluctuation, exceed the mixing length estimate (based on the linear growth rate and the linear mode width), by a power of the nonlinear enhancement factor. The radial scale lengths also increase at saturation, consistent with the notion of mode broadening as the saturation mechanism. The problem of the electron heat transport due to stochastic magnetic fields driven by NPGDT has been revisited. The reconsideration of the radial structure of magnetic flutter leads to estimates of the electron thermal diffusivity and magnetic fluctuation levels which differ substantially from previous calculations. Nonlinear interactions between different helicities have been considered. Nonlinear interactions with different radial modes other than

the principal peaked modes might be also interesting to consider. Also, one should self-consistently investigate effects of magnetic fluctuations (*not* driven by electrostatic modes) and the anomalous heat transport related to them.

In Chap. IV, we have studied the turbulence evolving from neoclassical resistivity-gradient-driven instabilities which can tap the density gradient expansion free energy source through the density dependence of the neoclassical resistivity. The density gradient coupling to the neoclassical rippling modes is salient when $\nu_{*e} \simeq 1$. Linear analyses show that the region where neoclassical rippling modes are significantly excited extends from the edge of the plasma to the region where $\nu_{*e} \leq 1$. Since these modes are non-dispersive, diamagnetic effects are negligible in comparison to the nonlinear decorrelation rate at saturation. Thus, the relevant regime is the strong turbulence regime. The turbulent radial diffusivities of the temperature and the density are obtained as eigenvalues of the renormalized eigenmode equations at steady state. These are substantially different from mixing length estimates. This feature of NRGDT contrasts with that of NPGDT, where only quantitative differences with mixing length estimates were found. This novel feature is due to the current decoupling which distinguishes the structure of NRGDT from its linear antecedent. The density gradient acts to enhance the level of turbulence, compared to that driven by the

temperature gradient alone. The saturated turbulent state is characterized by: current decoupling, the breakdown of Boltzmann relation, a radial mode scale of density fluctuations exceeding that of temperature fluctuations, implying that the density diffusivity exceeds the temperature diffusivity, and that density fluctuation levels exceed temperature fluctuation levels. Magnetic fluctuation levels are shown to be too feeble to induce any significant heat transport. An interesting extension of this work is to investigate the behavior of NRGDT in the presence of the bootstrap current. In particular, modification of the current decoupling would be interesting.

APPENDICES

Appendix A.

In this Appendix, it is shown that electrostatic turbulence cannot simultaneously underlie τ_R and τ_E in the ASDEX tokamak. To do this, we first assume that heat transport of both REs and bulk plasma is due to electrostatic turbulence and later we will show that this assumption leads to unphysical implications. For simplicity, only the electrostatic weak turbulence regime is considered here.

Starting from the electrostatic electron drift kinetic equation for untrapped electrons, one finds χ_e by following the same steps described in Sec. 2.3-A:

$$\chi_e = \pi \left(\frac{cT_e}{eB_0} \right)^2 \sum_{\vec{k}, \omega} k_\theta^2 \left| \frac{e\tilde{\phi}_{\vec{k}, \omega}}{T_e} \right|^2 \delta(\omega - \omega_D - k_\parallel v_\parallel). \quad (A.1)$$

Here, $\tilde{\phi}$ is the fluctuating electrostatic potential. The spectrum of $\tilde{\phi}$ can be written as

$$\left| \frac{e\tilde{\phi}_{\vec{k}, \omega}}{T_e} \right|^2 = \frac{\phi_0^2}{W_{mI}^{ES} I^{ES}} F^{ES}(m) S_{\vec{k}}^{ES} \left(\frac{x}{W_m^{ES}} \right) \frac{\Delta\omega_{\vec{k}}}{\pi [(\omega - \omega_{\vec{k}})^2 + \Delta\omega_{\vec{k}}]}. \quad (A.2)$$

Here, the superscript "ES" denotes electrostatic turbulence and

$$\phi_0^2 = \sum_{\vec{k}, \omega} \left| \frac{e\tilde{\phi}_{\vec{k}, \omega}}{T_e} \right|^2. \quad (A.3)$$

Equations (A.2) and (A.3) can be compared with Eqs. (2.13) and (2.11), respectively, and W_{mI}^{ES} , F^{ES} , $S_{\vec{k}}^{ES}$, and I^{ES} have same meanings as before with the replacement of “electrostatic” with “magnetic”. Since the ballistic frequency dominates for thermal electrons, we have

$$\chi_{e,th} = \frac{\pi \bar{k}_\theta L_s}{\overline{W}_{mI}^{ES} v_{\parallel,th}} \left(\frac{cT_e}{eB_0} \right)^2 \phi_0^2. \quad (A.4)$$

However, because of the large drift velocity across magnetic field lines for REs, we find

$$\chi_{e,R} = \frac{\pi \bar{k}_\theta L_s}{\overline{W}_{mI}^{ES} v_{\parallel,R}} \left(\frac{cT_e}{eB_0} \right)^2 \phi_0^2 S_{\vec{k}}^{ES} \left(\frac{\omega_{D,R}}{\bar{k}'_{\parallel} v_{\parallel,R} \overline{W}_m^{ES}} \right). \quad (A.5)$$

Then, comparing Eq. (A.5) with Eq. (A.4), one finds

$$S_{\vec{k}}^{ES} \left(\frac{\omega_{D,R}}{\bar{k}'_{\parallel} v_{\parallel,R} \overline{W}_m^{ES}} \right) = \frac{\tau_E v_{\parallel,R}}{\tau_R v_{\parallel,th}}. \quad (A.6)$$

For typical parameters, the right-hand side of (A.6) is about 10, which is unphysical because these modes are well localized around the rational surface, which implies $S_{\vec{k}} \leq 1$.

Appendix B.

In this Appendix, we briefly discuss the properties of neoclassical tearing instabilities driven by Δ' . We use the same notations as in Chap. III. These modes have symmetric $\tilde{\psi}$ and antisymmetric $\tilde{\phi}$ around the rational surface, while neoclassical pressure-gradient-driven instabilities have a twisting parity. Basic equations are:

$$-\frac{\gamma}{c}\tilde{\psi} - \nabla_{\parallel}\tilde{\phi} = \eta\tilde{J}_{\parallel} + \frac{c}{B_{\theta}}\eta\delta_e\frac{d}{dx}\tilde{P}, \quad (B.1)$$

$$\gamma\nabla_{\perp}^2\tilde{\phi} = \frac{B_{\theta}^2}{c^2\rho}\nabla_{\parallel}\tilde{J}_{\parallel} + \frac{B_{\theta}}{c\rho}\frac{d}{dx}\nabla_{\parallel}\tilde{P} + \frac{B_{\theta}^2}{c^2\rho}\tilde{\nabla}_{\parallel}J_{\parallel} + \frac{B_{\theta}}{c\rho}\frac{d}{dx}\tilde{\nabla}_{\parallel}P, \quad (B.2)$$

$$\gamma\tilde{P} + \tilde{v}_r\frac{dP}{dr} = 0, \quad (B.3)$$

$$\tilde{J}_{\parallel} = -\frac{c}{4\pi}\nabla_{\perp}^2\tilde{\psi}. \quad (B.4)$$

They are Ohm's law, vorticity evolution, pressure evolution, and Ampere's law.

We use $\tilde{v}_r = -ik_{\theta}c\tilde{\phi}/B$, since $c\tilde{\phi}/v_{\parallel}\tilde{\psi} \gg 1$, and $\tilde{\nabla}_{\parallel} = i(k_{\theta}\tilde{\psi}/B)(d/dr)$. By substituting Eqs. (B.3) and (B.4) into Eqs. (B.1) and (B.2), we have

$$\frac{\gamma}{c}\tilde{\psi} - i\frac{k_{\theta}}{L_s}x\tilde{\phi} = \frac{c\eta}{4\pi}\nabla_{\perp}^2\tilde{\psi} + \frac{k_{\theta}c^2\eta\delta_e}{BB_{\theta}\gamma}\left|\frac{dP}{dr}\right|\frac{d\tilde{\phi}}{dx}, \quad (B.5)$$

$$\gamma\nabla_{\perp}^2\tilde{\phi} = i\frac{k_{\theta}B_{\theta}^2}{4\pi c\rho L_s}x\nabla_{\perp}^2\tilde{\psi} - \frac{N_V}{\gamma}\frac{d}{dx}x\tilde{\phi} + i\frac{k_{\theta}B_{\theta}^2}{c^2\rho B}\frac{dJ_{\parallel}}{dr}\tilde{\psi} - i\frac{k_{\theta}B_{\theta}}{Bc\rho}\left|\frac{dP}{dr}\right|\frac{d\tilde{\psi}}{dx}. \quad (B.6)$$

The third and the fourth term in right-hand-side of Eq. (B.6) represent the kink term which can be neglected inside tearing layer, and neoclassical viscous damping due to perturbed magnetic fields. Without these terms and the first term

in left-hand-side of Eq. (B.5), the equations can describe neoclassical pressure-gradient-driven instabilities.

Outside the tearing layer, ideal MHD equations are valid, and $\tilde{\psi}$ satisfies:

$$\frac{B}{4\pi L_s} \nabla_{\perp}^2 \tilde{\psi} = \frac{1}{B_{\theta}} \left| \frac{dP}{dr} \right| \frac{1}{x} \frac{d\tilde{\psi}}{dx} - \frac{1}{c} \frac{dJ_{\parallel}}{dr} \frac{1}{x} \tilde{\psi}. \quad (B.7)$$

Therefore, the derivative of $\tilde{\psi}$ is discontinuous at $x = 0$, and one can usually define Δ' as

$$\Delta' = \lim_{x \rightarrow 0} \frac{1}{\tilde{\psi}} \frac{d\tilde{\psi}}{dx}.$$

It is given by:

$$\Delta' = -\frac{1}{\tilde{\psi}^2(0)} \int_0^{\infty} dx \left[\left(\frac{d\tilde{\psi}}{dx} \right)^2 + k_{\theta}^2 \tilde{\psi}^2 + \frac{4\pi L_s}{BB_{\theta}} \left| \frac{dP}{dr} \right| \frac{\tilde{\psi}}{x} \frac{d\tilde{\psi}}{dx} - \frac{4\pi L_s}{cB} \frac{dJ_{\parallel}}{dr} \frac{\tilde{\psi}^2}{x} \right]. \quad (B.8)$$

Therefore, neoclassical tearing modes can become unstabilized due to the pressure gradient as well as the current density gradient.

Inside the tearing layer, we use constant- ψ approximation, and Δ' is determined from:

$$\Delta' = \frac{4\pi}{\gamma c^2 \eta} \frac{1}{D} \left[\frac{N_V}{I} \int_0^{\infty} dx \frac{1}{x} \frac{d}{dx} x \tilde{\phi} + \gamma^2 \int_0^{\infty} dx \frac{1}{x} \frac{d^2}{dx^2} \tilde{\phi} \right], \quad (B.9)$$

where,

$$D = -i \frac{k_{\theta} B_{\theta}^2}{c^3 \eta \rho L_s} \tilde{\psi}(0).$$

When enoclassical effects dominate over the inertia, we can normalize as

$$x = X_0 X, \quad \text{and} \quad \phi = \frac{I\gamma^2}{N_V} DX_0 \Phi_N,$$

where $X_0 = N_V/F_B\gamma$ is the tearing layer width. Then, Φ_N satisfies:

$$\frac{I\gamma^3 F_B}{N_V^2} \frac{d^2}{dX^2} \Phi_N + \frac{d}{dX} X \Phi_N - \delta_e X \frac{d}{dX} \Phi_N - X^2 \Phi_N + X = 0. \quad (B.10)$$

Also,

$$\Delta' = \frac{4\pi C_1 \gamma}{c^2 \eta} X_0, \quad (B.11)$$

where C_1 is determined from

$$C_1 = \int_0^\infty dX \frac{1}{X} \frac{d}{dX} X \Phi_N + \frac{I\gamma^3 F_B}{N_V^2} \int_0^\infty dX \frac{1}{X} \frac{d^2}{dX^2} \Phi_N. \quad (B.12)$$

Inertia terms gives correction to γ through C_1 . The growth rate and the tearing layer width are then given by

$$\gamma = \frac{\Delta'^2 \tau^2 L_P}{2\pi C_1^2 L_s} \left(\frac{\epsilon}{q\beta_p} \right)^{-1} S_M^{-1} \tau_A^{-1}, \quad (B.13)$$

$$X_0 = \frac{C_1}{2\Delta' L_P} \frac{\epsilon}{q} \beta_p L_s. \quad (B.14)$$

The dependences on L_P , L_s , and β_p are somewhat misleading, because Δ' also depends on these quantities. When the inertia dominates over neoclassical effects, one recovers the usual $\gamma \sim \Delta'^{4/5} S_M^{-3/5} \tau_A^{-1}$ growth of tearing instabilities. However, neoclassical effects act to slow down linear growth of tearing

instabilities since they grow on the resistive time scale. Therefore, the nonlinear evolution near the rational surface will be dominated by the neoclassical pressure-gradient-driven instabilities.

References

1. H. P. Furth, *Nucl. Fusion* **15**, 487 (1975).
2. F. L. Hinton and R. D. Hazeltine, *Rev. Mod. Phys.* **48**, 239 (1976);
S. P. Hirshman and D. J. Sigmar, *Nucl. Fusion* **21**, 1079 (1981).
3. S. M. Kaye, *Phys. Fluids* **28**, 2327 (1985)
4. P.C. Liewer, *Nucl. Fusion* **25**, 543 (1985); W. M. Tang, *Nucl. Fusion* **18**, 1089 (1978).
5. J. D. Callen, *Phys. Rev. Lett.* **39**, 1540 (1977).
6. R. B. White, in *Handbook of Plasma Physics*, ed. by A. A. Galeev and R. N. Sudan (1983), Vol. I, p. 611.
7. A. B. Rechester and M. N. Rosenbluth, *Phys. Rev. Lett.* **40**, 38 (1978).
8. T. H. Stix, *Nucl. Fusion* **18**, (1978) 353 (1978); J. A. Krommes, C. Oberman, and R. G. Kleva, *J. Plasma Physics* **30**, 11 (1983); B. B. Kadomtsev and O. P. Pogutse, in *Plasma Physics and Controlled Nuclear Fusion Research*, 1978 (IAEA, Vienna, 1979), Vol. I, p. 649.
9. H. Dreicer, *Phys. Rev.* **115**, 238 (1959).
10. H. E. Mynick and J. D. Strachan, *Phys. Fluids* **24**, 695 (1981);
11. H. E. Mynick and J. A. Krommes, *Phys. Fluids* **23**, 1229 (1980); H. E. Mynick and J. A. Krommes, *Phys. Rev. Lett.* **43**, 1506 (1979); C. W.

- Barnes and J. D. Strachan, *Phys. Fluids* **26**, 2668 (1983).
12. H. P. Furth, J. Killeen, and M. N. Rosenbluth, *Phys. Fluids* **6**, 459 (1963).
 13. B. A. Carreras, L. Garcia, and P. H. Diamond, *Phys. Fluids* **30**, 1388 (1987).
 14. Z. G. An, P. H. Diamond, R. D. Hazeltine, J. N. Leboeuf, M. N. Rosenbluth, R. D. Sydora, T. Tajima, B. A. Carreras, L. Garcia, T. C. Hender, H. R. Hicks, J. A. Holmes, V. E. Lynch, and H. R. Strauss, in *Plasma Physics and Controlled Fusion Research*, 1984 (IAEA, Vienna, 1985), Vol. 2, p. 231.
 15. Y. T. Baidborodov, M. S. Ioffe, V. M. Petrov, and R. I. Sobolev, *J. Nucl. Energy C5*, 409 (1963); S. Yoshikawa, *Phys. Fluids* **17**, 178 (1974).
 16. A. H. Glasser, J. M. Greene, and J. L. Johnson, *Phys. Fluids* **19**, 567 (1976).
 17. H. P. Furth, J. Killeen, M. N. Rosenbluth, and B. Coppi, in *Plasma Physics and Controlled Fusion Research*, 1964 (IAEA, Vienna, 1965), Vol. I, p. 103.
 18. H. P. Furth, *Phys. Fluids* **28**, 1595 (1985).

19. S. V. Mirnov and I. B. Semenov, *Sov. Phys. JETP* **33**, 1134 (1971).
20. R. B. White, D. A. Monticello, M. N. Rosenbluth, and B. V. Waddell, *Phys. Fluids* **20**, 800 (1977).
21. S. von Goeler, W. Stodiek, and N. Sauthoff, *Phys. Rev. Lett.* **33**, 1201 (1974); M. A. Dubois, D. A. Marty, and A. Pochelon, *Nucl. Fusion* **20**, 1355 (1980).
22. B. B. Kadomtsev, *Sov. J. Plasma Phys.* **1**, 389 (1975); G. L. Jahns, M. Soler, B. V. Waddell, J. D. Callen, and H. R. Hicks, *Nucl. Fusion* **18**, 609 (1978).
23. P. H. Rutherford, *Phys. Fluids* **16**, 1903 (1973).
24. B. V. Waddell, B. A. Carreras, H. R. Hicks, J. A. Holmes, and D. K. Lee, *Phys. Rev. Lett.* **41**, 1386 (1978).
25. I. H. Hutchinson, *Phys. Rev. Lett.* **37**, 338 (1976); E. P. Gorbonov and K. A. Razumova, *Sov. J. of Atomic Energy*, **15**, 1105 (1963).
26. B. A. Carreras, P. H. Diamond, M. Murakami, J. L. Dunlap, J. D. Bell, H. R. Hicks, J. A. Holmes, E. A. Lazarus, V. K. Paré, P. L. Similon, C. E. Thomas, and R. M. Weiland, *Phys. Rev. Lett.* **50**, 503 (1983).
27. J. W. Connor and J. B. Taylor, *Phys. Fluids* **27**, 2676 (1984).
28. L. Garcia, P. H. Diamond, B. A. Carreras, and J. D. Callen, *Phys.*

- Fluids 28, 2147 (1985).
29. W. M. Tang, F. Romanelli, and S. Briguglio, *Phys. Fluids* 31, 2951 (1988); A. B. Hassam and J. F. Drake, *Phys. Fluids* 26, 133 (1983); A. Rogister, *Plasma Phys. and Controlled Fusion* 28, 547 (1986).
 30. B. B. Kadomtsev and O. P. Pogutse, in *Reviews of Plasma Physics*, ed. by M. Leontovich (Consultants Bureau, New York, 1970), Vol. V, p. 143.
 31. J. D. Callen, B. A. Carreras, P. H. Diamond, M. E. Benchikh-Lehocine, L. Garcia, and H. R. Hicks, in *Plasma Physics and Controlled Fusion Research*, 1982 (IAEA, Vienna, 1983), Vol. I, p. 297; B. A. Carreras, P. W. Gaffney, H. R. Hicks, and J. D. Callen, *Phys. Fluids* 26, 1231 (1982)
 32. P. H. Rutherford, in *Physics of Plasma Closed to Thermonuclear Conditions*, ed. by B. Coppi, et al. (Pergamon, New York, 1981), Vol. I, p. 143.
 33. T. S. Hahm, P. H. Diamond, P. W. Terry, L. Garcia, and B. A. Carreras, *Phys. Fluids* 30, 1452 (1987);
 34. D. R. Thayer and P. H. Diamond, *Phys. Fluids* 30, 3724 (1987).
 35. C. M. Surko and R. E. Slusher, *Science* 221, 817 (1983); S. J. Zweben

- and R. W. Gould, *Nucl. Fusion* **23**, 1625 (1983); S. J. Levinson, J. M. Beall, E. J. Powers, and R. D. Bengtson, *Nucl. Fusion* **24**, 527 (1984); P. C. Liewer, J. M. McChesney, S. J. Zweben, and R. W. Gould, *Phys. Fluids* **29**, 309 (1986); W. L. Rowan, C. C. Klepper, Ch. P. Ritz, R. D. Bengtson, K. W. Gentle, P. E. Philips, T. L. Rhodes, B. Richards, and A. J. Wooton, *Nucl. Fusion* **27**, 1105 (1987).
36. S. I. Braginskii, in *Reviews of Plasma Physics*, ed. by M. Leontovich (Consultants Bureau, New York, 1965), Vol. I, p. 205.
37. R. D. Hazeltine and F. L. Hinton, *Phys. Fluids* **16**, 1883 (1973); D. Pfirsch and A. Schlüter, Max Planck Institut Report MPI/PA/7/62 (1962).
38. H. R. Strauss, *Phys. Fluids* **19**, 134 (1976); B. V. Waddell, B. A. Carreras, H. R. Hicks, and J. A. Holmes, *Phys. Fluids* **22**, 896 (1979).
39. J. D. Callen, W. X. Qu, K. D. Siebert, B. A. Carreras, K. C. Shaing, and D. A. Spong, in *Plasma Physics and Controlled Fusion Research*, 1986 (IAEA, Vienna, 1987), Vol. II, p. 157.
40. R. J. Bickerton, J. W. Connor, and J. B. Taylor, *Nature (London) Phys. Sci.* **229**, 110 (1971).
41. F. L. Hinton and J. A. Robertson, *Phys. Fluids* **27**, 1243 (1984).

42. J. D. Callen and K. C. Shaing, *Phys. Fluids* **28**, 1845 (1985).
43. J. W. Connor and L. Chen, *Phys. Fluids* **28**, 2001 (1985).
44. P. H. Diamond, P. L. Similon, T. C. Hender, and B. A. Carreras, *Phys. Fluids* **27**, 1116 (1985); J. F. Drake and T. M. Antonsen, Jr., *Phys. Fluids* **28**, 544 (1985).
45. T. M. Antonsen, Jr., and B. Lane, *Phys. Fluids* **23**, 1205 (1980); P. J. Catto, W. M. Tang, and D. E. Baldwin, *Plasma Phys.* **23**, 639 (1981).
46. O. Gruber, W. Jilge, K. Bernhardt, A. Eberhagen, G. Fussmann, O. Gehre, J. Gernhardt, G. v. Gierke, E. Glock, G. Hass, G. Janeschitz, F. Karger, M. Keilhacker, O. Klüber, M. Kornherr, K. Lackner, G. Lisitano, H.-M. Mayer, K. McCormick, D. Meisel, V. Mertens, E. R. Müller, H. Neidermeyer, W. Poschenreider, H. Rapp, J. Roth, F. Ryter, F. Schneider, G. Siller, P. Smeulders, F. Söldner, E. Speth, A. Stäbler, K. Steuer, O. Vollmer, and F. Wagner, *Proceedings of 12th European Conference on Controlled Fusion and Plasma Physics* (Budapest, 1985), Vol. I, p. 18.
47. B. B. Kadomtsev and O. P. Pogutse, in *Plasma Physics and Controlled Nuclear Fusion Research*, 1984, (IAEA, Vienna, 1985), Vol. II, p. 69; B. B. Kadomtsev and O. P. Pogutse, *Sov. Phys.-JETP Lett.* **39**, 269

- (1984).
48. P. W. Terry and P. H. Diamond, *Phys. Fluids* **28**, 1419 (1985); P. W. Terry and W. Horton, Jr., *Phys. Fluids* **26**, 106 (1983); R. E. Waltz and R. R. Dominguez, *Phys. Fluids* **26**, 3338 (1983).
49. N. T. Gladd, J. F. Drake, C. L. Chang, and C. S. Liu, *Phys. Fluids* **23**, 1182 (1980); J. F. Drake and Y. C. Lee, *Phys. Fluids* **20**, 1341 (1977); A. B. Hassam, *Phys. Fluids* **23**, 38 (1980); A. B. Hassam, *Phys. Fluids* **23**, 2493 (1983).
50. R. H. Kraichnan, *J. Fluid Mech.* **5**, 497 (1959); T. H. Dupree and D. J. Tetreault, *Phys. Fluids* **21**, 425 (1978).
51. H. Knoepfel and D. A. Spong, *Nucl. Fusion* **19**, 785 (1979).
52. F. Wagner, G. Becker, K. Behringer, D. Cambell, A. Eberhagen, W. Engelhardt, G. Fussmann, O. Gehre, J. Gernhardt, G. v. Gierke, G. Hass, M. Huang, F. Karger, M. Keilhacker, O. Klüber, M. Kornherr, K. Lackner, G. Lisitano, G. G. Lister, H. M. Mayer, D. Meisel, E. R. Müller, H. Murmann, H. Niedermeyer, W. Poschenrieder, H. Rapp, H. Röhr, F. Schneider, G. Siller, E. Speth, A. Stäbler, K. H. Steuer, G. Venus, O. Vollmer, and Z. Yü, *Phys. Rev. Lett.* **49**, 1408 (1982); S. M. Kaye, M. G. Bell, K. Bol, D. Boyd, K. Brau, D. Buchenauer,

- R. Budny, A. Cavallo, P. Couture, T. Cowley, D. S. Darrow, H. Eubank, R. J. Fonck, R. Goldston, B. Grek, K. P. Jaehnig, D. Johnson, R. Kaita, H. Kugel, B. Leblanc, J. Manickam, D. Manos, D. Mansfield, E. Mazzucato, R. McCann, D. McCune, K. McGuire, D. Müller, A. Murdock, M. Okabayashi, K. Okano, D. K. Owens, D. E. Post, M. Reusch, G. L. Schmidt, S. Sesnic, R. Slusher, S. Suckewer, C. Surko, H. Takahashi, F. Tenny, H. Towner, J. Valley, *J. Nucl. Mater.* **121**, 115 (1984); N. Ohyabu, K. H. Burrell, J. DeBoo, S. Ejima, R. Groebner, D. Overski, W. Pfeiffer, R. Stambauch, R. Stockdale, C. Armentrout, J. Baur, F. Blau, G. Bramson, N. Brooks, R. Chase, E. Fairbank, C. Hsieh, G. Jahns, C. Kahn, A. Kellman, D. Knowles, A. Lieber, J. Lohr, T. Petrie, L. Rottler, D. Schissel, R. Seraydarian, J. Smith, R. Snider, H. St. John, E. Strait, T. Taylor, D. Vaslow, S. Wojtowicz, S. Wong, G. Zawadzki, and the Doublet III Operations, Neutral Beam, and Theory Groups, *Nucl. Fusion* **25**, 49 (1985).
53. C. W. Barnes, PhD Thesis, Princeton University, Princeton (1981).
54. C. W. Barnes and J. D. Strachan, *Nucl. Fusion* **22**, 1090 (1982).
55. F. W. Perkins, in *Heatings in Toroidal Plasmas 1984* (Proc. 4th Int. Symp. Rome, 1984), Vol. 2 p. 977.

56. H. P. Furth, *Bull. Am. Phys. Soc.* **30**, 1386 (1985).
57. F. Wagner, G. Becker, K. Behringer, D. Cambell, A. Eberhagen, W. Engelhardt, G. Fussmann, O. Gehre, J. Gernhardt, G. v. Gierke, G. Hass, M. Huang, F. Karger, M. Keilhacker, O. Klüber, M. Kornherr, K. Lackner, G. Lisitano, G. G. Lister, H. M. Mayer, D. Meisel, E. R. Müller, H. Murmann, H. Niedermeyer, W. Poschenrieder, H. Rapp, H. Röhr, F. Schneider, G. Siller, E. Speth, A. Stäbler, K. H. Steuer, G. Venus, O. Vollmer, and Z. Yü, in *Plasma Physics and Controlled Fusion Research*, 1982 (IAEA, Vienna, 1983), Vol. I, p. 43,.
58. J. L. Dunlap, personal communication, 1987; see also N. Ohya, G. L. Jahns, R. D. Stambaugh, and E. J. Strait, *Phys. Rev. Lett.* **58**, 120 (1987).
59. T. S. Hahm and P. H. Diamond, *Phys. Fluids* **30**, 133 (1987).
60. F. Wagner, G. Fussmann, T. Grave, M. Keilhacker, M. Kornherr K. Lackner, K. McCormick, E. R. Müller, A. Stäbler, G. Becker, K. Bernhardt, U. Ditte, A. Eberhagen, O. Gehre, J. Gernhardt, G. v. Gierke, E. Glock, O. Gruber, G. Hass, M. Hesse, G. Janeschitz, F. Karger, S. Kissel, O. Klüber G. Lisitano, H. M. Mayer, D. Meisel, V. Mertens, H. Murmann, W. Poschenrieder, H. Rapp, H. Röhr, F. Ryter, F. Schnei-

- der, G. Siller, P. Smeulders, F. Söldner, E. Speth, K.-H. Steuer, Z. Szymanski, and O. Vollmer, *Phys. Rev. Lett.* **53**, 1453 (1984).
61. F. Holzhauser, personal communication, 1987.
 62. A. A. Ware, *Phys. Rev. Lett.* **25**, 916 (1970).
 63. M. C. Zarnstorff, M. G. Bell, M. Bitter, R. J. Goldston, B. Grek, R. J. Hawryluk, K. Hill, D. Johnson, D. McCune, H. Park, A. Ramsey, G. Taylor, and R. Weiland, *Phys. Rev. Lett.* **60**, 1306 (1988).
 64. M. C. Zarnstorff and S. C. Prager, *Phys. Fluids* **29**, 308 (1986).
 65. M. N. Rosenbluth, S. T. Tsai, J. W. Van Dam, and M. G. Engquist, *Phys. Rev. Lett.* **51**, 1976 (1983); L. Chen, R. B. White, and M. N. Rosenbluth, *Phys. Rev. Lett.* **52**, 1122 (1984).
 66. S. M. Kaye, R. J. Goldston, M. G. Bell, K. Bol, M. Bitter, R. Fonck, B. Grek, R. J. Hawryluk, D. Johnson, R. Kaita, H. Kugel, D. Mansfield, D. McCune, K. McGuire, D. Mueller, M. Okabayashi, D. Owens, G. Schmidt, and P. Thomas, *Nucl. Fusion* **24**, 1303 (1984).
 67. H. Biglari and L. Chen, *Phys. Fluids* **29**, 2960 (1986); H. Biglari and P. H. Diamond, *Phys. Fluids* **30**, 3736 (1987).
 68. B. A. Carreras and P. H. Diamond, submitted to *Phys. Fluids*.
 69. M. Abramowitz and I. A. Stegun, *Handbook of Mathematical Functions*

(National Bureau of Standards, Washington, DC, 1970).

70. K. H. Burrell, et al., in *Plasma Physics and Controlled Fusion Research*, 1988 (IAEA, Vienna, 1989), in press.
71. A. Hasegawa and K. Mima, *Phys. Fluids* **21**, 87 (1978); T. Boutros-Ghali and T. H. Dupree, *Phys. Fluids* **24**, 1839 (1981).
72. N. Suzuki, et al., in *Plasma Physics and Controlled Fusion Research*, 1988 (IAEA, Vienna, 1989), in press.

VITA

Oh Jin Kwon was born in Taegu, Korea on the 25th of December, 1958, as the first son of Byung Dae and Sook Ja Kwon. After graduating from the Kyung-book Senior High School in Taegu, Korea in January, 1977, he entered the Seoul National University in Seoul, Korea. In February, 1981, he received a Bachelor of Science degree from the Seoul National University, majoring in physics. In March, 1981, he entered the Advanced Institute of Science and Technology in Seoul, Korea. He was awarded a Master of Art degree, majoring in high energy physics, from the Advanced Institute of Science and Technology in February, 1983. In March, 1983, he was employed by the Ajou University in Suweon, Korea, as a lab instructor. He entered the Graduate School of the University of Texas at Austin in August, 1984. In February, 1985, he was employed by the Institute for Fusion Studies as a graduate research assistant. In December, 1987, he moved to the University of California, San Diego, to finish his doctorate with Professor Patrick H Diamond.

Permanent Address: 2-106, Dong-Sung Joong-Ku
Taegu, 630, Korea

This thesis was set in \TeX by the author.